Covalent Stabilization of Self-assembled Structures of Block Copolymers Having Various Molecular Designs and Their Applications

by

Jiwon Kim

Supervised by

Professor **Kyoung Taek Kim**

A Dissertion
Submitted to the Faculty of
Seoul National University (SNU)
In Partial Fulfillment of
the Requirements for the Degree of
Doctor of Philosophy

February 2021

Department of Chemistry
Graduate School
Seoul National University

Covalent Stabilization of Self-assembled Structures of Block Copolymers Having Various Molecular Designs and Their Applications

가교 가능한 블록 공중합체의 자가조립 구조체 합성과 응용 연구

지도교수 **김 경 택**

이 논문을 이학박사 학위논문으로 제출함

2020년 12월

서울대학교 대학원

화학부 고분자화학 전공

김 지 원

김지원의 이학박사 학위논문을 인준함

2020년 12월

위 원 장 최 태 림 (인)

부위원장 김 경 택 (인)

위 원 손 병 혁 (인)

위 원 이 연 (인)

위 원 박 치 영 (인)

Abstract

Self-assembly of amphiphilic block copolymers into various nanostructures continues to be a significant topic in modern research on biomimetics such as smart delivery vehicles, nanoreactors, and cellular mimics. Furthermore, to utilize self-assembled nanostructures in physically and chemically harsh environments without loss of structural integrity, cross-linking of hydrophobic blocks within the bilayer membrane should be required to provide mechanical stability. It allows the covalently stabilized nanoparticles to be used as potential candidate for the formation of nanoreactors and drug delivery systems in chemically and mechanically harsh conditions.

In chapter 2, polymersomes composed of amphiphilic block copolymers containing polydimethylsiloxane with side-chain pendant vinyl groups were constructed. A reversibly deformable polymersome compartmentalizing membrane was obtained by cross-linkage of PEG-*b*-poly(dimethyl-*r*-methylvinyl)silane in a self-assembled bilayer via photo-radical generation in aqueous media. Polymersome-encapsulated hemoglobin bound oxygen reversibly, indicating the polymersomes could be used as O_2 carriers that reversibly deform without sacrificing structural integrity or oxygen transportability.

In chapter 3, a series of block copolymers synthesized by joining two structural modules, a branched poly(ethylene glycol) (PEG) hydrophilic block and linear/branched polyisoprene (PI) hydrophobic blocks. In addition to the block ratio and architecture of the block copolymer, PEG-*b*-PI, the length of the hydrophobic PI chain by adjusting its microstructure as a key structural parameter for the self-assembly of PEG-*b*-PI to form inverse cubic mesophases. The polymer cubosomes of these block copolymers can be covalently stabilized by the photo-radical-induced cross-linking of PI chains,

resulting in the formation of rubbery hydrophobic domain.

In chapter 4, we reported the synthesis of block copolymers (BCPs) incorporating a branched polyethylene glycol (PEG) hydrophilic block and randomly copolymerized styrene and isoprene units (p(St-*co*-Ip)) of different molecular weights as the hydrophobic component. The morphological transitions of self-assembled BCP structures are dependent on changes in the chain length of the hydrophobic block, which is determined by the regiospecificity of the isoprene units. The self-assembled structures could be covalently stabilized via intermolecular cyclization between the hydrophobic blocks. Notably, the cross-linked structures displayed a reversible swelling/deswelling ability in response to the type of solvent medium.

In chapter 5, block copolymers (BCPs) composed of hydrophilic polyethylene glycol (PEG) blocks and discrete poly(phenyllactic acid) (dPPLA) blocks having hydrazone-based photoswitches in the specific positions: (1) middle of hydrophobic PPLA chains and (2) junction of amphiphilic chains. The nanostructures were constructed via solution self-assembly or direct hydration of BCPs and placed under light source to induce *E/Z* isomerization of hydrazone-based photoswitches. We found that the configurational switching of this system can attribute the reduced hydrodynamic volume of hydrophobic chains, leading to the shape transformations of self-assembled nanoparticles.

Keywords: Amphiphilic block copolymer, Self-assembled nanostructure, Biomimetics, Polymer vesicles, Hemoglobin, Covalent stabilization, Polymer Cubosomes, Nanoreactors, hydrazone-based photoswitches, Photoisomerization.

Student Number: 2015-22610

Table of Contents

List of Figures

stiffness and mechanical stability achieved by cross-linking of the vesicles.

Figure 1-6. (A) Radical cross-linking using Irgacure 2959 leads to a polymerization of vinylic side chains of the polysiloxane. (B) Polymerization of the methacrylic side chain of the corresponding polymers. The cross-linking moieties are highlighted with boxes and examples for a complete reaction are shown.

Figure 1-7. Schematic representation of the epoxy-amine cross-linking of PGMA-*b*-P(HPMA-*r*-GlyMA) copolymer vesicles.

Figure 1-8. (A) Dual cross-linking through a ligand exchange in the ruthenium complex and photo-cross-linking though the methacrylamide side chain. (B) Poly(oxymetalates) based on molybdenum act as cross-linkers between PEO chains due to hydrogen bond formation.

Figure 1-9. A scheme of branched−linear block copolymers containing polystyrene hydrophobic blocks with indene pendant groups and their selfassembly toward complex inverse bicontinuous bilayers. The self-assembled structures were cross-linked by [2π + 2π]-cycloaddition of indene groups with irradiation of long-wavelength UV light (λ = 365 nm).

Figure 1-10. Schematic representation of photo-crosslinked and pH sensitive polymersomes for triggering the loading and release of cargo.

Figure 1-11. Schematic overview of the sequential postconjugation processes on a polymersome surface using covalent and noncovalent approach in combination with chemical structures of block copolymers having azide, methoxy, and adamantine functionalities.

Figure 1-12. Illustration of a polypeptide vesicle that exhibits intracellular esterase-triggered bilayer cross-linking to accelerate drug release without compromising the safety.

Figure 2-1. Schematic representation of the self-assembly of branched-linear block copolymers in solution and cross-linking of the poly(dimethyl-*r*-methylvinyl)silane (PDMVS) compartments by photo-generated radical coupling.

Figure 2-2. GPC analysis (A) and ^{1}H NMR spectrum (B) of PDMVS-*b*-PEG550$_3$.

Figure 2-3. Uncross-linked morphological transition upon reduction of the chain length of PDMVS. Cryo-EM images of (A) cylindrical micelles (PEG550$_3$-PDMVS15K), (B) polymersomes (PEG550$_3$-PDMVS20K), and (C) hexagonal nanoparticles (PEG550$_3$-PDMVS26K).

Figure 2-4. Cross-linked morphological transition upon reduction of the PDMVS chain length. TEM images of (A) cylindrical micelles of PEG550$_3$-PDMVS15K and (B) polymersomes of PEG550$_3$-PDMVS20K constructed by co-solvent self-assembly. (C) Cylindrical micelles of PEG550$_3$-PDMVS10K and (D) giant-sized polymersomes of PEG550$_3$-PDMVS15K formed by direct hydration.

Figure 2-5. (A) Dynamic light scattering (DLS) size plots of the cross- and uncross-linked polymersomes of PEG550$_3$-PDMVS20K in aqueous and THF solutions. TEM images of (B) unlinked polymersomes in water, cross-linked polymersomes (C) in water, and (D) in THF.

Figure 2-6. Results of multi-extrusion experiments of polymersomes of PEG550$_3$-*b*-PDMVS20K with 0.2 μm porous polycarbonate membrane filters. TEM images of polymersomes prepared by the following processes: (A) multi-extrusion (10 times) followed by cross-linking, (B) cross-linking followed by multi-extrusion (10 times). (C) DLS size plots of the cross-linked (blue) and uncross-linked (red) polymersomes in aqueous solution after multiple extrusions. (D) CLSM images of cross-linked vesicles containing

rhodamine B before extrusion (top) and after extrusion (bottom) (Scale bars = 5 μm). (E) Change of polymersome size with multiple extrusions.

Figure 2-7. Dynamic light scattering (DLS) size plots of polymersomes of PEG550$_3$-*b*-PDMVS self-assembled via co-solvent and direct hydration methods. The polymersomes encapsulating Rhodamine B stayed for 1 week without showing any change in their size and morphology.

Figure 2-8. Giant unilamellar vesicles of PEG-*b*-PDMVS. Micro-deformation of a polymersome observed by (A) optical and (B) confocal laser scanning microscopy. The arrow marks the upper portion of a projection aspirated by negative pressure into the micropipette. (C) Aspiration increased membrane tension and expanded the vesicle surface area.

Figure 2-9. Sequence of a locally cross-linked vesicle of PEG-*b*-PDMVS. The cross-linked vesicle was partially deflated (1 to 3) by a negative pressure and inflation under positive pressure brought the vesicle back to its original shape (4 to 6) (Scale bar = 20 μm).

Figure 2-10. Sequence of an uncross-linked vesicle of PEG-*b*-PDMVS. The uncross-linked polymersomes failed to retain their round-shape and then finally were ruptured under negative pressure (1 to 3) (Scale bar = 20 μm).

Figure 2-11. (A) Schematic of singlet O_2 generation by ZnTPP under yellow light. (B) UV-Vis absorbance spectra of cross-linked polymersomes with ZnTPP. (C) UV−Vis absorption spectra of ADPA with respect to the time of irradiation (λ_{max} = 560 nm) in the polymersomes of PEG550$_3$-*b*-PDMVS20K encapsulating ZnTPP. (D) Change in ADPA absorbance at 378 nm with increasing irradiation time.

Figure 2-12. (A) Absorptions of free ZnTPP with different amounts (B) Plotting of a calibration curve of free ZnTPP, and (C) Absorption of ZnTPP loaded vesicles after elimination of the effect of nanoparticle-induced

scattering.

Figure 2-13. (A) Absorptions of free COHb with different amounts (B) Plotting of suitable calibration curve of free COHb, and (C) Absorption of hemoglobin loaded vesicles after elimination of the effect of nanoparticle-induced scattering.

Figure 2-14. TEM image and DLS size plot for size-controlled polymersomes containing hemoglobin for oxygen transportation.

Figure 2-15. Polymersome-encapsulated hemoglobin tested for O_2 permeability. (A) UV-Vis spectra of oxygenated and deoxygenated HEP. (B) UV-Vis spectra from repeated oxygen-nitrogen bubbling processes. The changes in absorbance intensity at 538 and 572 nm with O_2 and N_2 saturation were observed.

Figure 3-1. Schematic representation of the solution self-assembly of branched-branched block copolymers of PEG550$_3$-*b*-PI(*1,2*)$_2$ into polymer cubosomes and the cross-linking of the PI compartments by photo-generated radical coupling. The cross-linked cubosomes maintained their structural integrity upon exchanging the solvent from water to THF.

Figure 3-2. 3-D images of (A) 1,2-cis and (B) 1,4-microstructures of PI chains. (C) ^{1}H NMR spectra of PI(*1,4*)(10K) and PI(*1,2*)(10K) showing the difference in microstructure of the repeating units.

Figure 3-3. (A) ^{1}H NMR spectra of PEG (red) and PI (black) structural modules and the PEG550$_3$-PI$_2$ (blue). (B) ^{1}H NMR spectra showing the disappearance of Si-CH$_2$ protons upon deprotection. (C) GPC spectra of synthesis of block copolymers by click chemistry.

Figure 3-4. Morphological transition from polymersomes to inverse micellar nanoparticles upon reduction of the chain length of PI. Cryo-TEM images of (A) polymersomes, (B) inverse micellar nanoparticles, and (C) mixed

Figure S4. UV-Vis spectra of COHb, metHb, deoxyHb, and oxyHb. The commercially available bovine hemoglobin was reduced by Sodium dithionite, followed by saturation with CO gas to obtain COHb.

Figure S5. ^{1}H NMR (500 MHz, $CDCl_3$) spectrum of branched hydrophilic block.

Figure S6. ^{1}H NMR (500 MHz, $CDCl_3$) spectrum of $PEG550_3$-*b*-PI_2.

Figure S7. (A) Dynamic light scattering (DLS) size plots of the uncross-linked (black) and cross-linked (red) polymersomes in aqueous and THF (blue). TEM images of (B) uncross-linked vesicles in water, and cross-linked vesicles (C) in water and (D) in THF.

Figure S8. (A) ^{1}H NMR and (B) ^{13}C NMR spectra of random copolymer, p(St-*co*-Ip)(1,4). The regiospecificities of the isoprene units showed predominantly 1,4-rich repeating unit (1,4-: 1,2-: 3,4- = 70-73: 0: 27-30) along the copolymer chain.

Figure S9. (A) ^{1}H NMR and (B) ^{13}C NMR spectra of random copolymer, p(St-*co*-Ip)(3,4). The regiospecificities of the isoprene units showed predominantly 3,4-rich repeating unit (1,4-: 1,2-: 3,4- = 0: 25-29: 71-75) along the copolymer chain.

Figure S10. 3-D images of (A) 1,4- units and bicyclic structure generated by the intramolecular Friedel-Craft cyclization of between isoprene units and the benzene ring of the adjacent styrene unit. Distance: 0.485 nm for 1,4 addition and 0.392 nm for bicyclic structure. (B) The reaction leads to a high Tg and robust mechanical properties to the random copolymer. The gummy product was converted to the powdery compound.

Figure S11. (A) ^{1}H NMR and (B) gel-permeation chromatography spectra of random copolymers, p(St-*co*-Ip)(1,4) and its cyclized product. Cationic cyclization of the obtained polymer was examined using CF_3SO_3H in

cyclohexane. $[CF_3SO_3H]_0$ = 5 wt%.

Figure S12. (A) ^{1}H NMR and (B) gel-permeation chromatography spectra of random copolymers, p(St-*co*-Ip)(3,4) and its cyclized product. Cationic cyclization of the obtained polymer was examined using CF_3SO_3H in cyclohexane. $[CF_3SO_3H]_0$ = 5 wt%.

Figure S13. ^{1}H NMR spectra of random copolymer, p(St-*co*-Ip)(1,4) (M_n = 14.5k) showing the disappearance of Si-CH_2 protons upon deprotection.

Figure S14. (A) ^{1}H NMR spectra and (B) GPC spectra of synthesis of p(St-*co*-Ip)(3,4)-*b*-PEG750$_3$ block copolymers by click chemistry: PEG (blue), p(St-*co*-Ip) (red) structural module, and p(St-*co*-Ip)-*b*-PEG (black).

Figure S15. (A) ^{1}H NMR and (B) Gel-permeation chromatography spectra of random copolymers containing dominantly 1,4-microstructures and its cyclized product. Cationic cyclization of the obtained polymer was examined using CF_3SO_3H in cyclohexane. $[CF_3SO_3H]_0$ =5 wt%.

Figure S16. Cryo-TEM images of self-assembled structures of (A) p(St-*co*-Ip)(1,4)-*b*-PEG750$_3$ (21.2k) and (B) p(St-*co*-Ip)(1,4)-*b*-PEG750$_3$ (25.0k).

Figure S17. TEM images of self-assembled structures showing the thickness of the bilayer membrane: (A) polymer vesicles of p(St-*co*-Ip)(3,4)-*b*-PEG750$_3$ (M_n = 19.2K) and (B) polymer vesicles of its cyclized BCPs.

Figure S18. ^{1}H NMR of (A) random copolymers, p(St-*co*-Ip)(1,4) and (B) its cyclized product. Cationic cyclization of the obtained polymer was examined using CF_3SO_3H in acetonitrile. $[CF_3SO_3H]_0$ = 5 wt%.

Figure S19. TEM images of (A) polymer vesicles of the cyclized p(St-*co*-Ip)(1,4)-*b*-PEG750$_3$ (M_n = 13.8K) in acetonitrile and (B) the uncross-linked polymer vesicles in THF.

Figure S20. ^{1}H NMR spectra of hydrazone-based photo-switches (THP-H1-

List of Tables

List of Schemes

Scheme S10. Synthesis of block copolymer having hydrazone-based photo-switches (PEG-H1-PPLA$_{17}$).

Chapter 1. Introduction

1.1 Morphological control of self-assembled nanostructures

The morphological control of nanostructures that are constructed by the self-assembly of macromolecular building blocks in solution is of practical importance because the shape and size of a nanostructure affects both its motion in solution and its interactions with surroundings, resulting in nanostructures with distinct kinetic and chemical behaviors.[1-7] In solution, block copolymers (BCPs) self-assemble to form micellar, vesicular, and periodic nanostructures. The morphology of these nanostructures is mainly dictated by the structural properties of the constituent BCPs such as the molecular weights and block ratios of their constituent polymer blocks.[8,9] The precise manipulation of the chemical structures and architectures of BCPs has been facilitated by advances in synthetic chemistry, including controlled polymerization techniques and coupling chemistries between well-defined macromolecules.[10-12]

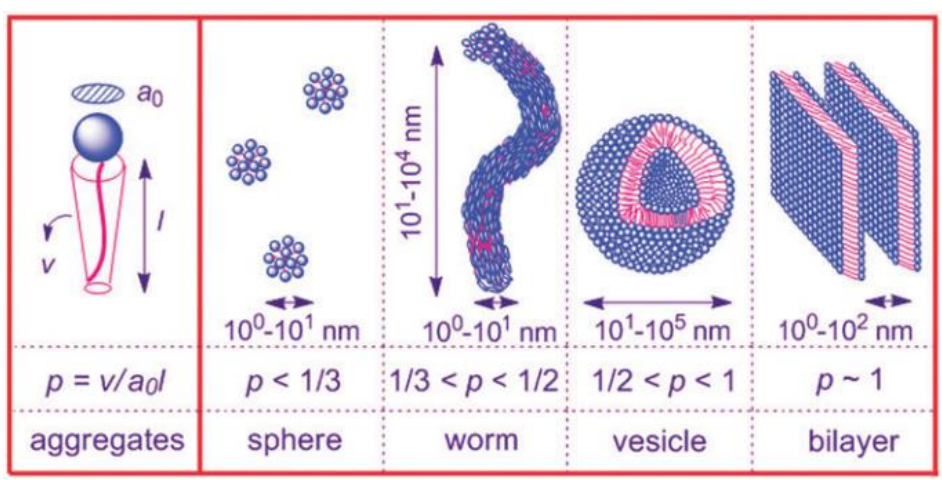

Figure 1-1. Relationship between the packing parameter (p) and the morphology of self-assembled surfactant aggregates.[17]

To form polymer vesicles, the packing parameter ($p = V/a_0l_c$ where domain volume (V) and chain length (l_c) of hydrophobic polymer block, and junction area (a_0) of hydrophilic block) of a BCP should range from 0.5 to 1.[10,14] In contrast, the formation of inverse mesophases requires this packing parameter to be greater than unity (Figure 1-1).[13,14] Inverse structures ($p > 1$) such as large compound vesicles, polymer cubosomes, hexagonal structures, and inverse micelles have been investigated. Among them, polymer cubosomes are cutting-edge structures with complex inner structures and large surface areas. Kim et al. (2014) reported colloidal inverse bicontinuous cubic structures.[15] These complex three-dimensionally ordered structures can be formed by the self-assembly of BCPs in solution, given that the architecture and molecular weight of the BCP are carefully adjusted during synthesis.

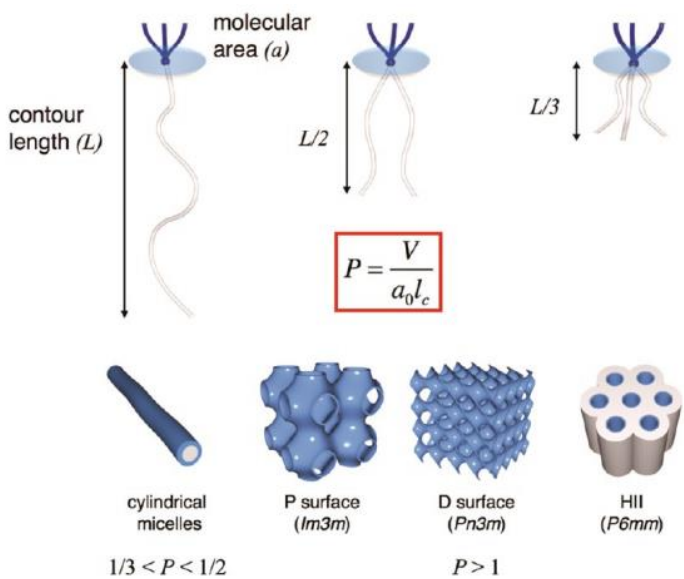

Figure 1-2. Schematic diagram of branched−branched BCPs and their self-assembly in solution. For a fixed molecular weight of the hydrophobic domain, the contour length of the hydrophobic chain (l) is reduced proportionally upon increasing the number of chains comprising the branched hydrophobic block. P represents the packing parameter of a BCP, where V is the volume of the hydrophobic block, a_0 is the interfacial area of the hydrophilic block, and l_c is the critical length of the hydrophobic block.[16]

Furthermore, the structural requirements for forming inverse bicontinuous cubic structures have been elucidated, which consist of triply periodic minimal surfaces of block copolymers with dissimilar lattices and periodicities (Figure 1-2 and 1-3).[16] At the same block ratio (i.e., weight fraction of the hydrophilic block), a BCP comprising a dendritic or branched hydrophilic block with a linear hydrophobic block favors the formation of inverse mesophases in solution, which is in direct contrast to the formation of polymer vesicles by the self-assembly of chemically identical linear BCP.[15–17] Because the packing parameter (p) of a BCP is primarily determined by its block ratio, we postulated that this marked difference in the self-assembled morphologies of chemically identical BCPs could arise from differences in their p values. These differences stem from the presence or absence of steric bulk in the hydrophilic block. To rationalize this phenomenon, we hypothesized that the presence of a sterically bulky hydrophilic block increases the interfacial area at the junction between two polymer blocks (a_0).

However, fine-tuning the chemical structures of BCPs requires arduous synthesis, which limits the availability and application of tailored soft nanostructures. Therefore, a non-synthetic method for controlling the morphology of self-assembled BCP nanostructures is desired and would allow BCP nanostructures of varying shapes and surface chemistries to reach their maximum potential. Control of BCP nanostructure formation using a non-synthetic pathway would entail manipulating solvent affinity for the constituent polymer blocks and blending BCPs of differing molecular weights and block ratios.[15,16] An interesting approach involves the application of external stimuli to control BCP conformation. Such conformation changes directly influence the structural parameters governing the in-solution morphology of the self-assembled structure (Figure 1-4).[17–23] This approach to morphology control may also allow the *in situ* change of the nanostructure morphology via the introduction or removal of stimuli-inducing molecules.

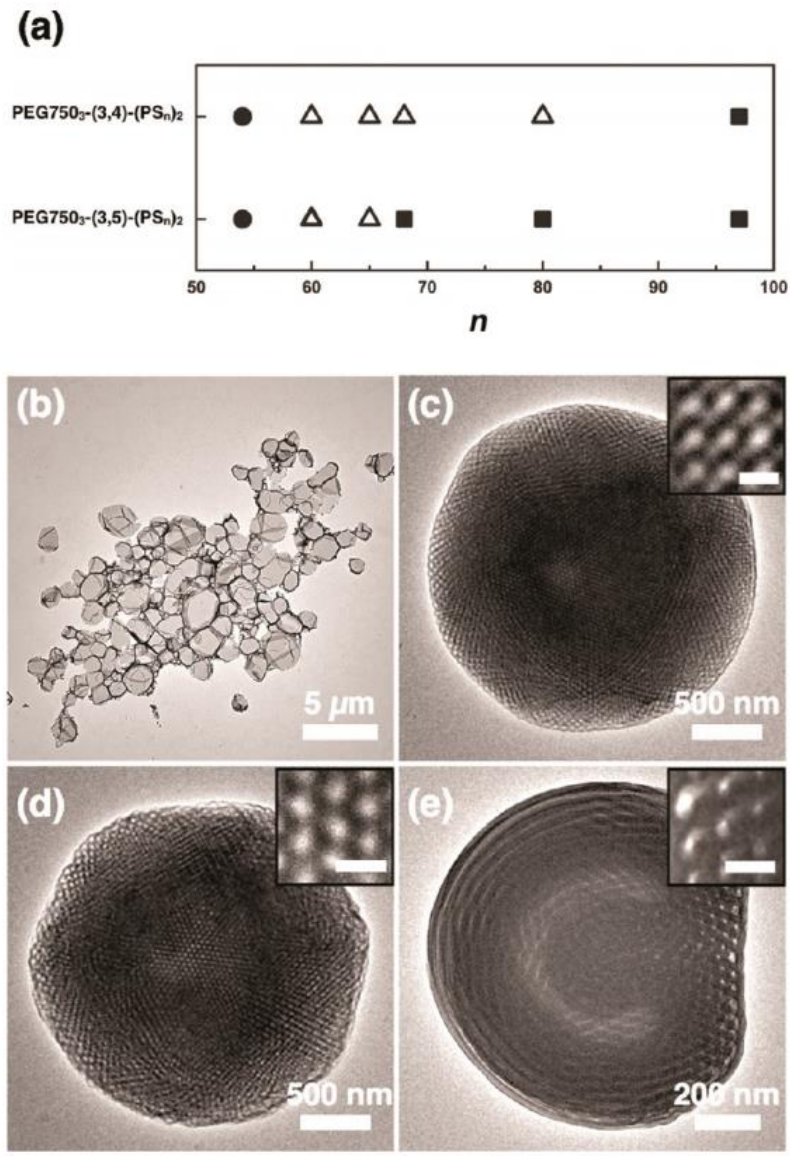

Figure 1-3. (A) Simple phase diagrams for solution self-assembly of bbBCPs (1 wt% in dioxane) with respect to the molecular weight of the PS chains. *n* indicates the number-average degree of polymerization of the PS chains (filled circle: vesicle; open triangle: cubosome; filled square: hexasome). (B−E) TEM images showing representative morphologies of self-assembled structures of PEG750$_3$-(3,5)-(PS$_n$)$_2$ at varying DP$_n$ values of the PS chains: (B) flat lamella and polymer vesicles (n = 54, f_{PEG} = 20.0%); (C, D) polymer cubosomes (n = 60, f_{PEG} = 18.0% for c and n = 65, f_{PEG} = 16.6% for d); (E) polymer hexasomes (n = 80, f_{PEG} = 13.5%). The insets are magnified views of the internal lattices (scale bars = 50 nm).[14]

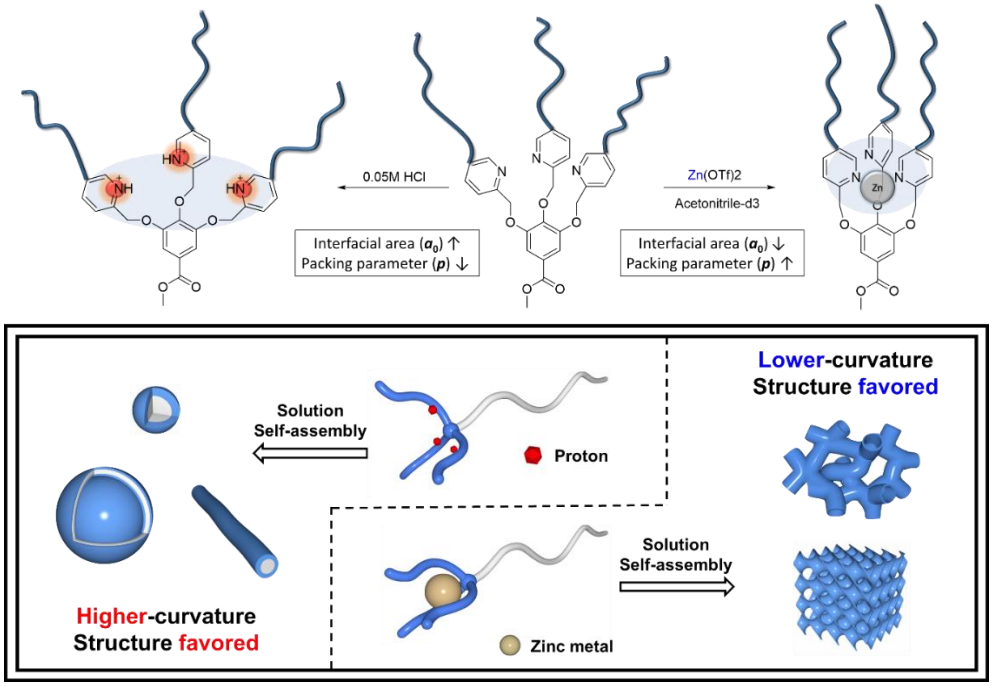

Figure 1-4. Schematic of the stimuli-induced conformational changes of a hydrophilic block containing three pyridyl groups that respond to the presence of stimuli, such as pH changes and the addition of metal cations.[22]

1.2 Covalent stabilization of self-assembled nanostructures via cross-linking

The application of self-assembled nanostructures in physically and chemically harsh environments requires additional mechanical stability for maintaining structural integrity. This is provided by cross-linking the hydrophobic polymer blocks within the nanostructure bilayer membrane.[24-30] The first application of cross-linking to polymersomes was reported by Discher et al. (2002). The reported cross-linking of a PEG-*b*-PB block copolymer was achieved using covalent stabilization afforded by radical polymerization of the residual polybutadiene (PB) double bonds.[31,32] The vesicles present maintained their shape in solution while retaining all of the

encapsulated sucrose solution. It was also reported that complete cross-linking was not necessary when the gel point had been reached. Later works report the use of radical cross-linking as the primary method employed for polymersomes.[31] The resulting cross-linked membranes were tested for stability using a simple dehydration–rehydration cycle, wherein a vesicle was sucked into a micropipette from an aqueous solution (Figure 1-5). Both the surface elastic moduli and sustainable wall were stressed to 10^3 atm, which were several orders of magnitude greater than any natural lipid membrane could endure.

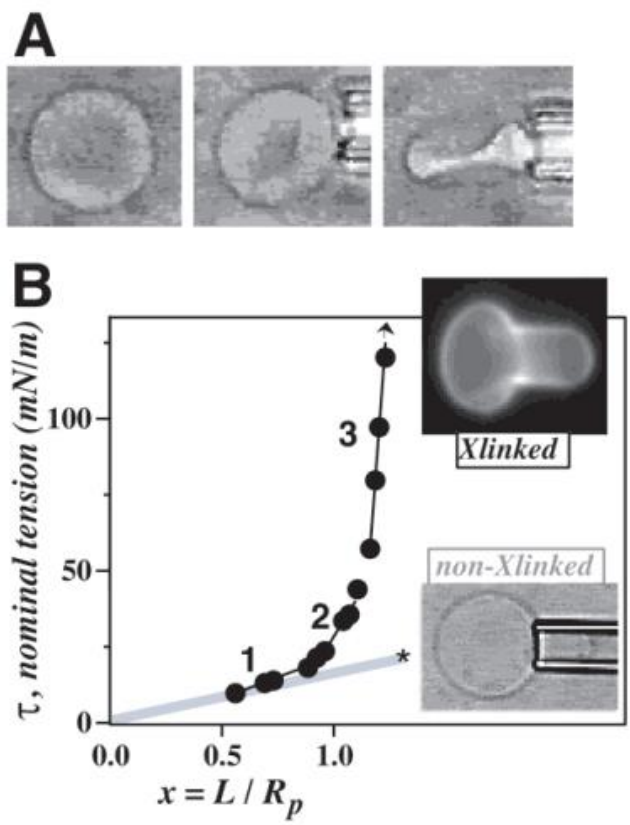

Figure 1-5. Deformability of cross-linked vesicles in comparison with non-cross-linked vesicles. (A) Cross-linked polymer vesicles tested for stability by a simple dehydration-rehydration cycle. (B) Increased elastic stiffness and mechanical stability achieved by cross-linking vesicles.[31]

Kim et al. (2019) used a photo-radical generator, 2-hydroxy-4'-(2-hydroxyethoxy)-2-methylpropiophenone (Irgacure 2959), for radical cross-linking of polymer vesicles (Figure 1-6A).[33] Photoinitiation is advantageous to initiation via peroxodisulfate as it proceeds at room temperature. An increase in mechanical stability was indirectly found when multi-extrusion through a 0.2 μm filter left the diameter of cross-linked vesicles unaltered, while their non-cross-linked counterparts reduced in diameter. In addition, the E-moduli of the giant polymer vesicles prepared via direct hydration increased from 18.7 mN/m to 224.1 mN/m, revealing that the mechanical properties of the membrane were enhanced as a result of cross-linking. Kong et al. (2014) also employed radical photo-cross-linking using Irgacure 2959 to covalently stabilize polymersomes of poly(2-hydroxyethyl-co-2-methacryloxyethyl-co-octadecyl aspartamide (Figure 1-6B).[34] Cross-linking was performed by polymerizing methacrylate units using UV irradiation. The hydroxyl groups along the hydrophilic chain of the polymer were then employed to conjugate a fluorescent probe to the polymer, so as to track them inside a mouse body.

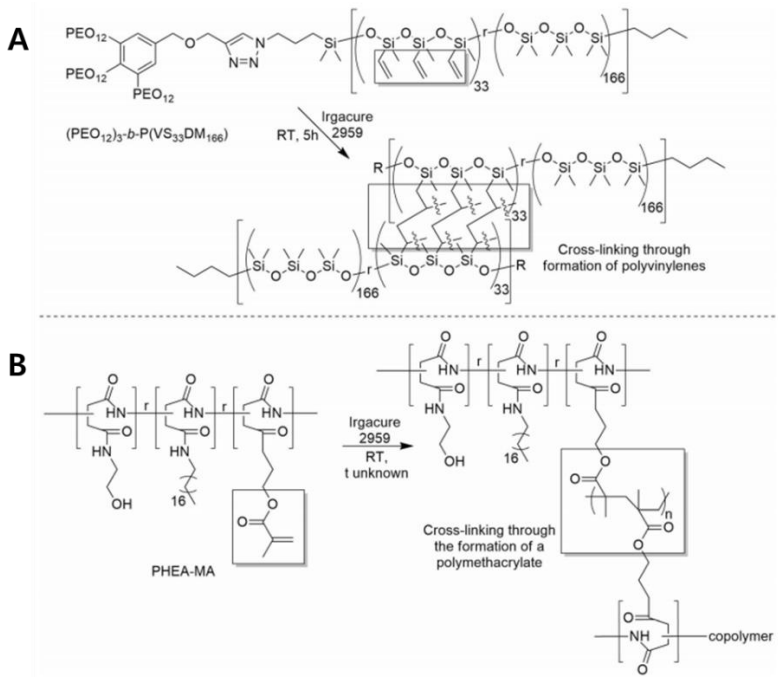

Figure 1-6. (A) Radical cross-linking using Irgacure 2959 leading to the polymerization of vinylic side chains of polysiloxane. (B) Polymerization of the methacrylic side chain of the corresponding polymers. The cross-linking moieties are highlighted with boxes and examples of a complete reaction are shown.[33,34]

Armes at al. (2012) produced cross-linked vesicles from PGMA-*b*-P (HPMA-*r*-GlyMA) by polymerization-induced self-assembly (PISA).[35] Bifunctional amines were used for cross-linking the vesicles through a ring-opening reaction of the epoxide. *O*-Reilly et al. (2019) employed a variety of cross-linkers such as Jeffamine (bifunctional PEO, PPO) and small aliphatic amines including ethylenediamine and butyldiamine amongst others.[36] They discovered that using small-molecule amines led to shrinkage of vesicle diameters (180 to 125 nm), while bifunctional PEO amines caused membrane swelling and produced larger diameters of approximately 240 nm.

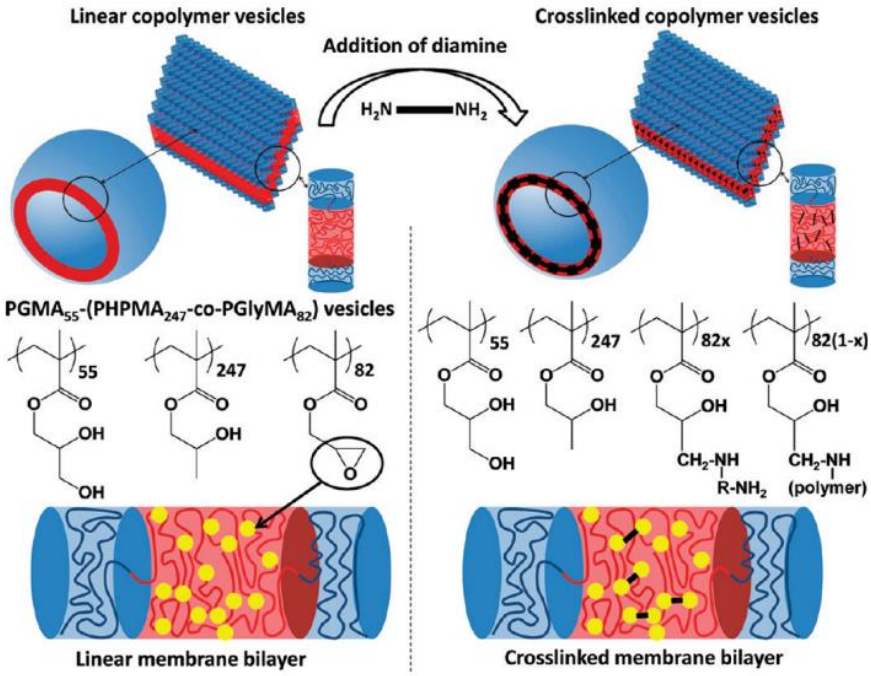

Figure 1-7. Schematic representation of the epoxy-amine cross-linking of PGMA-*b*-P(HPMA-*r*-GlyMA) copolymer vesicles.[34]

Yoshida et al. (2015) employed a combination of two cross-linking methods to covalently stabilize the vesicles of PEO-*b*-P(NIPAAm-*r*-NAPMAm-*r*-NAPMAmRu(bpy)-*r*-NAPMAmMA) (Figure 1-8A). In this system, photopolymerization of the methacrylic units formed irreversible cross-linking bonds within the polymer membrane. Furthermore, the ruthenium complex acted as a partial cross-linker through intermolecular ligand exchange, which finally interconnected two polymer chains.[35] Most cross-linking processes have been conducted in the hydrophobic block of the polymer membranes. However, Zhu et al. (2017) chose a different approach by cross-linking the PEO domain. They constructed polymer vesicles of PEO-*b*-PCL wherein PEO chains were cross-linked using Mo polyoxometalates (POMs) (Figure 1-8, Bottom) to control the shape and mechanical stability of polymersomes in aqueous suspensions.[36] The stimuli-responsive properties of

the POMs were introduced into the POM-dressed polymersomes after the interaction of POMs with the PEO blocks.

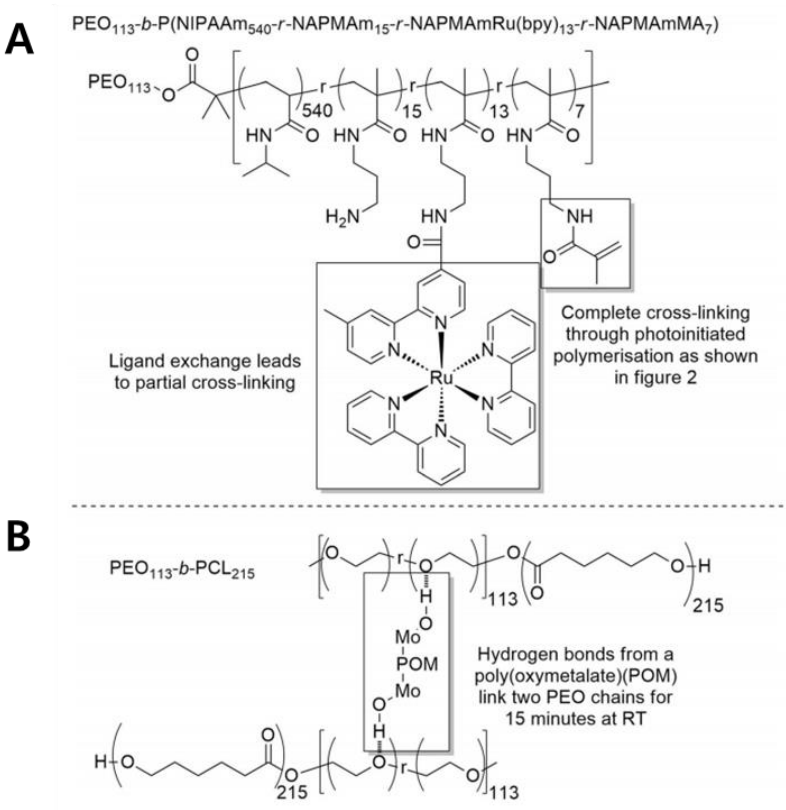

Figure 1-8. (A) Dual cross-linking through a ligand exchange in the ruthenium complex and photo-cross-linking though the methacrylamide side chain. (B) Poly(oxymetalates) based on molybdenum act as cross-linkers between PEO chains due to hydrogen bond formation.[35,36]

Covalent stabilization of complex 3-D periodic structures was performed to develop smart nanoreactors. Inverse bicontinuous cubic mesophases of BCPs are an emerging class of mesoporous structures composed of well-defined periodic minimal structures of BCP bilayers, in which two non-intersecting water channel networks are embedded in a long-range three-dimensional order. The transient structures formed by the self-assembly of macromolecular building blocks may require covalent fixing by

cross-linking of organized molecules to allow their use in harsh conditions. Jeong et al. (2017) reported the cross-linking of hydrophobic compartments of complex self-assembled nanostructures of amphiphilic block copolymers by the [2π + 2π]-cycloaddition of indene moieties present in a hydrophobic block based on polystyrene (PS).[37] This method produced an infinite polymer network within the hydrophobic compartments of the self-assembled structures without using additional reagents or causing morphological changes during cross-linking (Figure 1-9).

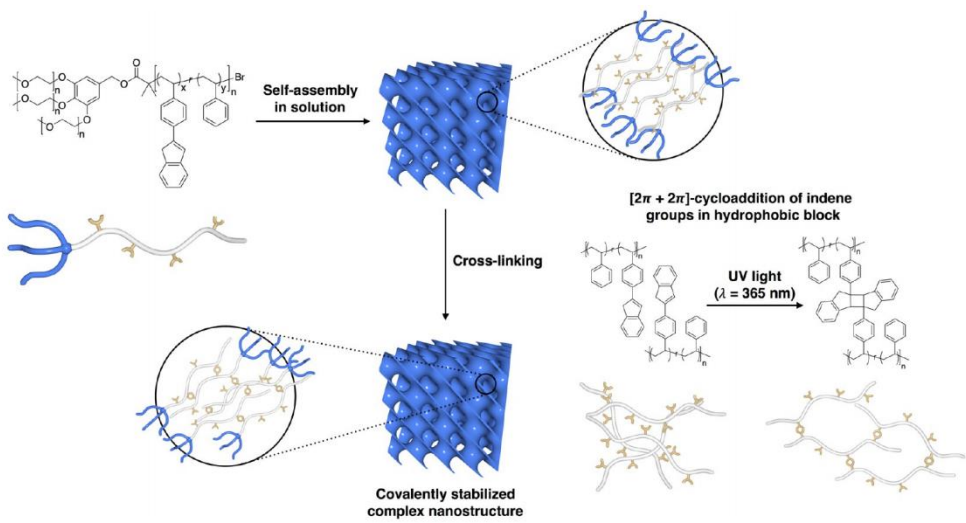

Figure 1-9. Scheme depicting branched−linear block copolymers containing polystyrene hydrophobic blocks with indene pendant groups and their self-assembly towards complex inverse bicontinuous bilayers. The self-assembled structures were cross-linked by [2π + 2π]-cycloaddition of indene groups under long wave UV irradiation (λ = 365 nm).[37]

While cross-linked cubic mesophases of BCPs demonstrate enhanced stability under chemical stresses, the mechanical properties of these mesophases require modifications to allow for their use in various other applications, including those wherein they are employed as responsive photonic crystals and for ultrafiltration.[38-41] The introduction of cross-linkable hydrophobic polymers with low glass transition temperatures to BCPs may

represent a very attractive strategy because the resultant cross-linked mesophases would exhibit elasticity and resist physical stress without fracture. Kim et al. (2019) reported block copolymers composed of branched hydrophilic PEG blocks and hydrophobic polyisoprene (PI).[17] The prepared BCPs in solution self-assembled into colloidal particles of inverse mesophases including polymer cubosomes. This was dependent on the hydrophobic block chain length, which can be adjusted by varying the molecular weight and microstructure of the repeating unit. Furthermore, the polymer cubosomes showed reversible swelling/deswelling without losing their structural integrity in response to the presence of organic solvents.

1.3 Potential applications of cross-linked nanostructures

Cross-linked vesicles bearing membranes responsive to different stimuli have emerged as promising candidates for nanoreactors and drug delivery systems.[42-48] Polymersomes can be tailored to desired applications using different strategies. Voit et al. first reported photo-cross-linked and pH-sensitive polymer vesicles in 2011 (Figure 1-10).[49] The hydrophobic block consisted of polymerized pH-sensitive diethylaminoethyl methacrylate (DEA) and the photo-cross-linker 3,4-dimethyl maleic imidobutyl methacrylate (DMIBMA). Polymer vesicles were typically prepared via the self-assembly of BCPs using the so-called pH switch method. Upon protonation of PDEA along the hydrophobic chain, the vesicles exhibited a defined swelling and returned to their original size at pH >8. This system exhibits potential for establishing pH-stable and permeable vesicles, and is suitable for application in biomedicine as nanocarriers.[50,51]

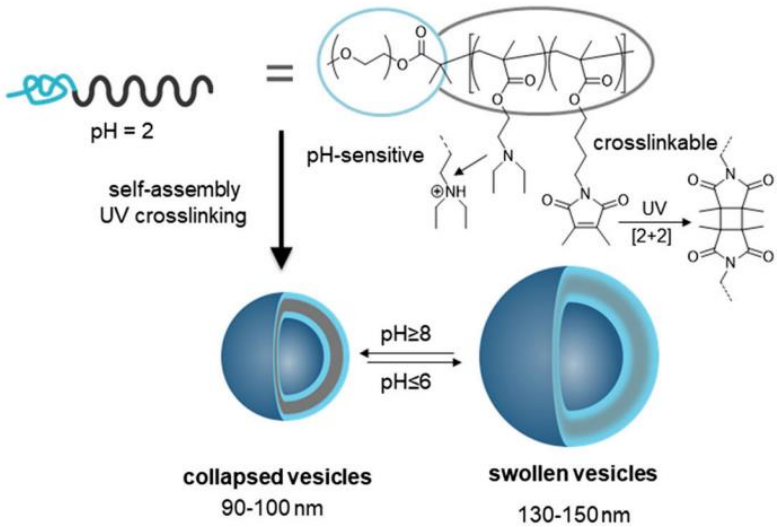

Figure 1-10. Schematic representation of photo-cross-linked and pH sensitive polymersomes for triggering the loading and release of cargo.[49]

Similar pH- and light-sensitive block copolymers were synthesized using a cross-linker (2-hydroxy-4-(methacryloyloxy) benzophenone, BMA) as a side chain of the hydrophobic block to prepare photo-cross-linked polymersomes. In addition, various functional groups (N_3, NH_2, and adamantine groups) were introduced to the hydrophilic end group (Figure 1-11).[52-54] The end groups allowed further functionalization using different methods. For the covalent approach, nitroveratryloxycarbonyl-protected amine (NVOC) molecules (as light-responsive moieties) were introduced into the surface of polymer vesicles via azide-alkyne click chemistry. For the noncovalent approach, strong adamantine-cyclodextrin host-guest interactions were used. This stepwise procedure enabled the establishment of pH- and light-responsive multifunctional polymersomes.

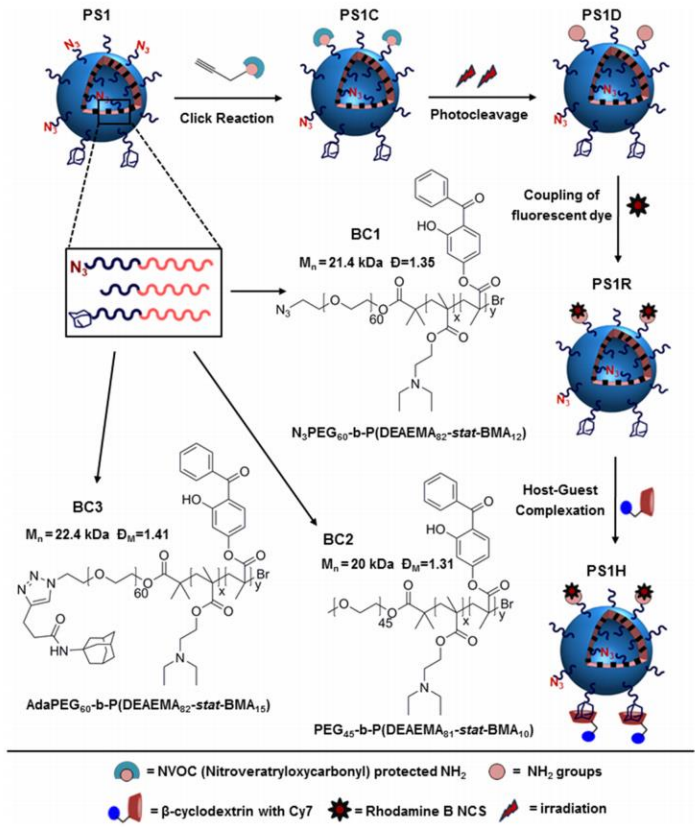

Figure 1-11. Schematic overview of sequential postconjugation processes conducted on a polymersome surface, using covalent and noncovalent approaches, in combination with chemical structures of block copolymers having azide, methoxy, and adamantine functionalities.[53]

Red blood cells (RBCs) are the oxygen-carrying cells abundant in blood. The discoidal RBCs exhibit remarkable deformability under mechanical stress, which enables their passage through capillaries with smaller diameters without loss of their structural integrity. To mimic RBCs using polymer vesicles, Kim et al. (2019) synthesized PEG-*b*-poly(dimethyl-*r*-methylvinyl)siloxane block copolymers composed of a siloxane chain as a hydrophobic block with low glass-transition temperatures (T_g).[33] The covalently cross-linked polymer vesicles exhibited superior mechanical robustness while maintaining deformability under physical stress. Moreover,

polymersome-encapsulated hemoglobin successfully bound oxygen reversibly and indicated that cross-linked polymer vesicles containing the siloxane bond could be used as O_2 carriers, which reversibly deformed without sacrificing structural integrity or oxygen transportability.

Enzyme-responsive polypeptide vesicles have attracted significant attention for use in precision theranostics owing to their biocompatibility and biodegradability. Duan et al. (2020) reported amphiphilic PEG-polypeptide copolymers containing esterase-labile carbamate-caged primary amines (Figure 1-12).[55] 4-Acetoxybenzyl carbamate, an esterase-responsive moiety, was incorporated into the poly-L-lysine (PLL) side chain using the postmodification method. The prepared PEG-*b*-PLL(N-acetoxybenzyl acetate) copolypeptides successfully self-assembled into vesicular structures. Esterase-triggered self-immolative decaging reactions quickly led to the release of the primary amine moiety of the monomers. The transition of the bilayer membrane of vesicles from hydrophobic to partially hydrophilic allowed the vesicles to undergo an amidation reaction. This process preserved the nanostructures while permeabilizing the vesicle membrane.

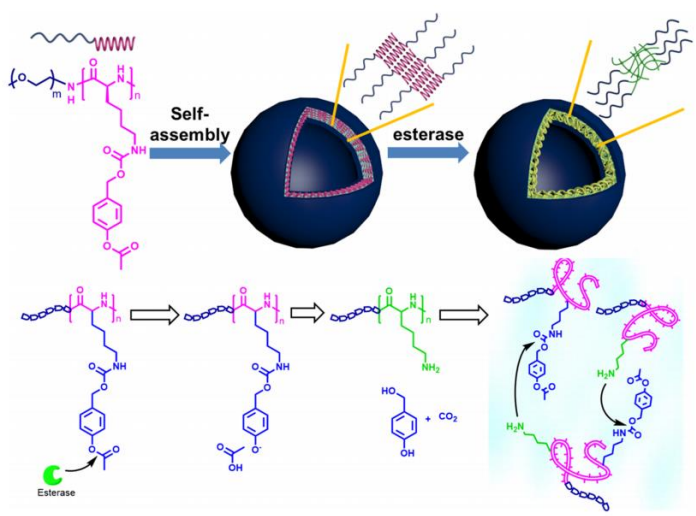

Figure 1-12. A polypeptide vesicle exhibiting intracellular esterase-triggered bilayer cross-linking, aiding in accelerated drug release, without

compromising safety.[55]

1.4 Summary of thesis

This dissertation reports the synthesis of amphiphilic block copolymers containing different hydrophobic chains. The molecular structures of these copolymers were tailored to specific applications. Utilization of self-assembled nanostructures in physically and chemically harsh environments required the use of cross-linking to maintain structural integrity. Various cross-linking methods, such as photo-generated radical coupling and intermolecular Friedel–Crafts alkylation, were applied to provide covalent stabilization of the self-assembled structures. This allowed for the potential use of covalently stabilized nanoparticles in the formation of nanoreactors, and as drug delivery systems.

In Chapter 2, polymersomes composed of amphiphilic block copolymers containing polydimethylsiloxane with side-chain pendant vinyl groups were constructed. A reversibly deformable polymersome compartmentalizing membrane was obtained by cross-linkage of PEG-*b*-poly(dimethyl-*r*-methylvinyl)silane in a self-assembled bilayer via photo-radical generation in aqueous media. Polymersome-encapsulated hemoglobin bound oxygen reversibly, indicating that the polymersomes could be used as O_2 carriers that reversibly deform without sacrificing structural integrity or oxygen transportability.

In Chapter 3, a series of block copolymers was synthesized by joining two structural modules, a branched poly(ethylene glycol) (PEG) hydrophilic block, and linear/branched polyisoprene (PI) hydrophobic blocks. In addition to the block ratio and block copolymer (PEG-*b*-PI) architecture, the length of the hydrophobic PI chain is also a key structural parameter in the self-

assembly of PEG-*b*-PI to an inverse cubic mesophase, because it adjusts the copolymer microstructure. The polymer cubosomes of these block copolymers were covalently stabilized by the photo-radical-induced cross-linking of PI chains, resulting in the formation of a rubbery hydrophobic domain.

Chapter 4 reports the synthesis of block copolymers (BCPs) by incorporating a branched polyethylene glycol (PEG) hydrophilic block and randomly copolymerized styrene and isoprene units (p(St-*co*-Ip)) of different molecular weights, which functioned as the hydrophobic component. The morphological transitions of self-assembled BCP structures are dependent on changes in the chain length of the hydrophobic block. This is determined by the regiospecificity of the isoprene units. The self-assembled structures were covalently stabilized via intermolecular cyclization between the hydrophobic blocks. Notably, the cross-linked structures displayed a reversible swelling/deswelling ability dependent on solvent medium.

In Chapter 5, it was revealed that block copolymers (BCPs) comprised hydrophilic polyethylene glycol (PEG) blocks and discrete poly(phenyllactic acid) (dPPLA) blocks with hydrazone-based photoswitches in specific positions. To observe the effect of light-induced configurational switching of photoswitches, they were embedded in two different positions within the BCP chains, namely: (1) at the middle of the hydrophobic PPLA chains and (2) at the junction of the amphiphilic chains. The nanostructures were constructed via solution self-assembly of BCPs and irradiated (wavelength = 405 nm) to induce *E/Z* isomerization of the hydrazone-based photoswitches. We found that the configurational switching of this system contributes to reducing the hydrodynamic volume of the hydrophobic chains, thereby leading to shape transformations of the self-assembled nanoparticles.

Excerpts from the following chapters have already been published:

Chapter 2: Kim, J.; Jeong, S.; Shin, K.; Kim, K. T. Cross-linked Polymersomes with Reversible Deformability and Oxygen Transportability. *Biomacromolecules* **2019**, *20*, 2430–2439.

Chapter 3: Kim, J.; Yoon, M.; Jin, S-M.; Lee, J.; La, Y.; Lee, E.; Kim, K. T. Polymer Cubosomes of Block Copolymers Having Cross-linkable Soft Hydrophobic Blocks. *Polym. Chem.* **2019**, *20*, 3778–3785.

Chapter 4: Kim, J.; Wang, V.; Kim, K. T. Block Copolymers Composed of Main-Chain Cyclic Polymers: Morphology Transition and Covalent Stabilization of Self-assembled Nanostructures via Intra- and Inter-chain cyclization of Styrene-*co*-Isoprene Blocks. *Macromolecules* **2020**, *53,* 10725–10733.

1.5 References

1. van Hest, J. C. M.; Delnoye, D. A. P.; Baars, M. H. P.; van Genderen, M. H. P. Meijer, E. W. Polystyrene-Dendrimer Amphiphilic Block Copolymers with a Generation-Dependent Aggregation. *Science* **1995**, *268*, 1592−1595.
2. Zhang, L.; Eisenberg, A. Multiple Morphologies of "Crew-Cut" Aggregates of Polystyrene-*b*-poly(acrylic acid) Block Copolymers. *Science* **1995,** *268*, 1728−1731.
3. Kim, K. T.; Meeuwissen, S. A.; Nolte, R. J. M.; van Hest, J. C. M. Smart nanocontainers and nanoreactors. *Nanoscale* **2010,** *2,* 844−858.
4. Renggli, K.; Baumann, P.; Langowska, K.; Onaca, O.; Bruns, N.; Meier, W. Selective and Responsive Nanoreactors. *Adv. Funct. Mater.* **2011,** *21,* 1241−1259.
5. Brinkhuis, R. P.; Rutjes, F. P. J. T.; van Hest, J. C. M. Polymeric vesicles in biomedical applications. *Polym. Chem.* **2011,** *2,* 1449−1462.
6. Massignani, M.; Lopresti, C.; Blanazs, A.; Madsen, J.; Armes, S. P.; Lewis, A. L.; Battaglia, G. Controlling Cellular Uptake by Surface Chemistry, Size, and Surface Topology at the Nanoscale. *Small* **2009,** *5,* 2424−2432.
7. Onaca, O; Enea, R.; Hughes, D. W.; Meier, W. Stimuli-Responsive Polymersomes as Nanocarriers for Drug and Gene Delivery. *Macromol. Biosci.* **2009**, *9*, 129−139.
8. Zhang, L. Yu, K.; Eisenberg, A. Ion-Induced Morphological Changes in "Crew-Cut" Aggregates of Amphiphilic Block Copolymers. *Science* **1996,** *272,* 1777−1779.
9. Zhang, L.; Eisenberg, A. Multiple morphologies of "crew-cut" aggregates of polystyrene-b-poly(acrylic acid) block copolymers. *J. Am. Chem. Soc.* **1996,** *118,* 3168−3181.

10. Mai, Y.; Eisenberg, A. Self-assembly of block copolymers *Chem. Soc. Rev.* **2012,** *41,* 5969−5985.
11. Israelachvili, J. N.; Mitchell, J.; Ninham, B. W. Theory of self-assembly of hydrocarbon amphiphiles into micelles and bilayers. *J. Chem. Soc., Faraday Trans. 2* **1976,** *72,* 1525−1568.
12. He, X.; Liang, H.; Huang, L.; Pan, C. Complex Microstructures of Amphiphilic Diblock Copolymer in Dilute Solution. *J. Phys. Chem. B* **2004**, *108*, 1731−1735.
13. Cho, A.; La, Y.; Jeong, M. G.; Moon, H. R.; Ryu, J. H.; Shin, T. J.; Kim, K. T. Mix-and-Match Assembly of Block Copolymer Blends in Solution. *Macromolecules* **2017**, *50*, 3234−3243.
14. Kim, J.; Yoon, M.; Jin, S-M.; Lee, E.; Kim, K. T. Polymer Cubosomes of Block Copolymers Having Cross-linkable Soft Hydrophobic Blocks. *Polym. Chem.* **2019,** *10,* 3778−3785.
15. La, Y.; Park, C.; Shin, T. J.; Joo, S. H.; Kang, S.; Kim, K. T. Mesoporous monoliths of inverse bicontinuous cubic phases of block copolymer bilayers. *Nat. Chem.* **2014,** *6,* 534−541.
16. Cho, A.; La, Y.; Shin, T. J.; Park, C.; Kim, K. T. Structural Requirements of Block Copolymers for Self-Assembly into Inverse Bicontinuous Cubic Mesophases in Solution. *Macromolecules* **2016,** *49,* 4510−4519.
17. La, Y.; An, T. H.; Shin, T. J.; Park, C.; Lee, E.; Kim, K. T. A Morphological Transition of Inverse Mesophases of a Branched-Linear Block Copolymer Guided by Using Cosolvents. *Angew. Chem. Int. Ed.* **2015,** *54,* 10483−10487.
18. Rodríguez-Hernández, J.; Lecommandoux, S. Reversible inside-out micellization of pH-responsive and water-soluble vesicles based on polypeptide diblock copolymers. *J. Am. Chem. Soc.* **2005**, *127*, 2026−2027.
19. Lovett, J. R.; Warren, J. W.; Ratcliffe, L. P. D.; Kocik, M. K.; Armes, S.

P. pH-Responsive Non-Ionic Diblock Copolymers: Ionization of Carboxylic Acid End-Groups Induces an Order-Order Morphological Transition. *Angew. Chem. Int. Ed.* **2015**, *54*, 1279−1283.

20. Moughton, A. O.; O'Reilly, R. K. Thermally induced micelle to vesicle morphology transition for a charged chain end diblock copolymer. *Chem. Commun.* **2010**, *46,* 1091−1093.
21. Machado, C. A.; Tran, R.; Jenkins, T. A.; Pritzlaff, A. M.; Sims, M. B.; Sumerlin, B. S.; Savin, D. A. UV-induced vesicle to micelle transition: a mechanistic study. *Polym. Chem.* **2019,** *10,* 6037−6046.
22. Jeong, M. G.; Kim, J.; Kwon, J. H.; Kim, K. T. Morphological transition of nanostructure of self-assembled block copolymers by stimuli-induced conformational changes in the hydrophilic block. *J. Polym. Sci.* **2020,** *58,* 1153−1162.
23. Kim, J.; Wang, V.; Kim, K. T. Block Copolymers Composed of Main-Chain Cyclic Polymers: Morphology Transition and Covalent Stabilization of Self-Assembled Nanostructures via Intra- and Interchain Cyclization of Styrene-*co*-isoprene Blocks. *Macromolecules* **2020,** doi.org/10.1021/acs.macromol.0c02020.
24. Che, H.; Cao, S.; van Hest, J. C. M. Feedback-induced temporal control of "breathing" polymersomes to create self-adaptive nanoreactors. *J. Am. Chem. Soc.* **2018,** *140*, 5356–5359.
25. Che, H.; van Hest, J. C. M. Stimuli-responsive polymersomes and nanoreactors. *J. Mater. Chem. B* **2016,** *4,* 4632–4647
26. Feng, A.; Yuan, J. Smart nanocontainers: progress on novel stimuli-responsive polymer vesicles. *Macromol. Rapid Commun.* **2014,** *35*, 767–779.
27. Grafe, D.; Gaitzsch, J.; Appelhans, D.; Voit, B. Cross-linked polymersomes as nanoreactors for controlled and stabilized single and cascade enzymatic reactions. *Nanoscale* **2014,** *6*, 10752–10761.

28. Louzao, I.; van Hest, J. C. M. Permeability effects on the efficiency of antioxidant nanoreactors. *Biomacromolecules* **2014,** *14*, 2364–2372.
29. Peters, R. J. R. W. Marguet, M.; Marais, S.; Fraaije, M. W.; van Hest, J. C. M.; Lecommandoux, S. Cascade reactions in multicompartmentalized polymersomes. *Angew. Chemie. In. Ed*. **2014,** *53*, 146–150.
30. Marguet, M.; Bonduelle, C.; Lecommandoux, S. Multicompartmentalized polymeric systems: towards biomimetic cellular structure and function. *Chem. Soc. Rev.* **2013,** *42*, 512–529.
31. Discher, D. E.; Discher, B. M.; Bermudez, H.; Hammer, D. A.; Won, Y. Y.; Bates, F. S. Cross-linked polymersome membranes: vesicles with broadly adjustable properties. *J. Phys. Chem. B* **2002,** *106*, 2848–2854.
32. Won, Y. Y.; Davis, H. T.; Bates, F. S. Giant wormlike rubber micelles. *Science* **1999,** *283*, 960–963.
33. Kim, J.; Jeong, S.; Shin, K.; Kim, K. T. Cross-linked Polymersomes with Reversible Deformability and Oxygen Transportability. *Biomacromolecules* **2019**, *20*, 2430–2439.
34. Lai, M. H.; Lee, S.; Smith, C. E.; Kim, K.; Kong, H. Tailoring polymersome bilayer permeability improves enhanced permeability and retention effect for bioimaging. *ACS Appl. Mater. Interfaces* **2014,** *6*, 10821–10829.
35. Chambon, P.; Blanazs, A.; Battaglia, G.; Armest, S. P. How does cross-linking affect the stability of block copolymer vesicles in the presence of surfactant? *Langmuir* **2012,** *28*, 1196–1205.
36. Varlas, S.; Foster, J. C.; Georgiou, P. G.; Keogh, R.; Husband, J. T.; Williams, D. S.; O'Reilly, R. K. Tuning the membrane permeability of polymersome nanoreactors developed by aqueous emulsion

polymerization-induced self-assembly. *Nanoscale* **2019,** *11*, 12643–12654.

37. Jeong, M. G.; Kim, K. T. Covalent Stabilization of Inverse Bicontinuous Cubic Structures of Block Copolymer Bilayers by Photodimerization of Indene Pendant Groups of Polystyrene hydrophobic Blocks. *Macromolecules* **2017,** *50,* 223−234
38. Kanai, T.; Yamamoto, S.; Sawada, T. Swelling of Gel-Immobilized Colloidal Photonic Crystals in Ionic Liquids. *Macromolecules* **2011,** *44,* 5865−5867.
39. Smith, L. C.; Lind, J. U.; Nielsen, C. H.; Christiansen, M. B.; Buss, T.; Larsen, N. B.; Kristensen, A. Enhanced transduction of photonic crystal dye lasers for gas sensing via swelling polymer film. **2012,** *36,* 1392−1394.
40. Zhang, Y.; Fu, Q.; Ge, J. Photonic sensing of organic solvents through geometric study of dynamic reflection spectrum. *Nat. Commun.* **2015,** *6,* 7510−7516.
41. Lencki, R. W.; Williams, S. Effect of nonaqueous solvents on the flux behavior of ultrafiltration membranes. *J. Memb. Sci.* **1995,** *101,* 43−51.
42. Liu, X.; Yaszemski, M. J.; Lu, L. Expansile crosslinked polymersomes for pH sensitive delivery of doxorubicin. *Biomater. Sci.* **2006,** *4,* 245–249.
43. Mai, B. T.; Barthel, M.; Marotta, R.; Pellegrino, T. Crosslinked pH-responsive polymersome via Diels-Alder click chemistry: a reversible pH-dependent vesicular nanosystem. *Polymer* **2009,** *165,* 19–27.
44. Deng, Z.; Qian, Y.; Yu, Y.; Liu, G.; Hu, J.; Zhang, G.; Liu, S. Engineering intracellular delivery nanocarriers and nanoreactors from oxidation-responsive polymersomes via synchronized bilayer cross-linking and permeabilizing inside live cells. *J. Am. Chem. Soc.* **2016,** *138,* 10452–10466.
45. Xu, H.; Meng, F.; Zhong, Z. Reversibly crosslinked temperature-

responsive nano-sized polymersomes: synthesis and triggered drug release. *J. Mater. Chem.* **2019,** *19,* 4183–4190.

46. Kim, B. S.; Chuanoi, S.; Suma, T.; Anraku, Y.; Hayashi, K.; Naito, M.; Kim, H. J.; Kwon, I. C.; Miyata, K.; Kishimura, A.; Kataoka, K. Self-assembly of siRNA/PEG-b-catiomer at integer molar ratio into 100 nm-sized vesicular polyion complexes (siRNAsomes) for RNAi and codelivery of cargo macromolecules. *J. Am. Chem. Soc.* **2019,** *141,* 3699–3709.
47. Sun, H.; Meng, F.; Cheng, R.; Deng, C.; Zhong, Z. Reduction and pH dual-bioresponsive crosslinked polymersomes for efficient intracellular delivery of proteins and potent induction of cancer cell apoptosis. *Acta. Biomater.* **2014,** *10,* 2159–2168.
48. Ke, W.; Li, J.; Mohammed, F.; Wang, Y.; Tou, K.; Liu, X.; Wen, P.; Kinoh, H.; Anraku, Y.; Chen, H.; Kataoka, K.; Ge, Z. Therapeutic polymersome nanoreactors with tumor-specific activable cascade reactions for cooperative cancer therapy. *ACS Nano* **2019,** *13,* 2357–2369.
49. Gaitzsch, J.; Appelhans, D.; Grafe, D.; Schwille, P.; Voit, B. Photo-crosslinked and pH sensitive polymersomes for triggering the loading and release of cargo. *Chem. Commun.* **2011,** *47,* 3466–3468.
50. Gaitzsch, J.; Appelhans, D.; Wang, L.; Battaglia, G.; Voit, B. Synthetic bio-nanoreactor: mechanical and chemical control of polymersome membrane permeability. *Angew. Chem. Int. Ed.* **2012,** *51,* 4448–4451.
51. Gaitzsch, J.; Appelhans, D.; Janke, A.; Strempel, M.; Schwille, P.; Voit, B. Cross-linked and pH sensitive supported polymer bilayers from polymersomes – studies concerning thickness, rigidity and fluidity. *Soft Matter* **2014,** *10,* 75–82.
52. Yassin, M. A.; Appelhans, D.; Wiedemuth, R.; Formanek, P.; Boye, S.; Lederer, A.; Temme, A.; Voit, B. Overcoming concealment effects of targeting moieties in the PEG Corona: controlled permeable

polymersomes decorated with Folate-antennae for selective targeting of tumor cells. *Small* **2015,** *11,* 1580–1591.

53. Iyisan, B.; Kluge, Jr.; Formanek, P.; Voit, B.; Appelhans, D. Multifunctional and dual-responsive polymersomes as robust nanocontainers: design, formation by sequential post-conjugations, and pH-controlled drug release. *Chem. Mater.* **2016,** *28,* 1513–1525.
54. Iyisan, B.; Siedel, A. C.; Gumz, H. Yassin, M.; Kluge, J.; Gaitzsch, J.; Formanek, P.; Moreno, S.; Voit, B.; Appelhans, D. Dynamic docking and undocking processes addressing selectively the outside and inside of polymersomes. *Macro. Rapid Commun.* **2017,** *38,* 1700486.
55. Duan, W.; Ji, S.; Guan, Y.; Mu, X.; Fang, S.; Lu, Y.; Zhou, X.; Sun, J.; Li, Z. Esterase-Responsive Polypeptide Vesicles as Fast-Response and Sustained-Release Nanocompartments for Fibroblast-Exempt Drug Delivery. Biomacromolecules **2020,** *21,* 5093–5103.

Chapter 2. Cross-linked Polymersomes with Reversible Deformability and Oxygen Transportability

2.1 Abstract

Polymersomes are of interest as nanocarriers due to their physical and chemical robustness, which arises from the macromolecular nature of their block copolymer components. However, the physical robustness of polymersomes impairs transmembrane diffusion and responsiveness to mechanical forces. Polymer nanocarriers that can reversibly deform under stress while maintaining structural integrity and transmembrane diffusivity are desired for development of gas transport vehicles. Here, we report polymersomes composed of amphiphilic block copolymers containing polydimethylsiloxane with side-chain pendant vinyl groups. A reversibly deformable polymersome compartmentalizing membrane was obtained by cross-linkage of PEG-*b*-poly(dimethyl-*r*-methylvinyl)silane in a self-assembled bilayer via photo-radical generation in aqueous media. The covalently cross-linked polymersomes exhibited superior physical robustness compared to unlinked polymersomes while maintaining deformability under stress. Transmembrane oxygen diffusion was confirmed when lumen-encapsulated Zn-porphyrin generated singlet O_2 under irradiation, and the anthracene-9,10-dipropionic acid O_2 quencher was consumed. Polymersome-encapsulated hemoglobin bound oxygen reversibly, indicating the polymersomes could be used as O_2 carriers that reversibly deform without sacrificing structural integrity or oxygen transportability.

2.2 Introduction

Nature compartmentalizes enzymes and protein machinery within cells and cellular organelles to enable relayed chemical reactions in a sequential manner for signal transduction and biochemical transformations. The strategy of sequestering functional components within protective shells in a spatially resolved fashion has been adopted to develop smart delivery vehicles, nanoreactors, and cellular mimics.[1–3] For these applications, polymer micro- and nanocapsules have been studied intensively as material and molecular cargo containers. Nanocontainers capable of communicating with the surrounding environment via molecular transport through their compartmentalizing membranes are highly desired.[4–13] For example, semi-permeable membranes composed of polyion complexes have been used successfully to create micro- and nanocapsules with innate polymer membrane micropores that allow diffusion.[14–15] Self-assembly of block copolymers (BCPs) in solution is an essential means by which to create polymeric nano- and microcontainers of various sizes and shapes.[16–19] The physical properties and chemical functions of the resulting containers can be tailored during the design and synthesis of their BCP components. Polymersomes that resemble cells and cellular organelles have attracted special attention as synthetic compartments. Limited transport of small molecules through polymersome vesicular membranes can be overcome by reconstitution of channel proteins, sacrificial porogens, and stimuli-responsive polymers in the membranes.[20–25] Polymersomes that are permeable to guest molecules can compartmentalize macromolecules, such as enzymes, within their inner lumina while allowing free diffusion of small molecules through their membranes.

Controlling polymersome responses to external forces without compromising their structural integrity and transmembrane diffusivity

remains a challenge. Red blood cells (RBCs) are oxygen-carrying cells that are abundant in blood. Discoidal RBCs exhibit remarkable deformability under mechanical stress, which enables their passage though capillaries with smaller diameters without loss of structural integrity.[26–28] In order to achieve the low elastic modulus exhibited by RBCs, the polymersome bilayer membranes should be composed of hydrophobic block copolymers with low glass-transition temperatures (T_g). However, the structural integrity of these polymersomes could be lost if they are subjected to extreme dilution or strong sheer forces, which may lead to disintegration or fission of the polymersomes. Cross-linking of the hydrophobic polymer blocks within the bilayer membrane would lend mechanical stability to the polymersomes, but the diffusivity of small molecules through the cross-linked membrane might be compromised.[29-34]

Here, we report the formation of highly deformable and mechanically robust polymersomes that can transport oxygen. The polymersomes are composed of amphiphilic BCPs containing polydimethylsiloxane (PDMS) groups and vinyl pendants along their polymer chains (Figure 2-1). Self-assembly of the BCPs leads to formation of polymersomes with bilayer membranes that are made fluidic by the low T_g of the PDMS block, and cross-linking occurs through photo-radical coupling of the vinyl groups. The obtained polymersomes exhibited excellent mechanical stability, which was confirmed with measurements of the elastic moduli of the membranes by micropipette aspiration. Multiple extrusions of the polymersomes through a porous membrane filter did not change their diameters, demonstrating the deformability of the cross-linked polymersomes. The gas permeability of the polymersomes was evaluated by encapsulation of zinc tetraphenylporphyrin (ZnTPP) within their inner compartments. Photosensitized conversion of triplet oxygen to singlet oxygen by the encapsulated ZnTPP resulted in formation of the endoperoxide of anthracene dipropionic acid (ADPA)

outside the cross-linked polymersomes, suggesting the facile diffusion of oxygen molecules through the cross-linked membranes.[35, 50] In addition, hemoglobin-encapsulating polymersome (HEP) was prepared by direct hydration of BCP thin films. The reversible binding of oxygen to HEP was confirmed by repeated exposure of the cross-linked polymersomes to oxygen and nitrogen. Our results suggest that deformable cross-linked polymersomes with encapsulated oxygen-binding proteins have potential for use as oxygen-transporting vehicles with mechanical responses that resemble those exhibited by RBCs.

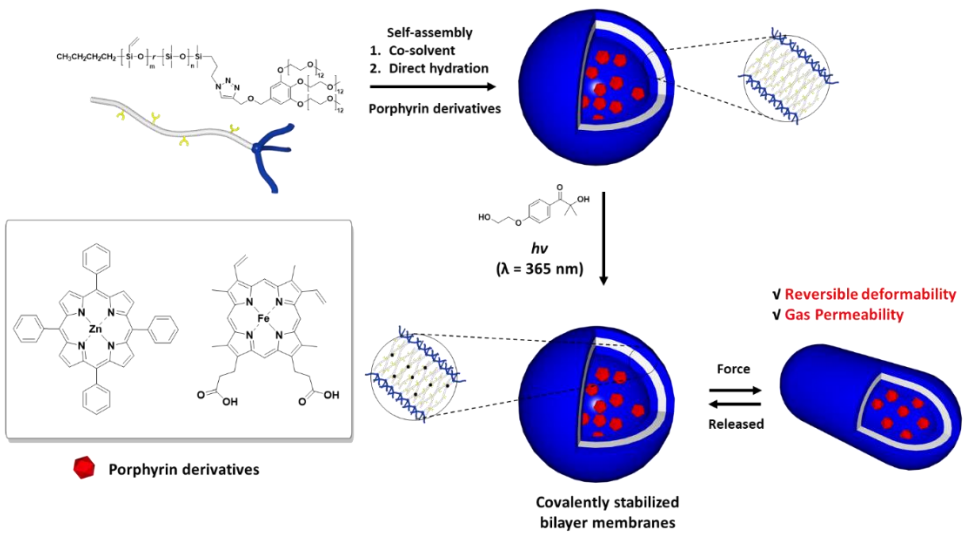

Figure 2-1. Schematic representation of the self-assembly of branched-linear block copolymers in solution and cross-linking of the poly(dimethyl-*r*-methylvinyl)silane (PDMVS) compartments by photo-generated radical coupling.

2.3 Experimental Section

Materials. Unless otherwise noted, all reagents and chemicals were purchased from Sigma Aldrich, Alfa Aesar, and TCI and used as received.

Hexamethylcyclotrisiloxane monomer was purified by sublimation apparatus before use. 1,3,5-trivinyl-1,3,5-trimethylcyclosiloxane was purchased from Gelest. Tetrahydrofuran (THF) was refluxed over a mixture of Na and benzophenone under N_2 and distilled before use. All reactions were performed under N_2 unless otherwise noted.

Methods. ^{1}H and ^{13}C NMR spectra were recorded on a Agilent 500-MR DD2 spectrometer, using $CDCl_3$ as a solvent. Molecular weights of block copolymers were measured by Agilent 1260 Infinity GPC system equipped with a PL gel 5 μm mixed D column (Agilent Technologies) and differential refractive index detectors. THF was used as an eluent with a flow rate of 1 mL min^{-1} at 30 °C and the analytical sample was filtered by using PTFE filter before injection. A PS standard (Agilent Technologies) was used for calibration. Transmission electron microscopy (TEM) was performed on a Hitachi 7600 operating at 100 kV and a JEOL JEM-2100 operating at 200 kV. Specimens were prepared by placing a drop of the solution on a carbon-coated Cu grid (200 mesh, EM Science). After 30 min, the remaining solution on a grid was removed with a filter paper, and the grid was dried overnight. The morphologies of polymer nanostructures were measured by analyzing TEM images with Image^{J} software. Dynamic light scattering (DLS) was performed at a Malvern Zetasizer Nano-S. UV light source was Uvitec Cambridge LF-215.LM (365 nm/312 nm, 15 W). The multi-extruder (LiposoFast-Basic) was purchased from AVESTIN, Inc. and it consists of a stainless steel housing, membrane support, two 1.0 mL syringes, and 50 polycarbonate membranes with 200 nm pore diameter. Differential scanning calorimetry (DSC) was carried out under N_2 gas at a scan rate of 10 ^{o}C min^{-1} with a TA Instruments Q10. UV-vis spectrometry (UV-via) was measured on a Jasco V-630 spectrophotometer. Optical and fluorescence microscopy images of giant sized polymersomes in which nile red (Sigma Aldrich, λ_{ex} = 515-560 nm, λ_{em} > 590 nm) was embedded on the hydrophobic membranes were obtained

using Zeiss LSM710 Confocal microscope and Nikon Eclipse TE2000-U. 5 - 10 μL of concentration of fluorescently labeled polymersomes was placed on confocal dish. Glass micropipette for aspiration was purchased from Hilgenberg (made of borosilicate glass, tip bent 35 °, diameter = 5 μm). Cryogenic transmission electron microscopy (cryo-TEM) images were taken from Talos L120C operating at 120 kV. The cryo-TEM experiments performed with a thin film of aqueous sample solution (5 μL) transferred to a quantifoil supported grid (copper, 200 mesh, EM science) by the plunge-dipping method. The thin aqueous films were prepared at ambient temperature and with a humidity of 97-99% within custom-built environmental chamber in order to prevent water evaporation from the sample solution. The excess liquid was blotted with filter paper for 1-2 s, and the thin aqueous films were rapidly vitrified by plunging them into liquid ethane (cooled by liquid N_2) at its freezing point.

Synthesis of *ω*-chloro-PDMVS. Under nitrogen atmosphere, 1.6 M *n*-Butyllithium (100 μL, 0.160 mmol) was added in one portion to a solution of hexamethylcyclotrisiloxane (1.73 g, 7.80 mmol) and 1,3,5-trivinyl-1,3,5-trimethylcyclosiloxane (420 μL, 1.56 mmol) in dry THF (30 mL) at 0 °C. The mixture was stirred overnight to warm slowly to room temperature and then quenched with a 5-fold excess of 3-chloropropyldimethyl -chlorosilane. The solution was precipitated into a vigorously stirring mixture of methanol (50 mL) and triethylamine (2 mL) and centrifuged to isolate the crude polymer. The product was precipitated twice more in methanol (2 x 50 mL) and dried in vacuo to afford *ω*-chloro-PDMVS as a colorless viscous liquid. Yield: 2.01 g, 92 %. ^{1}H NMR (500 MHz, $CDCl_3$) 6.01 – 5.72(m, -$CHCH_2$), 3.52(t, 2H), 1.81(m, 2H), 1.32(m, 4H), 0.89(t, 3H), 0.65(m, 2H), 0.64 – 0.53(m, 2H) ppm.

Synthesis of *ω*-azido-PDMVS. To a solution of ω-chloro-PDMVS (2.00 g, 0.20 mmol) in THF (50 mL) was added sodium azide (0.130 mg, 2.00 mmol)

and tetrabutylammonium bromide (0.645 mg, 2.00 mmol). The resulting suspension was refluxed at 80 ºC for 36 h. Thre reaction mixture was precipitated three times in MeOH (3 x 30 mL). The remains were re-dispersed between hexane and H_2O and the organic phase was washed with another portion of H_2O and brine. The resulting solution was dried over anhydrous $MgSO_4$, filtered, and concentrated in vacuo to afford the pure polymer as a colorless viscous liquid. Yield: 1.62 g, 80 %. ^{1}H NMR (500 MHz, $CDCl_3$) 6.01 – 5.72(m, -$CHCH_2$), 3.24(t, 2H), 1.64(m, 2H), 1.32(m, 4H), 0.89(t, 3H), 0.57(m, 2H), 0.64 – 0.53(m, 2H) ppm.

Synthesis of PEG550$_3$-*b*-PDMVS. CuBr (40 mg) was dried in vacuum for 15 min. *N,N,N′,N″,N″*-pentamethyldiethylenetriamine (PMDETA) (80 mg) mixed with THF (1.5 mL) was added and the mixture was stirred in N_2 for 15 min. To this solution, a solution of PEG550$_3$-propargyl ether (0.06 g, 0.033 mmol) and ω-azido-PDMVS (0.85 g, 0.131 mmol) in THF(3 mL) was added. The mixture was degassed by bubbling N_2 for 15 min. After degassing, the click reaction was proceeded at 40 °C until completion. The reaction was quenched by dilution with dichloromethane and filtered through a pack of silica with $CHCl_3$ to remove the excess ω-azido-PDMVS. To collect the click product, a mixed eluent (dichloromethane : methanol = 90:10 v/v) was used. The filtered solution was concentrated on a rotary evaporator to afford a pure block copolymer as pale yellow viscous liquid. The resulting block copolymers were purified by flash column chromatography and preparative size-exclusion chromatography (prep-SEC), resulting in the branched-linear BCPs with narrow molecular weight distribution.

2.4 Results and Discussion

Modular Synthesis of Cross-linkable Block Copolymers

Poly(dimethylsiloxane)s containing randomly distributed pendant vinyl groups were synthesized by anionic ring-opening copolymerization of hexamethylcyclotrisiloxane (D_3) and 1,3,5-trivinyl-1,3,5-trimethylcyclotrisiloxane (V_3) using *n*-butyllithium as an initiator (Scheme 2-1). After complete consumption of the monomers over 1 h, the polymerization reaction was quenched with 1-chloropropyldimethylchlorosilane to afford a chloromethyl group at each chain end. The polymers were purified by precipitation in cold methanol and subsequently reacted with NaN_3 in tetrahydrofuran (THF) in the presence of tetrabutylammonium bromide (TBAB).[37] The resulting poly(dimethyl-*r*-methylvinyl)silanes with azide end groups (PDMVS-N_3) were analyzed by gel-permeation chromatography (GPC) and exhibited well-defined molecular weights and molecular weight distributions. ^{1}H NMR analysis of PDMVS-N_3 indicated the molar fraction of polymers with vinyl-containing repeating units was ~17%, which was consistent with the feed ratio of the two monomers (D_3:V_3 = 5:1 mol/mol). For the modular construction of BCPs, we employed a branched polyethylene glycol (PEG) unit as the hydrophilic module. When a branched hydrophilic block is combined with a hydrophobic block to form a BCP, the larger size of the branched hydrophilic block sterically hinders chain stretching in the hydrophobic polymer block during self-assembly. We anticipated this property in the branched PEG blocks would facilitate self-assembly to form bilayer structures (i.e. polymersomes).

Four BCPs (PEG550$_3$-*b*-PDMVS) were synthesized by the Cu(I)-catalyzed click reaction between the hydrophilic module and PDMVS-N_3 (Scheme 2-1). The block copolymers were made using a range of block ratios, which were defined by the molecular weight fractions of the PEG domain,

f_{PEG}. The click reaction was monitored by GPC, and the appearance of a peak corresponding to the higher molecular weight BCP (Figure 2-2A) signaled completion. Each block copolymer was purified by flash column chromatography and preparative size-exclusion chromatography (prep-SEC) to yield a branched-linear BCP with a narrow molecular weight distribution (Table 2-1). The successful synthesis of the BCPs by the click reaction of the structural modules was confirmed by ^{1}H NMR (Figure 2-2B).

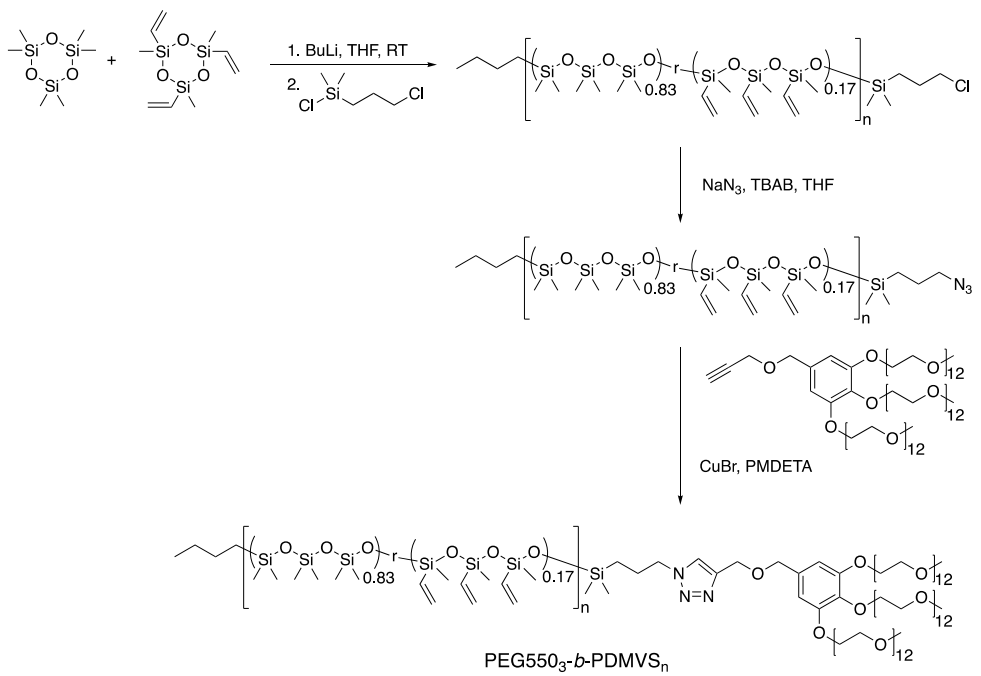

Scheme 2-1. Synthesis of hydrophobic modules and block copolymers by azide-alkyne 1,3-dipolar cycloaddition.

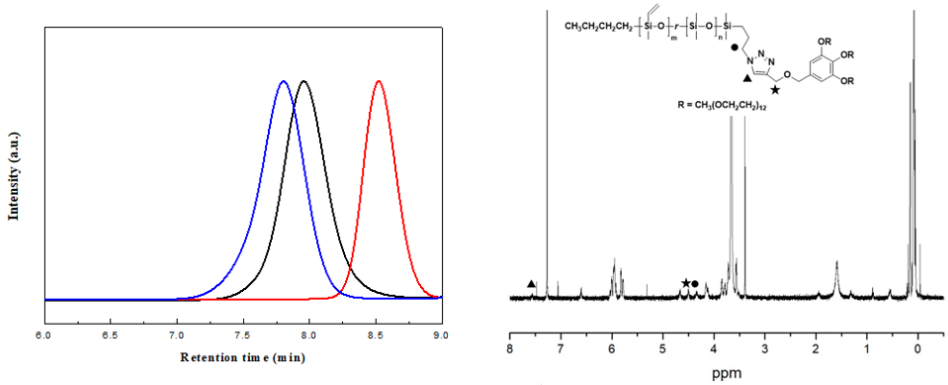

Figure 2-2. GPC analysis (A) and ^{1}H NMR spectrum (B) of PDMVS-*b*-PEG550$_3$.

Table 2-1. Characterization of block copolymers (BCPs)

Entry	BCPs	M_n (g/mol)[a]	$Đ$ [a]	DP_n(MVS)[b]	DP_n(DMS)[b]	f_{PEG} (%)[c]
1	PEG550$_3$-*b*-P(DM$_{63}$-*r*-MV$_{12}$)S	10200	1.10	12	63	28.9
2	PEG550$_3$-*b*-P(DM$_{120}$-*r*-MV$_{21}$)S	14700	1.11	20	120	15.5
3	PEG550$_3$-*b*-P(DM$_{166}$-*r*-MV$_{33}$)S	20000	1.10	33	166	10.9
4	PEG550$_3$-*b*-P(DM$_{244}$-*r*-MV$_{45}$)S	25800	1.12	45	244	7.5

[a]Number average molecular weight (M_n) and molecular weight distribution (D) determined by GPC using polystyrene (PS) standards. Elution was performed with THF at a flow rate of 1 mL/min at 30 ℃. [b]DP_n determined by ^{1}H NMR integration. [c]Molecular weight fraction of the PEG domain relative to the PMVS and PDMS blocks (1650 g/mol for PEG550$_3$).

Self-Assembly of BCPs and Photocross-linking of Self-Assembled Structures in Solution

The BCPs were comprised of identical hydrophilic blocks and a series of PDMVS blocks with different molecular weights (MWs). Hence, each BCP had a unique PEG molecular weight fraction (f_{PEG}). The BCPs self-assembled into nanostructures via a co-solvent method. Dioxane was

employed as the common solvent for both polymer blocks, and water served as the selective solvent. Due to the low T_g of the core-forming PDMVS block, the self-assembled structures could only be observed by cryogenic transmission electron microscopy (cryo-TEM). Cryo-TEM images of the self-assembled structures (Figure 2-3) revealed that PEG550$_3$-PDMVS20K self-assembled into polymersomes, while PEG550$_3$-PDMVS10K and 15K formed spherical and cylindrical micelles. Among them, PEG550$_3$-PDMVS26K containing the hydrophobic block with the highest MW formed hexosomes, or nanoparticles composed of the inverse-hexagonal phase. The observed morphologies of the self-assembled structures indicated that BCPs with low f_{PEG} values were guided to form bilayer-based structures, such as polymersomes and inverse-hexagonal phases.

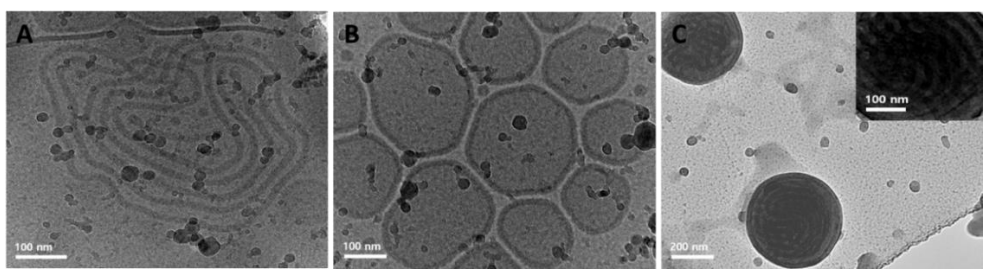

Figure 2-3. Uncross-linked morphological transition upon reduction of the chain length of PDMVS. Cryo-EM images of (A) cylindrical micelles (PEG550$_3$-PDMVS15K), (B) polymersomes (PEG550$_3$-PDMVS20K), and (C) hexagonal nanoparticles (PEG550$_3$-PDMVS 26K).

To impart structural robustness to the self-assembled BCP structures, we carried out covalent cross-linking of BCPs by free-radical coupling of the pendant vinyl groups tethered to their PDMS backbones. The photo-radical generator, 2-hydroxy-4'-(2-hydroxyethoxy)2-methylpropiophenone (Irgacure 2959, Sigma), was introduced to dispersions of the self-assembled BCP structures in water, followed by irradiation with UV light (λ = 365 nm, 8 W) for 5 h. After cross-linking, the dispersions were purified by size-

exclusion chromatography (SEC) on a Sephadex^{TM} G-100 column (GE Healthcare Life Sciences, Marlborough, MA).

The self-assembled BCP structures could then be analyzed by conventional TEM, because their physical robustness was increased by cross-linking. The TEM images of the self-assembled BCP structures shown in Figure 2-4A and 2-4B indicated that cross-linking of the hydrophobic PDMVS domains did not alter the morphology of the structures. In addition, all structures maintained their morphology upon exchange of the solvent from water to THF by dialysis. This indicated the covalent stabilization of the transient BCP assembled structures. Cross-linked polymersomes could also be observed with conventional TEM due to their enhanced physical stability.

The cross-linked polymersomes of PEG550$_3$-PDMVS20K retained their structures upon exchange of the medium from water to THF, indicating the compartmentalizing membrane of the polymersome was covalently stabilized by cross-linking of the PDMS domains in the bilayer membrane. The average diameter of the cross-linked polymersomes measured by dynamic light scattering (DLS) analysis increased from 505 nm in water to 742 nm in THF, suggesting swelling of the cross-linked PDMS domains in the polymersome bilayer membrane. Upon exchange of the medium from THF to water, the cross-linked PEG550$_3$-PDMVS20K polymersomes returned to their original diameter (Figure 2-5).

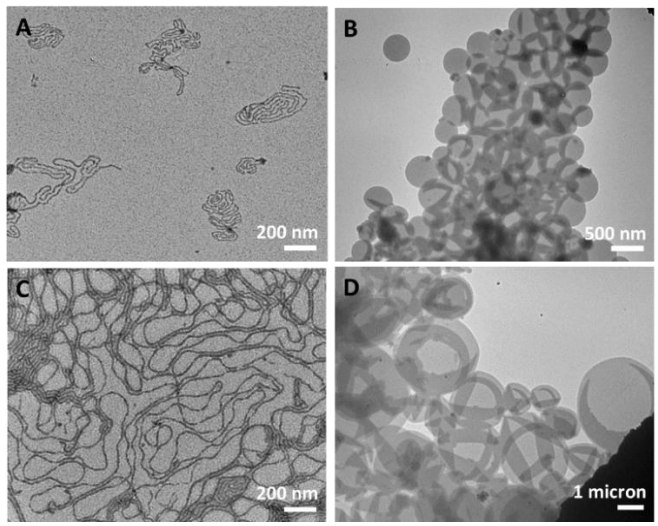

Figure 2-4. Cross-linked morphological transition upon reduction of the PDMVS chain length. TEM images of (A) cylindrical micelles of PEG550$_3$-PDMVS15K and (B) polymersomes of PEG550$_3$-PDMVS20K constructed by co-solvent self-assembly. (C) Cylindrical micelles of PEG550$_3$-PDMVS10K and (D) giant-sized polymersomes of PEG550$_3$-PDMVS15K formed by direct hydration.

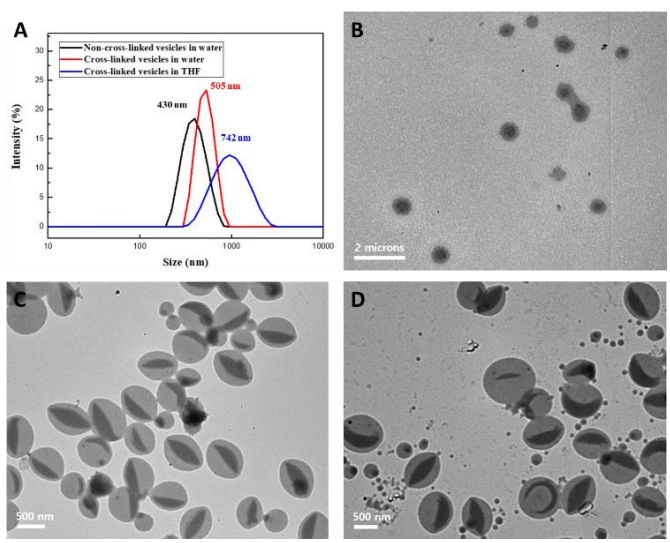

Figure 2-5. (A) Dynamic light scattering (DLS) size plots of the cross- and uncross-linked polymersomes of PEG550$_3$-PDMVS20K in aqueous and THF solutions. TEM images of (B) unlinked polymersomes in water, cross-linked polymersomes (C) in water, and (D) in THF.

The BCPs made with PDMS as the hydrophobic block could be dispersed by direct hydration of BCP thin films in water without requiring an organic solvent to mobilize the hydrophobic polymer blocks during self-assembly. The structures of the BCPs that self-assembled in water (Figure 2-4C and 2-4D) had morphologies similar to those observed in self-assembled structures formed by the co-solvent method. Interestingly, the cylindrical micelles of $PEG550_3$-PDMVS10K (Figure 2-4C) were significantly longer than the cylindrical micelles of $PEG550_3$-PDMVS15K formed by the co-solvent method (Figure 2-4A). Similarly, the direct hydration of $PEG550_3$-PDMVS15K generated giant polymersomes. These were imaged by confocal laser scanning microscopy (CLSM) following labeling of the hydrophobic bilayer membrane compartment with Nile red dye (3μm Nile red in 1.5 mL dioxane + 1 mL H_2O). The difference of observed morphology of self-assembled structures of $PEG550_3$-*b*-PDMVSs via different dispersion methods (co-solvent vs. direct hydration) was summarized in Table 2-2 in the supporting information.

Table 2-2. Difference of observed morphology of self-assembled structures

Entry	BCPs	Solution self-assembly	Direct hydration
1	$PEG550_3$-PDMVS10K	Spherical micelles	Cylindrical micelles
2	$PEG550_3$-PDMVS15K	Cylindrical micelles	Polymersomes
3	$PEG550_3$-PDMVS20K	Polymersomes	Nanoparticles
4	$PEG550_3$-PDMVS26K	Hexosomes	No dispersion

Reversible Deformation of Cross-linked Polymersomes

The compartmentalizing membranes of the polymersomes of PEG550$_3$-PDMVS20K were fluidic due to the low T_g of the PDMVS block, which was determined through application of shear force to the polymersomes. Unlinked polymersomes of PEG550$_3$-PDMVS20K were subjected to 10 extrusions through a 0.2 μm membrane filter, which reduced their diameter from 500 nm to 200 nm. In contrast, the diameter of the cross-linked polymersomes was not altered by the extrusion procedure. When the cross-linked polymersomes containing encapsulated rhodamine were subjected to multiple extrusions (10 times), no dye leakage was observed (Figure 2-6). These results confirmed the cross-linked polymersomes could be highly deformed by physical stress without losing their structural integrity. Polymersomes encapsulating rhodamine B stayed in water for an extended period without showing any change in their size and morphology (Figure 2-7).

To investigate changes in the physical properties of the polymersome bilayer membranes that resulted from cross-linking, we measured the elastic moduli of the polymersomes by micropipette aspiration. Giant polymersomes with diameters >10 μm were prepared by direct hydration of the PEG550$_3$-PDMVS15K thin films. Pressure was applied to draw the membranes into the capillary, which reduced the diameter of the polymersomes. By measuring the surface area of each polymersome, the elastic modulus of the membrane (K_a) was determined by $\sigma = K_a\alpha$ (equation 1). Here, σ represents the membrane tension. The area strain, α, is determined by A/A_0, where A_0 is the initial membrane area and A is the change in area due to application of pressure.[39,40]

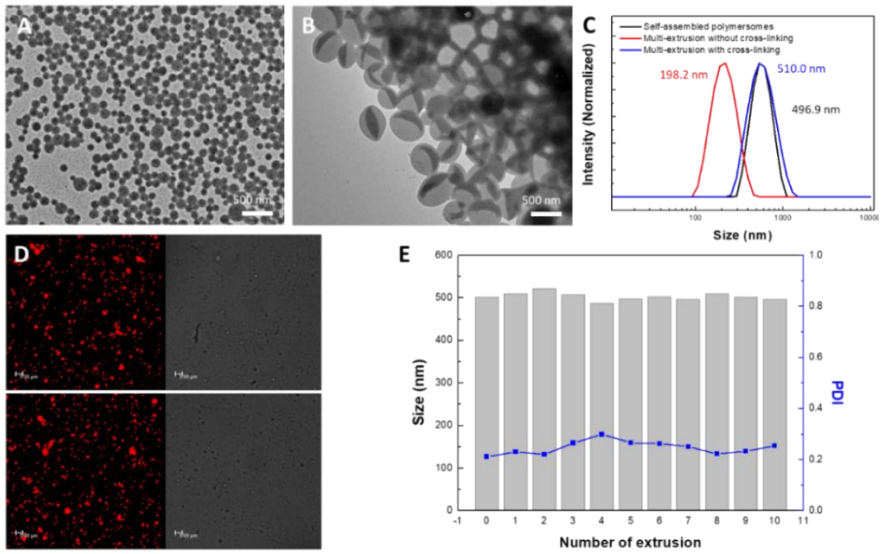

Figure 2-6. Results of multi-extrusion experiments of polymersomes of $PEG550_3$-*b*-PDMVS20K with 0.2 µm porous polycarbonate membrane filters. TEM images of polymersomes prepared by the following processes: (A) multi-extrusion (10 times) followed by cross-linking, (B) cross-linking followed by multi-extrusion (10 times). (C) DLS size plots of the cross-linked (blue) and uncross-linked (red) polymersomes in aqueous solution after multiple extrusions. (D) CLSM images of cross-linked vesicles containing rhodamine B before extrusion (top) and after extrusion (bottom) (Scale bars = 5 µm). (E) Change of polymersome size with multiple extrusions.

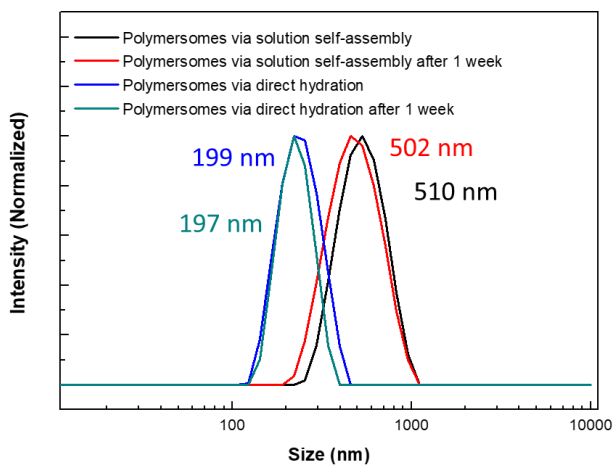

Figure 2-7. Dynamic light scattering (DLS) size plots of polymersomes of $PEG550_3$-b-PDMVS self-assembled via co-solvent and direct hydration methods. The polymersomes encapsulating Rhodamine B stayed for 1 week without showing any change in their size and morphology.

Giant polymersomes of PEG550$_3$-PDMVS15K had an elastic modulus of 18.7 mN/m before cross-linking. After cross-linking, the modulus of the polymersomes increased to 224.1 mN/m, which was comparable to the previously reported value of the shear elastic modulus of healthy RBC measured by micropipette aspiration (approximately 550 mN/m).[41,42] The results reflect an increase in physical stability brought about by covalent stabilization of the PDMS bilayer membrane compartment (Figure 2-8). In addition, the giant cross-linked polymersomes of PEG550$_3$-PDMVS15K exhibited reversible shape changes upon exposure to external force by aspiration. We applied high negative pressure through the capillary, followed by high positive pressure, to both unlinked and cross-linked vesicles. The cross-linked polymersomes underwent the deflation-inflation cycle without losing structural integrity (Figure 2-9). [43,44] In contrast, the uncross-linked polymersomes did not retain their structures under the same stresses (Figure 2-10). This result suggested that deformation of the PEG-*b*-PDMVS polymersomes was reversible due to the elasticity of the cross-linked hydrophobic bilayer compartment.

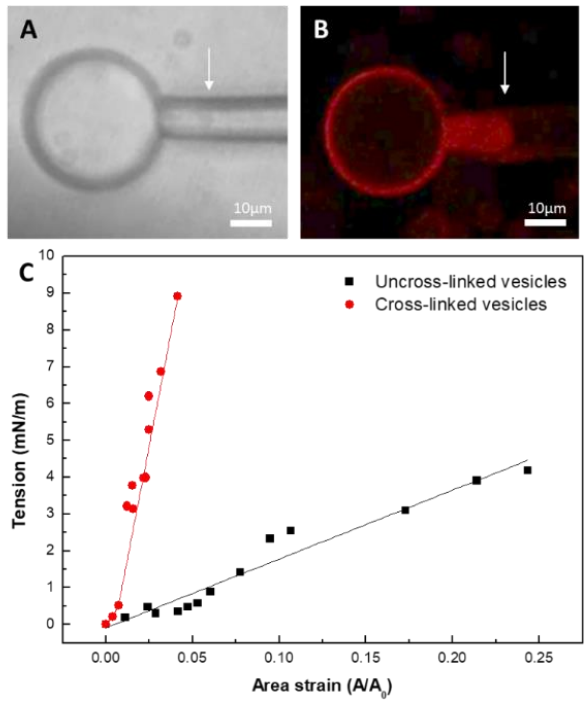

Figure 2-8. Giant unilamellar vesicles of PEG-*b*-PDMVS. Micro-deformation of a polymersome observed by (A) optical and (B) confocal laser scanning microscopy. The arrow marks the upper portion of a projection aspirated by negative pressure into the micropipette. (C) Aspiration increased membrane tension and expanded the vesicle surface area.

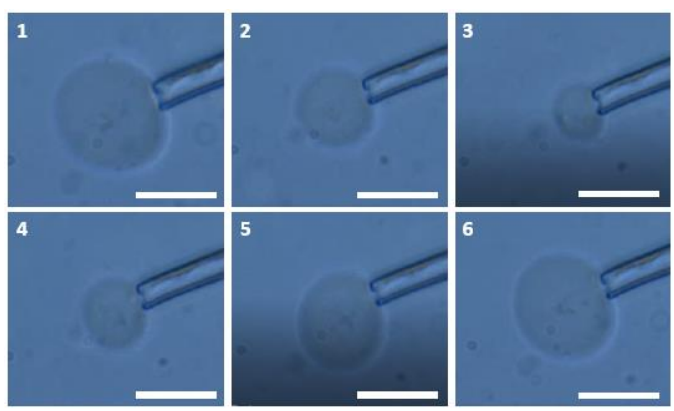

Figure 2-9. Sequence of a locally cross-linked vesicle of PEG-*b*-PDMVS. The cross-linked vesicle was partially deflated (1 to 3) by a negative pressure and inflation under positive pressure brought the vesicle back to its original shape (4 to 6) (Scale bar = 20 μm).

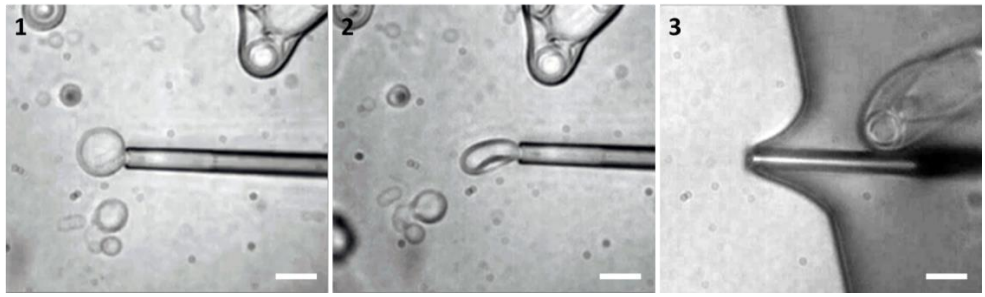

Figure 2-10. Sequence of an uncross-linked vesicle of PEG-*b*-PDMVS. The uncross-linked polymersomes failed to retain their round-shape and then finally were ruptured under negative pressure (1 to 3) (Scale bar = 20 μm).

Oxygen Permeability of Reversibly Deformable Polymersomes

We hypothesized that the compartmentalizing membrane, which consisted of cross-linked thin films of PDMVS, would make our polymersomes highly permeable to gas molecules, particularly oxygen. The photosensitized generation of singlet oxygen has been investigated for a number of applications, such as photodynamic therapy (PDT).[45–47] We surmised that polymersomes with encapsulated ZnTPP would be excellent candidates for biological singlet oxygen generation if their compartmentalizing membranes allowed free diffusion of oxygen. Zn(II)-tetraphenylporphyrin (ZnTPP) has been widely used as a photosensitizer to transfer energy to molecular triplet oxygen and to generate singlet oxygen. To determine their permeability to oxygen, we encapsulated ZnTPP within the polymersomes by a co-solvent method. Water (2 mL) was slowly added to a solution of the $PEG550_3$-PDMVS20K in dioxane that also contained 2 mg ZnTPP. Following addition of water, the resulting suspension was dialyzed against water, and unencapsulated ZnTPP was removed by SEC. After cross-linking of the ZnTPP-loaded polymersomes, UV-Vis absorption spectra contained the expected peaks, the major peaks being the Soret band in the

blue region and the Q-band in the red region. The spectra thus indicated the presence of ZnTPP within the polymersomes (Figure 2-11B).

The encapsulation efficiency was estimated by measuring the absorption of ZnTPP at 424 nm, which was compared to the calibration curve of free ZnTPP in THF (Figure 2-12).[46] The ZnTPP encapsulation efficiency was 0.19 wt.% relative to the BCP mass. Singlet oxygen generation was monitored by observing consumption of the singlet oxygen quencher, anthracene-9,10-dipropionic acid disodium salt (ADPA), to form its endoperoxide.[36,50] The ZnTPP-loaded polymersomes were placed under yellow light (λ = 560 nm) in the presence of ADPA. Results showed that 95% of the ADPA was consumed within 35 min (Figure 2-11C and 2-11D). This suggested that oxygen molecules could access the encapsulated photosensitizing ZnTPP within the polymersomes, and that the triplet oxygen generated could diffuse out through the cross-linked polymersome membrane.

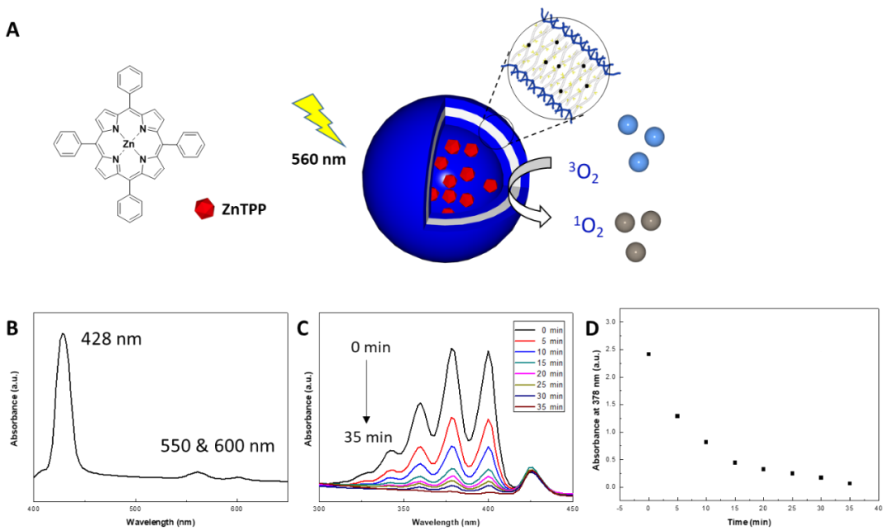

Figure 2-11. (A) Schematic representation of singlet O_2 generation by ZnTPP under yellow light. (B) UV-Vis absorbance spectra of cross-linked polymersomes with ZnTPP. (C) UV−Vis absorption spectra of ADPA with respect to the time of irradiation (λ_{max} = 560 nm) in the polymersomes of PEG550$_3$-b-PDMVS20K encapsulating ZnTPP. (D) Change in ADPA absorbance at 378 nm with increasing irradiation time.

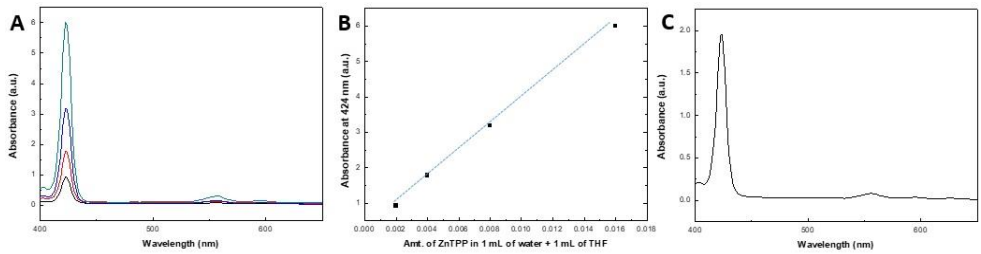

Figure 2-12. (A) Absorptions of free ZnTPP with different amounts (B) Plotting of a calibration curve of free ZnTPP, and (C) Absorption of ZnTPP loaded vesicles after elimination of the effect of nanoparticle-induced scattering.

The cross-linked polymersomes of $PEG550_3$-PDMVS15K exhibited reversible deformation when subjected to physical forces and spatial confinement, which resembled the physical responses exhibited by RBCs. To investigate the possibility of using the cross-linked polymersomes as oxygen-transporting vehicles, we encapsulated hemoglobin (Hb) in the aqueous compartment of the polymersomes of $PEG550_3$-PDMVS15K. To prevent unwanted oxidation of Hb to methemoglobin (metHb) during the preparation of hemoglobin-encapsulating polymersomes (HEPs), Hb was complexed with carbon monoxide (CO) to prepare carboxyhemoglobin (COHb) before encapsulation.[27,28,61] For encapsulation of COHb, the $PEG550_3$-*b*-PDMVS15K was directly hydrated in this solution at 4 ºC for 16 h. The resulting hemoglobin-encapsulating polymersomes (HEPs) were extruded through a 0.2 μm polycarbonate membrane filter to adjust their diameter to 200 nm.[62] Unencapsulated Hb was removed from the aqueous suspension by dialysis against PBS with a 100 K cutoff. We estimated the encapsulation efficiency (EE%) of Hb by measuring the absorption of the dispersion after purification. The absorption of the dispersion was measured by UV-vis spectrometer, which was compared to the calibration plot obtained using COHb in PBS. The estimated EE% was 8.37% (Figure 2-13). After cross-linking of the polymersomes with Irgacure 2959 under 8 W UV illumination

at 365 nm, the formation of polymersomes of uniform diameter was confirmed by DLS analysis. The average diameter of the polymersomes was 184.2 nm, and their polydispersity index was 0.212 (Figure 2-14).

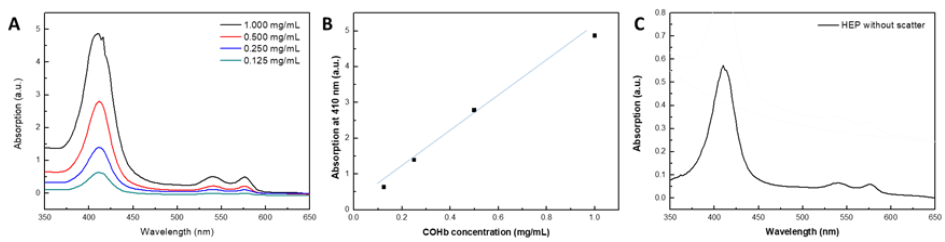

Figure 2-13. (A) Absorptions of free COHb with different amounts (B) Plotting of suitable calibration curve of free COHb, and (C) Absorption of hemoglobin loaded vesicles after elimination of the effect of nanoparticle-induced scattering.

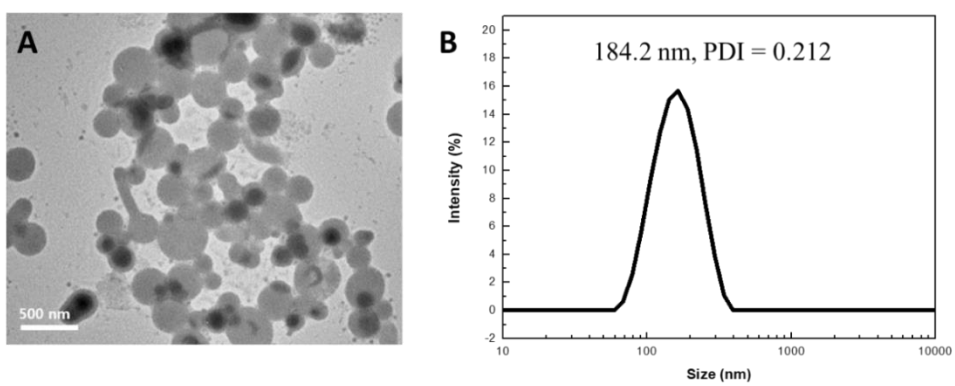

Figure 2-14. TEM image and DLS size plot for size-controlled polymersomes containing hemoglobin for oxygen transportation.

Oxygen binding in the cross-linked polymersomes with encapsulated Hb was investigated by UV-vis spectrometry. After introducing oxygen to the suspension by bubbling for 60 min, characteristic oxyHb absorption peaks were visible in the spectrum at 412, 538, and 572 nm (Figure 2-15A). The suspension was sealed off from the surrounding air and deoxygenated by

purging with nitrogen gas for 150 min. The absorption peaks of deoxygenated hemoglobin (deoxyHb) appeared in the spectrum of the suspension at 430 and 556 nm (Figure 2-15A).[63,65,66] When the deoxyHb vesicle suspension was exposed to oxygen, the characteristic peaks for oxyHb were observed again. The oxygen-nitrogen exchange process was repeated at least three times, and the resulting spectral data are shown in Figure 2-15B. These findings confirmed that the HEP was able to bind and release oxygen reversibly. We were also able to demonstrate the potential of HEP as an oxygen carrier based on the similarity of its bioactivity to that of free hemoglobin.

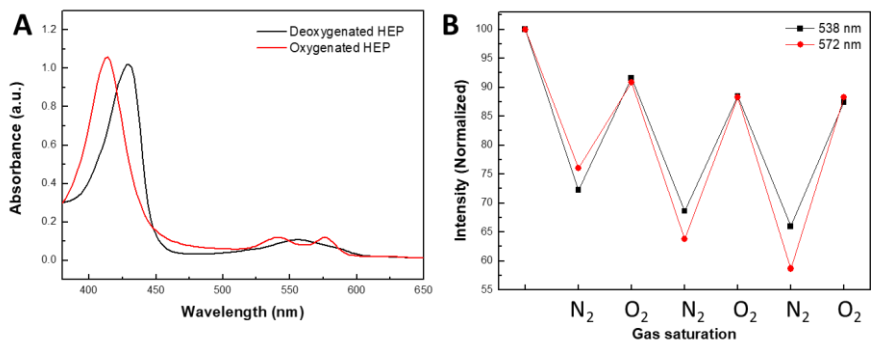

Figure 2-15. Polymersome-encapsulated hemoglobin tested for O_2 permeability. (A) UV-Vis spectra of oxygenated and deoxygenated HEP. (B) UV-vis spectra from repeated oxygen-nitrogen bubbling processes. The changes in absorbance intensity at 538 and 572 nm with O_2 and N_2 saturation were observed.

2.5 Conclusion

In summary, we report the synthesis of highly deformable and mechanically robust polymersomes capable of oxygen transport. The polymersomes were composed of amphiphilic block copolymers constructed with poly(dimethyl-*r*-methylvinyl)siloxane (PDMVS) as a hydrophobic block. Owing to the low T_g of the core block, these BCPs were able to self-assemble regardless of the presence or absence of organic solvents. All self-

assembled structures were covalently stabilized by cross-linking between vinyl pendants on their hydrophobic chains in the presence of a photo-radical generator in water. The cross-linked PEG-*b*-PDMVS polymersomes retained structural integrity under harsh conditions, such as the application of extreme shear force and exposure to organic solvents. In addition, quantitative mechanical measurement via micropipette aspiration indicated that the cross-links imparted structural toughness to the polymersomes without impairing their deformability. We encapsulated two porphyrin derivatives, ZnTPP and hemoglobin, within the inner compartments of the polymersomes. The permeability of the cross-linked PDMS membrane to oxygen demonstrated the polymersomes were capable of transporting gas molecules through their membranes without sacrificing their physical integrity. This work thus provides motivation to pursue use of polymeric nano-compartments as cellular mimics that can store and transport selected small molecules.

2.6 References

1. Buddingh', B. C.; van Hest, J. C. M. Artiicial Cells: Synthetic Compartments with Life-like Functionality and Adaptivity. *Acc. Chem. Rev.* **2017**, *50*, 769−777.
2. Rideau, E.; Dimova, R.; Schwille, P.; Wurm, F. R.; Landfester, K. Liposomes and polymersomes: a comparative review towards cell mimicking. *Chem. Soc. Rev.* **2018**, *47*, 8572−8610.
3. Tu, Y.; Peng, F.; Adawy, A.; Men, Y.; Abdelmohsen, L. K. E. A.; Wilson, D. A. Mimicking the Cell: Bio-Inspired Functions of Supramolecular Assemblies. *Chem. Rev.* **2016**, *116*, 2023−2078.
4. Kuiper, S. M.; Nallani, M.; Vriezema D. M.; Cornelissen, J. J. L. M.; van Hest, J. C. M.; Nolte, R. J. M.; Rowan, A. E. Enzymes containing porous polymersomes as nano reaction vessels for cascade reactions. *Org. & Biomol. Chem.* **2008**, *6*, 4315−4318.

5. Schatz, C.; Louguet, S.; Le Meins, J. F.; Lecommandoux, S. Polysaccharide-block-polypeptide Copolymer Vesicles: Towards Synthetic Viral Capsids. *Angew. Chem., Int. Ed.* **2009**, *48*, 2572−2575.
6. LoPresti, C.; Lomas, H.; Massignani, M.; Smart, T.; Battaglia, G. Polymersomes: Nature Inspired Nanometer Sized Compartments. *J. M*
7. Cai, Y.; Aubrecht, K. B.; Grubbs, R. B. Thermally Induced Changes in Amphiphilicity Drive Reversible Restructuring of Assemblies of ABC Triblock Copolymers with Statistical Polyether Blocks. *J. Am. Chem. Soc.* **2011**, *133*, 1058−1065.
8. Chandrawati, R.; Caruso, F. Biomimetic Liposome- and Polymersome-Based Multicompartmentalized Assemblies. *Langmuir,* **2012**, *28*, 13798−13807.
9. Zhang, X. Y.; Tanner, P.; Graff, A.; Palivan, C. G.; Meler, W. Mimicking the cell membrane with block copolymer membranes. *Journal of Polymer Science Part A: Polymer Chemistry* **2012**, *50*, 2293−2318.
10. Scarpa, E.; Janeczek, A. A.; Hailes, A.; de Andres, M. C.; Grazia, A. D.; Oreffo, R. O.; Newman, T. A.; Evans, N. D. Polymersome nanoparticles for delivery of Wnt-activating small molecules. Nanomedicine: Nanotechnology, *Biology, and Medicine* **2018**, *14*, 1267−1277.
11. Georgieva, J. V.; Brinkhuis, R. P.; Stojanov, K.; Weijers, C. A.; Zuilhof, H.; Rutjes, F. P.; Hoekstra, D.; van Hest, J. C. M.; Zuhorn, I. S. Peptide-Mediated Blood-Brain Barrier Transport of Polymersomes. *Angew. Chem. Int. Ed.* **2012**, *51*, 8339−8342.
12. Brinkhuis, R. P.; Stojanov, K.; Laverman, P.; Eilander, J.; Zuhorn, I. S.; Rutjes, F. P.; van Hest, J. C. M. Size Dependent Biodistribution and SPECT Imaging of ^{111}In-labeled Polymersomes. *Bioconjugate Chem.* **2012**, *23*, 958−965.

13. Marguet, M.; Bonduelle, C.; Lecommandoux, S. Multicompartmentalized polymeric systems: towards biomimetic cellular structure and function. *Chem. Soc. Rev.* **2013**, *42*, 512−529.
14. Chen, H.; Xiao, L.; Anraku, Y.; Mi, P.; Liu, X.; Cabral, H.; Inoue, A.; Nomoto, T.; Kishimura, A.; Nishiyama, N.; Kataoka, K. Polyion Complex Vesicles for Photoinduced Intracellular Delivery of Amphiphilic Photosensitizer. *J. Am. Chem. Soc.* **2014**, *136*, 157−163.
15. Li, J.; Liang, L.; Liang, J.; Wu, W.; Zhou, H.; Guo, J. Constructing Asymmetric Polyion Comlex Vesicles via Template Assembling Strategy; Formulation Control and Tunable Permeability, *Nanomaterials* **2017**, *7*, 387−397.
16. Discher, D. E.; Eisenberg, A. Polymer Vesicles. *Science* **2002**, *297*, 967−973.
17. Kim, K. T.; Zhu, J. H.; Meeuwissen, S. A.; Cornelissen, J.; Pochan, D. J.; Nolte, R. J. M.; van Hest, J. C. M. Polymersome Stomatocytes: Controlled Shape Transformation in Polymer Vesicles. *J. Am. Chem. Soc.* **2010**, *132*, 12522−12524.
18. Jeong, M. G.; van Hest, J. C. M.; Kim, K. T. Self-assembly of dendritic-linear block copolymers with fixed molecular weight and block ratio. *Chem. Commun.* **2012**, *48*, 3590−3592.
19. Rikken, R. S. M.; Engelkamp, H.; Nolte, R. J. M.; Maan, J. C.; van Hest, J. C. M.; Wilson, D. A.; Christianen, P. C. M. Shaping polymersomes into predictable morphologies via out-of-equilibrium self-assembly. *Nat. Comm.* **2016**, *7*, 12606−12612.
20. Che, H.; van Hest, J. C. M. Stimuli-responsive polymersomes and nanoreactors. *J. Mater. Chem. B* **2016**, *4*, 4632−4647.
21. Meng, F. H.; Zhong, Z. Y.; Feijen, J. Stimuli-Responsive Polymersomes for Programmed Drug Delivery. *Biomacromolecules* **2009**, *10*, 197−209.

22. Liu, G. J.; Ma, S. B.; Li, S. K.; Cheng, R.; Meng, F. H.; Liu, H. Y.; Zhong, Z. Y. The Highly Efficient Delivery of Exogenous Proteins into Cells M
23. Kim, H.; Kang, Y. J.; Kang, S.; Kim, K.T. Monosaccharide-Responsive Release of Insulin from Polymersomes of Polyboroxole Block Copolymers at Neutral pH. *J. Am. Chem. Soc.* **2012**, *134*, 4030−4033.
24. Kim, H.; Kang, Y. J.; Jeong, E. S.; Kang, S.; Kim, K. T. Glucose-Responsive Disassembly of Polymersomes of Sequence-Specific Boroxole-Containing Block Copolymers under Physiological Relevant Conditions. *ACS Macro Lett.* **2012**, *1*, 1194−1198.
25. So, S.; Yao, L.; Lodge, T. P. Permeability of Rubbery and Glassy Membranes of Ionic Liquid Filled Polymersome Nanoreactors in Water. *J. Phys. Chem. B* **2015**, *119*, 15054−15062.
26. Doshi, N.; Zahr, A. S.; Bhaskar, S.; Lahann, J.; Mitragotri, S. Red blood cell-mimicking synthetic biomaterial particles. *Proc. Natl. Acad. Sci. U.S.A.* **2009**, *106*, 21495−21499.
27. Arifin, D. R.; Palmer, A. F. Determination of Size Distribution and Encapsulation Efficiency of Liposome-Encapsulated Hemoglobin Blood Substitutes Using Asymmetric Flow Field-Flow Fractionation Coupled with Multi-Angle Static Light Scattering. *Biotechnol. Prog.* **2003**, *19*, 1798−1811.
28. Arifin, D. R.; Palmer, A. F. Polymersome Encapsulated Hemoglobin: A Novel Type of Oxygen Carrier. *Biomacromolecules* **2005**, *6*, 2172−2181.
29. Lin, H.; Kai, T.; Freeman, B. D.; Kalakkunnath, S.; Kalika, D. S. *Macromolecules* **2005**, *38*, 8381−8393.
30. Le Meins, J. F.; Sandre, O.; Lecommandoux, S. Recent trends in the tuning of polymersomes' membrane properties. *Eur. Phys. J. E* **2011**, *34*, 14.

31. Checot, F.; Lecommandoux, S.; Klok, H. A.; Gnanou, Y. From supramolecular polymersomes to stimuli-responsive nano-capsules based on poly(diene-b-peptide) diblock copolymers. *Eur. Phys. J. E* **2003**, *10*, 25−35.
32. Cheng, R.; Meng, F.; Ma, S.; Xu, H.; Liu, H.; Jing, X.; Zhong, Z. Reduction and temperature dual-responsive crosslinked polymersomes for targeted intracellular protein delivery. *J. Mater. Chem.* **2011**, *21*, 19013−19020.
33. Deng, Z.; Qian, Y.; Yu, Y.; Liu, G.; Hu, J.; Zhang, G.; Liu, S. Engineering Intracellular Delivery Nanocarriers and Nanoreactors from Oxidation-Responsive Polymersomes via Synchronized Bilayer Cross-linking and Permeabilizing Inside Live Cells. *J. Am. Chem. Soc.* **2016**, *138*, 10452−10456.
34. Gaitzsch, J.; Canton, I.; Appelhans, D.; Battaglia, G.; Voit, B. Cellular Interactions with Photo-Cross-Linked and pH-Sensitive Polymersomes: Biocompatibility and Uptake Studies. *Biomacromolecules* **2012**, *13*, 4188−4195.
35. Bermudez, H.; Brannan, A. K.; Hammer, D. A.; Bates, F. S.; Discher, D. E. Molecular Weight Dependence of Polymersome Membrane Structure, Elasticity, and Stability. *Marcromolecules* **2002**, *35*, 8203−8208.
36. Lindig, B. A.; Rodgers, M. A. J.; Schaap, A. P. Determination of the lifetime of singlet oxygen in water-d2 using 9,10-anthracenedipropionic acid, a water-soluble probe. *J. Am. Chem. Soc.* **1980**, *102*, 5590−5593.
37. Zhang, M.; Rupar, P. A.; Feng, C.; Lin, K.; Lunn, D. J.; Oliver, A.; Nunns, A.; Whittell, G. R.; Manners, I.; Winnik, M. A. Modular Synthesis of Polyferrocenylsilane Block Copolymers by Cu-Catalyzed Alkyne/Azide "Click" Reactions. *Macromolecules* **2013**, *46*, 1296−1304.

38. Dollase, T.; Spiess, H. W.; Gottlieb, M.; Yerushalmi-Rozen, R. Crystallization of PDMS: The effect of physical and chemical crosslinks. *Europhys. Lett.* **2002**, *60*, 390−396.
39. Discher, B. M.; Won, Y. Y.; Ege, D. S.; Lee, J. C. M.; Bates, F. S.; Discher, D. E.; Hammer, D. A. Polymersomes: Tough Vesicles Made from Diblock Copolymers. *Science* **1999**, *284*, 1143−1146.
40. Discher, B. M.; Bermudez, H.; Hammer, D. A.; Discher, D. E. Cross-linked Polymersome Membranes: Vesicles with Broadly Adjustable Properties. *J. Phys. Chem B* **2002**, *106*, 2848−2854.
41. Tomaiuolo, G. Biomechanical properties of red blood cells in health and disease towards microfluidics. *Biomicofluidics* **2014**, *8*, 051501
42. Evans, E. A. New membrane concept applied to the analysis of fluid shear- and micropipette-deformed red blood cells. *Biophys. J.* **1973**, *13*, 941−954.
43. Mabrouk, E.; Cuvelier, D.; Pontani, L.; Xu, B.; Levy, D.; Keller, P.; Brochard-Wyart, F.; Nassoy, P.; Li, M. Formation and material properties of giant liquid crystal polymersomes. *Soft Matter* **2009**, *5*, 1870−1878.
44. Ahmed, F.; Hategan, A.; Discher, D. E.; Discher, B. M. Block Copolymer Assemblies with Cross-link Stabilization: From Single-Component Monolayers to Bilayer Blends with PEO-PLA. *Langmuir* **2003**, *19*, 6505−6511.
45. Merkel, T. C.; Bondar, V. I.; Nagai, K.; Freeman, B. D.; Pinnau, I. Gas Sorption, Diffusion, and Permeation in Poly(dimethylsiloxane). *Journal of Polymer Science Part B: Polymer Physics* **2000**, *38*, 415−434.
46. Robb, W. L. Thin Silicone Membranes-Their Permeation Properties and Some Applications. *Ann. N.Y. Acad. Sci.* **1968**, *146*, 119−137.
47. DeRosa, M. C.; Crutchley, R. J. Photosensitized singlet oxygen and its applications. *Coordination Chemistry Reviews* **2002**, *233*, 351−371.

48. Zarrintaj, P.; Ahmadi, Z.; Hosseinnezhad, M.; Saeb, M. R.; Laheurte, P.; Mozafari, M. Photosensitizers in medicine: Does nanotechnology make a difference? *Materials Today: Proceedings* **2018**, *5*, 15836−15844.
49. Hong, E. J.; Choi, D. G.; Shim, M. S. Targeted and effective photodynamic therapy for cancer using functionalized nanomaterials. *Acta Pham. Sin. B.* **2016**, *6*, 297−307.
50. Yeow, J.; Shanmugam, S.; Corrigan, N.; Kuchel, R. P.; Xu, J.; Boyer, C. A Polymerization-Induced Self-Assembly Approach to Nanoparticles Loaded with Singlet Oxygen Generators. *Macromolecules* **2016**, *49*, 7277−7285.
51. Zheng, S.; Beissinger, R.; Sherwood, R. L.; McCormick, D. L.; Lasic, D. D.; Martin, F. J. Liposome-encapsulated hemoglobin: a red blood cell substitute. *J. Liposome Res.* **1993**, *3*, 575−588.
52. Patton, J. N.; Palmer, A. F. Engineering Temperature-Sensitive Hydrogel Nanoparticles Entrapping Hemoglobin as a Novel Type of Oxygen Carrier. *Biomacromolecules* **2005**, *6*, 2204−2212.
53. Arifin, D. R.; Palmer, A. F. Stability of Liposome Encapsulated Hemoglobin Dispersions. *Artificial Cells, Blood Substitutes, and Biotechnology* **2005**, *33*, 113−136.
54. Eike, J. H.; Palmer, A. F. Effect of Glutaraldehyde Concentration on the Physical Properties of Polymerized Hemoglobin-Based Oxygen-Carriers. *Biotechnol. Prog.* **2004**, *20*, 1225−1232.
55. Eike, J. H.; Palmer, A. F. Effect of Cl^- and H^+ on the Oxygen Binding Properties of Glutaraldehyde-Polymerized Bovine Hemoglobin-Based Blood Substitutes. *Biotechnol. Prog.* **2004**, *20*, 1543−1549.
56. Sakai, H.; Tomiyama, K.; Sou, K.; Takeoka, S.; Tsuchida, E. Poly(ethylene glycol)-Conjugation and Deoxygenation Enable Long-Term Preservation of Hemoglobin-Vesicles as Oxygen Carriers in a Liquid State. *Bioconjugate Chem.* **2000**, *11*, 425−432.

57. Huang, Y.; Takeoka, S.; Sakai, H.; Abe, H.; Hirayama, J.; Ikebuchi, K.; Ikeda, H.; Tsucaida, E. Complete Deoxygenation from a Hemoglobin Solution by an Electrochemical Method and Heat Treatment for Virus Inactivation. *Biotechnol. Prog.* **2002**, *18*, 101−107.
58. Chang, T. M. S. Blood substitutes: principles, methods, products, and clinical trials; Karger: New York, 1997.
59. Phillips, W. T.; Klipper, R. W.; Awasthi, V. D.; Rudolph, A. S.; Cliff, R.; Kwasiborski, V.; Goins, B. A. Polyethylene glycol-modified liposome-encapsulated hemoglobin; a long circulating red cell substitute. *J. Pharmacol. Exp. Ther.* **1999**, *288*, 665−670.
60. Bhadra, D.; Bhadra, S.; Jain, P.; Jain, N. K. Pegnology: a review of PEG-ylated system. *Pharmazie* **2002**, *57*, 5−29.
61. Ghatge, M. S.; Ahmed, M. H.; Omar, A. S.; Pagae, P. P.; Rosef, S.; Kellogg, G. E.; Abdulmalik, O.; Safo, M. K. Crystal structure of carbonmonoxy sickle hemoglobin in R-state conformation. *J. Struc. Biol.* **2016**, *194*, 446−450.
62. Xiong, Y.; Liu, Z. Z.; Georgieva, R.; Smuda, K.; Steffen, A.; Sendeski, M.; Voigt, A.; Patzak, A.; Baumler, H. Nonvasoconstrictive Hemoglobin particles as Oxygen Carriers. *ACS Nano* **2013**, *7*, 7454−7461.
63. Russo, S. F.; Sorstokke, R. B. Hemoglobin: Isolation and Chemical Properties. *J. Chem. Educ,* **1973**, *50*, 347−350.
64. Zwart, A.; Buursma, A.; van Kampen, E. J.; Zijistra, W. G. Multicomponent Analysis of Hemoglobin Derivatives with a Reversed-Optics Spectrophotometer. *Clin. Chem.* **1984**, *30*, 373−379.
65. Zijistra, W. G.; Buursma, A.; Meeuwsen-van der Roest, W. Absorption Spectra of Human Fetal and Adult Oxyhemoglobin, De-Oxyhemoglobin, Carboxyhemoglobin, and Methemoglobin. *Clin. Chem.* **1991**, *37*, 1633−1638.

66. Wang, W.; Liu, S.; Huang, Y.; Jing, X.; Xie, Z. Biodegradable dextran vesicles for effective haemoglobin encapsulation. *J. Mater. Chem. B* **2015**, *3*, 5753−5759.

Chapter 3. Polymer Cubosomes of Block Copolymers Having Cross-linkable Soft Hydrophobic Blocks

3.1 Abstract

Inverse bicontinuous cubic mesophases of block copolymers are an emerging class of mesoporous structures consisting of block copolymer bilayers, in which well-defined reticulated pore networks are intertwined in a long-range crystalline order. Polymer cubosomes, colloidal particles consisting of inverse cubic mesophases of block copolymers may find applications in ultrafiltration and affinity-based separation if the physical properties of their self-assembled structures could be optimized to maintain their structural integrity under physical and chemical stresses. In particular, highly ordered triply periodic mesoporous structures showing reversible swelling can be directly synthesized via solution self-assembly of block copolymers into polymer cubosomes and their subsequent cross-linking. Here we report a series of block copolymers synthesized by joining two structural modules, a branched poly(ethylene glycol) (PEG) hydrophilic block and linear/branched polyisoprene (PI) hydrophobic blocks. In addition to the block ratio and architecture of the block copolymer, PEG-*b*-PI, we suggest the length of the hydrophobic PI chain by adjusting its microstructure as a key structural parameter for the self-assembly of PEG-*b*-PI to form inverse cubic mesophases. The polymer cubosomes of these block copolymers can be covalently stabilized by the photo-radical-induced cross-linking of PI chains, resulting in the formation of rubbery hydrophobic domain. In contrast to uncross-linked polymer cubosomes, the cross-linked structures retained their structures under ambient conditions without water, and exhibited reversible swelling-deswelling upon exposure to organic solvents.

3.2 Introduction

Porous polymers are indispensable media serving the stationary phase for separation, filtration, chromatography, catalysis, and biomedical applications.[1–8] For these applications, it is desirable to exercise precise control over the dimension and spatial arrangement of pores embedded in polymer membranes and monoliths.[9-12] Also, the surface functionality of these porous polymers could greatly benefit applications such as affinity-based separation and chiral separation of pharmaceuticals and biomolecules.[1,13] Recently, block copolymers (BCPs) have been highlighted as promising materials to prepare porous polymer films having precisely defined pore sizes and spatial arrangements of pores.[14–17] BCPs self-assemble to form periodic arrangements of different chemical compositions in the bulk. After pore formation by selective removal of the dispersed domain consisting of chemically labile polymer blocks, the distribution of chemical compositions within the BCP films and monoliths can be translated to well-defined sizes of pores and their spatial arrangements.[18–20]

Inverse bicontinuous cubic mesophases of BCPs are an emerging class of mesoporous structures composed of well-defined periodic minimal surfaces of BCP bilayers, in which two non-intersecting water channel networks are embedded in a long-range three-dimensional order. BCPs could form colloidal particles (polymer cubosomes) or monolithic films composed of inverse cubic mesophases of the BCP bilayers in solution. Similar to the crystallographic characteristics of lipid cubic mesophases,[27–33,47] triply periodic minimal surfaces having symmetries corresponding to the Schwarz P and D surfaces ($Im\bar{3}m$ and $Pn\bar{3}m$ space group, respectively) and Schoen G surface ($Ia\bar{3}d$ space group) were found from the cubic mesophases of

BCPs. These lattices translate into the spatial arrangement of mesoporous networks embedded within BCP cubic mesophases, of which the size of the pore is dictated by the molecular weight of a BCP. With a large surface area (>100 m^2g^{-1}) and pore volume (>1 cm^2g^{-1}) arising from the bicontinuous channel networks, the resultant polymer cubosomes and monolithic mesoporous films could be mesoporous materials potentially useful for separation, bioreactors, and nanotemplating.[21,22]

However, transient structures formed by the self-assembly of macromolecular building blocks might be necessary to be covalently fixed by the cross-linking of the organized molecules for their applications under harsh conditions. Although the cross-linked cubic mesophases of BCPs could show enhanced stability under chemical stresses,[34] the mechanical properties of the mesophases have yet to be adjusted for application. In particular, triply periodic minimal surface of BCPs can be directly used as mesoporous materials that can change their pore size and periodicity reversibly without losing their structural integrity in response to external stimuli such as solvents and physical force. These materials are promising in responsive photonic crystals and ultrafiltration.[35-38] To this end, the introduction of cross-linkable hydrophobic polymers having a low glass transition temperature (T_g) to the BCPs could be a very attractive strategy because the resultant cross-linked mesophases would exhibit elasticity and resist physical stress without fracture.

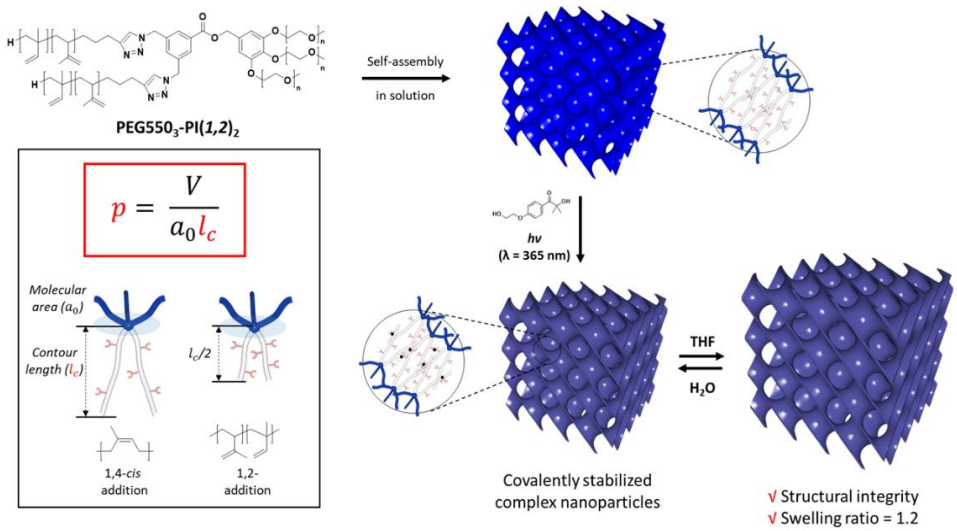

Figure 3-1. Schematic representation of the solution self-assembly of branched-branched block copolymers of PEG550$_3$-*b*-PI(*1,2*)$_2$ into polymer cubosomes and the cross-linking of the PI compartments by photo-generated radical coupling. The cross-linked cubosomes maintained their structural integrity upon exchanging the solvent from water to THF.

Here we report the modular synthesis of a series of branched-branched BCPs composed of branched hydrophilic PEG blocks and hydrophobic polyisoprene (PI) blocks as the structural modules. We introduce the PI chains as the hydrophobic blocks to construct the BCPs because their low T_g and the reactive vinyl groups in the repeating unit provide a means to precisely tune the physical properties of the self-assembled structures upon cross-linking (Figure 3-1). We show that the length of the polymer chains constituting the hydrophobic block is a decisive factor that guides the self-assembly of BCPs into inverse cubic mesophases in solution. The BCPs in solution self-assembled into colloidal particles of inverse mesophase including polymer cubosomes and hexosomes depending on the contour length of the PI chain, which

can be adjusted by varying the molecular weight and microstructure of the repeating unit. The polymer cubosomes exhibited reversible swelling/deswelling without losing their structural integrity in response to the presence of organic solvents.

3.3 Results and Discussion

Design and synthesis of block copolymers

The critical packing parameter of an amphiphile is defined by $p = V/a_0 l_c$, where V is the volume of the hydrophobic domain, a_0 is the cross-sectional area of the hydrophilic group, and l_c is the critical length of the hydrophobic part.[40] When the value of p exceeds unity, the amphiphile favors forming inverse mesophases in solution. We previously suggested that the architecture of the dendritic or branched hydrophilic block, in combination with the block ratio, defined here by the molecular weight fraction of the hydrophilic PEG chains (f_{PEG}), plays a crucial role in tuning the phase behavior of the BCP in solution.[39]

In this work, we chose a simple branched PEG hydrophilic block and PI hydrophobic block having a low T_g as the structural modules to prepare amphiphilic BCPs (Scheme 3-1). The branched PEG block was synthesized by alkylation of oligomeric PEG chains (M_n = 550 g mol^{-1}, $Đ$ = 1.08) to methyl 3,4,5-trihydroxybenzoate, followed by reduction of the methyl ester into a hydroxymethyl group. To this core, azide groups were introduced by substitution at the focal benzyl chloride, which afforded the hydrophilic module PEG550$_3$-N$_3$. The hydrophilic module PEG550$_3$-(3,5)-N$_3$ having two azide groups at predetermined locations was prepared by introducing 3,5-

azidomethylbenzoid acid to the benzyl alcohol core by the Steglich esterification.

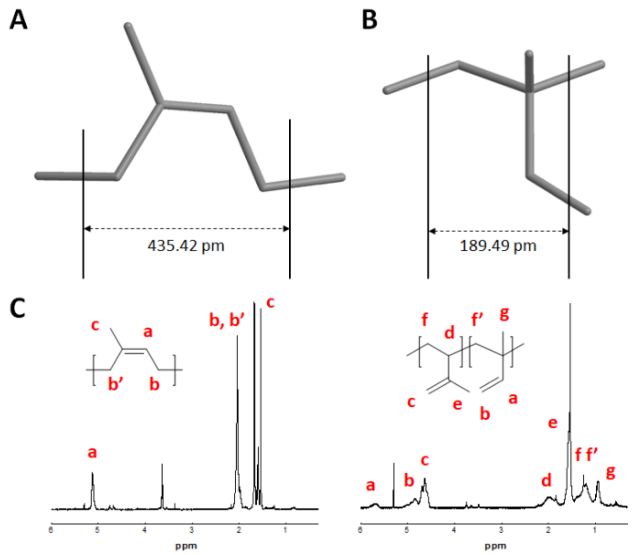

Figure 3-2. 3-D images of (A) 1,2-cis and (B) 1,4-microstructures of PI chains. (C) ^{1}H NMR spectra of PI(*1,4*)(10K) and PI(*1,2*)(10K) showing the difference in microstructure of the repeating units.

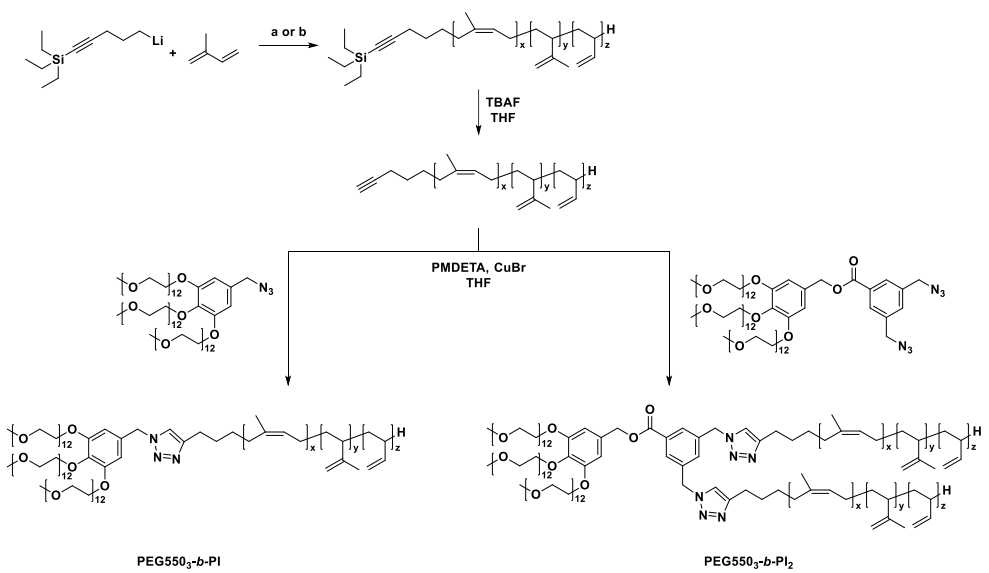

Scheme 3-1. Synthesis of PEG-b-PI block copolymers composed of branched hydrophilic PEG blocks and linear/branched hydrophobic polyisoprene (PI) blocks. a: cyclohexane, 35 ^{o}C. 2h; b: THF, -76 ^{o}C, 1h.

Table 3-1. Characterization of polyisoprene

Entry	M_n (g mol^{-1})[a]	Đ [a]	DP_n[b]	1,4:3,4:1,2[c]	Extended length (nm)[d]
PI(*1,4*)(10K)	9780	1.20	143	94:0:6	60
PI(*1,4*)(13K)	12880	1.17	189	94:0:6	80
PI(*1,4*)(15K)	14600	1.08	214	94:0:6	90
PI(*1,4*)(33K)	33500	1.32	492	94:0:6	209
PI(*1,2*)(10K)	10500	1.09	154	0:38:62	29

[a] Number-average molecular weight and molecular weight distribution determined by GPC. [b] Number-average degree of polymerization estimated by the molecular weight. [c] Ratio between microstructures of the repeating unit of the PI chain calculated by ^{1}H NMR integration. [d] Fully-extended chain length calculated based on the microstructure of the repeating unit.

For the hydrophobic blocks, we anionically polymerized isoprene with triethylsilyl-1-propynyl lithium as an initiator.[35] Polymerization was conducted in cyclohexane for 2 h at 35 ℃, which predominantly showed the repeating unit of the 1,4-cis microstructure along the PI backbone in ^{1}H NMR spectrum. When the polymerization was carried out in THF at –78 ℃, 1,2- or 3,4- microstructures with pendant vinyl groups along the PI backbone were observed by ^{1}H NMR spectroscopy (Figure 3-2C). The change of the repeating unit microstructure of the PI chains was quantified by integrating the peaks of the ^{1}H NMR spectra. which showed that the PI chain polymerized in cyclohexane consisted of the 1,4-cis microstructure (~94%) having an internal alkene and the PI chain polymerized in THF was composed of 1,2- and 3,4-microstructures (>90%) having pendant vinyl groups. By altering the microstructure of the PI backbone, we were able to differentiate the PI chain length at the same molecular weight (Figure 3-2). The resultant PI chains showed well-defined molecular weights and molecular weight distributions by GPC analysis (Table 3-1). The triethylsilyl protecting group was removed by reacting the PI with

tetrabutylammonium fluoride, resulting in the PI chains with an acetylene end group. The complete deprotection of the triethylsilyl groups was confirmed by ^{1}H-NMR spectroscopy (Figure. 3-3B).

The synthesized modules were combined to form BCPs by Cu(I)-catalyzed azide–alkyne click chemistry in THF (Scheme 3-1). After confirming completion of the reaction by GPC, the resulting BCP with linear and branched PI hydrophobic blocks was purified by repeated precipitation in methanol, followed by column chromatography on SiO_2 with CH_2Cl_2 as an eluent to remove any unreacted PI chains. The resulting BCP showed a unimodal peak on GPC, of which the molecular weight corresponded to the increased molecular weight upon completion of the click reaction between the structural modules (Figure 3-3C). Additionally, ^{1}H NMR integration was used to confirm the successful synthesis of BCPs by the click reaction of the structural modules (Figure 3-3A). A comparison of the peak integration corresponding to the PEG and PI chains provided the number-average degree of the repeating units (DP_n) of the PI chains by assuming the molecular weight of the PEG domain was 1650 g mol^{-1} for $PEG550_3$. The estimated DPn showed good agreement with the Mn value obtained by GPC (Table 3-2).

Table 3-1. Characterization of block copolymers (BCPs)

Entry	M_n (g mol^{-1})[a]	$Đ$ [a]	DP_n(PI)[b]	f_{PEG} (%)[c]	PI chain length (nm)[d]
PEG550$_3$-PI(*1,4*)(33K)	29800	1.23	493	5.5	209
PEG550$_3$-PI(*1,4*)(15K)$_2$	24900	1.29	214	6.6	90
PEG550$_3$-PI(*1,4*)(13K)$_2$	23800	1.21	189	6.9	80
PEG550$_3$-PI(*1,4*)(10K)$_2$	22700	1.13	114	7.3	60
PEG550$_3$-PI(*1,2*)(10K)$_2$	21000	1.10	120	7.9	29

[a]Number average molecular weight (M_n) and molecular weight distribution ($Đ$) determined by GPC using polystyrene (PS) standards. Elution was performed with THF at a flow rate of 1 mL min^{-1} at 30 °C. [b]DP_n determined by ^{1}H NMR integration. [c]Block ratio defined by the molecular weight of PEG chains. [d]Fully-extended chain length calculated based on the microstructure of the repeating unit.

We first studied the self-assembly of a series of PEG550$_3$-PI and PEG550$_3$-PI$_2$ (Scheme 3-1) to elucidate the structural requirement of the BCPs to form inverse mesophases in aqueous solution. The BCPs were dissolved in dioxane at a typical concentration of 10 mg mL^{-1}. To this solution, water was slowly introduced at a rate of 2 mL h^{-1} via a syringe pump. The organic solvent was removed from the aqueous suspension by dialysis against water. The resulting aqueous suspension was inspected by dynamic light scattering (DLS), which provided the hydrodynamic diameter of the self-assembled structures in water. These nanostructures remained suspended in water for a period of 2 weeks without any change in the diameters as examined by DLS. For the direct observation of the self-assembled structures of BCPs in water, the cryogenic transmission electron microscopy (cryo-TEM) was performed.[46]

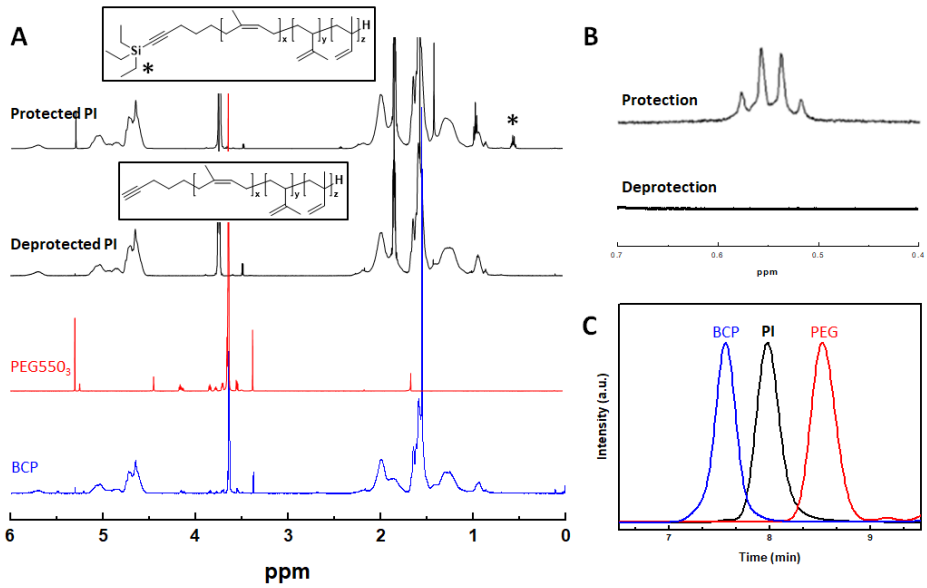

Figure 3-3. (A) ^{1}H NMR spectra of PEG (red) and PI (black) structural modules and the PEG550$_3$-PI$_2$ (blue). (B) ^{1}H NMR spectra showing the disappearance of Si-CH$_2$ protons upon deprotection. (C) GPC spectra of synthesis of block copolymers by click chemistry.

We compared the morphology of the self-assembled structures of two BCPs, PEG550$_3$-PI(*1,4*)(33K) and PEG550$_3$-PI(*1,4*)(15K)$_2$, having similar molecular weights of hydrophobic blocks (f_{PEG} = 8.1% and 9.9%, respectively). The branched-linear BCP, PEG550$_3$-PI(*1,4*)(33K) with a long PI chain (fully extended chain length of the PI chain, L_{PI} = 207 nm) self-assembled into polymer vesicles (polymersomes, Figure 3-4A). Non-circular shaped polymersomes were observed from the vitrified solution, which may arise from the confinement of soft polymersomes within the cavity of the porous carbon support of the TEM grid used for the experiments.

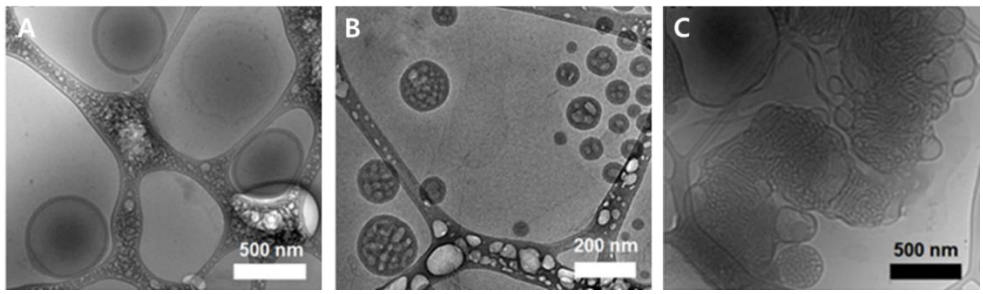

Figure 3-4. Morphological transition from polymersomes to inverse micellar nanoparticles upon reduction of the chain length of PI. Cryo-TEM images of (A) polymersomes, (B) inverse micellar nanoparticles, and (C) mixed structures of large polymersomes and disordered bicontinuous phases formed from PEG550$_3$-PI(*1,4*)(33K), PEG550$_3$-PI(*1,4*)(15K)$_2$, and PEG550$_3$-PI(*1,4*)(10K)$_2$ respectively.

PEG550$_3$-PI(*1,4*)(15K)$_2$, which possesses two shorter PI chains (L_{PI} = 90 nm) self-assembled into nanoparticles having internal inverse micellar phases, in which small water-containing cavities were packed without a cubic crystalline order (Figure 3-4B). These inverse micellar nanoparticles were distinguished from bicontinuous inverse mesophases such as polymer cubosomes and hexosomes having an ordered array of interior water channels. Inverse micellar phases of BCPs would require the *p* value of the BCP to be greater than those of BCPs forming polymer vesicles and inverse cubic and hexagonal phases.[22] Therefore, this result confirms that the branched architecture introduced into the hydrophobic block should contribute to the reduction of the length of the hydrophobic domain, resulting in an increase of the *p* value of the BCP.

When we reduced the molecular weight of the PI chains comprising the hydrophobic block without changing the architecture of the BCP, the resulting PEG550$_3$-PI(*1,4*)(13K)$_2$ (f_{PEG} = 6.9%, L_{PI} = 80 nm) self-assembled into the mixed structures of hexagonal phases and

bicontinuous mesophases (Figure 3-5). In contrast, PEG550$_3$-PI(*1,4*)(10K)$_2$ (f_{PEG} = 7.3%, L_{PI} = 60 nm) self-assembled into mixed structures of large polymersomes and disordered bicontinuous phases of the BCP bilayers (Figure 3-4C). This morphological transition from inverse micellar nanoparticles, hexosomes, to bilayer mesophases may be caused by the increase of the block ratio. Therefore, at the block ratio of 7.3%, we further reduced the hydrophobic polymer chain length by adopting PI chains with dominant 1,2-microstructures along the backbone. Notably, the resulting BCP, PEG550$_3$-PI(*1,2*)(10K)$_2$ (f_{PEG} = 12%, L_{PI} = 29 nm) self-assembled into polymer cubosomes, of which the average diameter was measured to be 980 nm by DLS (polydispersity: 0.260) (Figure 3-5). We reasoned that the formation of polymer cubosomes from the solution self-assembly of PEG550$_3$-PI(*1,2*)(10K)$_2$ was attributed to the decreased length of the PI chains having 1,2-microstructures along the backbone (L_{PI} = 29 nm) compared to the length of the PI chains having a 1,4-*cis* microstructure (L_{PI} = 60 nm) at the same molecular weight. Assuming that the volume of the hydrophobic chains (V) with same molecular weight should be identical, the reduced chain length of the PI chain consisting of 1,2- and 3,4-rich microstructure could contribute to the increase of the p value of the resulting BCP.

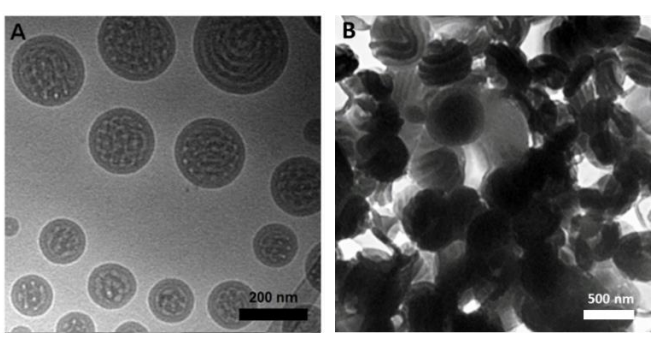

Figure 3-5. (A) Cryo-TEM and (B) TEM images of mixed structures of hexagonal structures of PEG550$_3$-PI(*1,4*)(13K)$_2$.

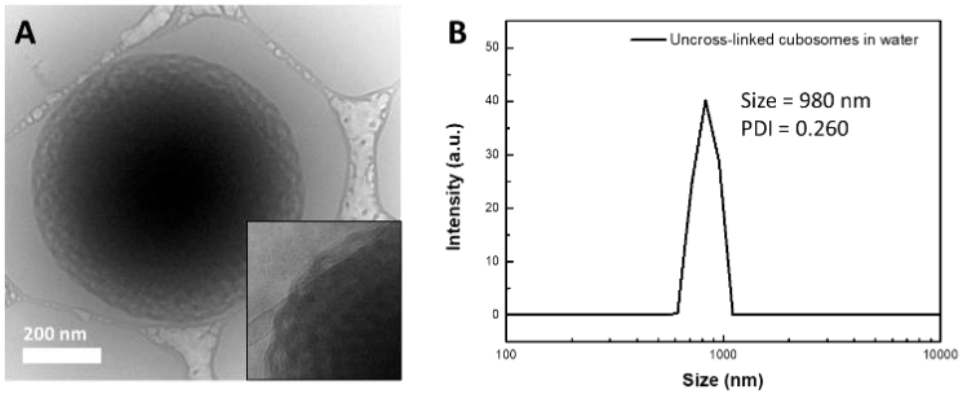

Figure 3-6. (A) Cryo-TEM images and (B) dynamic light scattering (DLS) result of polymer cubosomes formed from PEG550$_3$-PI(*1*,*2*)(10K)$_2$.

Covalent stabilization of polymer cubosomes of PEG-*b*-PI.

In order to covalently stabilize these self-assembled polymer cubosomes, we cross-linked the PI chains by using a water-soluble photo-radical generator (Irgacure 2959, Sigma) under UV light irradiation (λ = 348 nm) for 5 h. The covalent stabilization of polymer cubosomes of PEG550$_3$-PI(*1*,*2*)(10K)$_2$ was confirmed by replacing the dispersion medium from water to THF. The average diameter of the polymer cubosomes was measured by DLS: the average diameter of the polymer cubosomes changed from 1044 nm in water to 1244 nm in THF.

The intensity of the scattered light from the THF dispersion of the polymer cubosomes indicated the presence of polymer cubosomes in the dispersion without dissociation to individual block copolymers. When the medium was changed from THF and water, the average diameter was again changed to 1100 nm. This change of the average diameter of polymer cubosomes in solution suggested the covalent

stabilization of the self-assembled structures by cross-linking (Figure 3-7A). Differential scanning calorimetry (DSC) experiments of the pristine and cross-linked particles of PEG550$_3$-PI(*1,2*)(10K)$_2$ showed an increase of the T_g from 12 ℃ for the pristine particles to 37 ℃ for the cross-linked particles, indicating the formation of covalent bonds between the PI chains (Figure 3-7B).

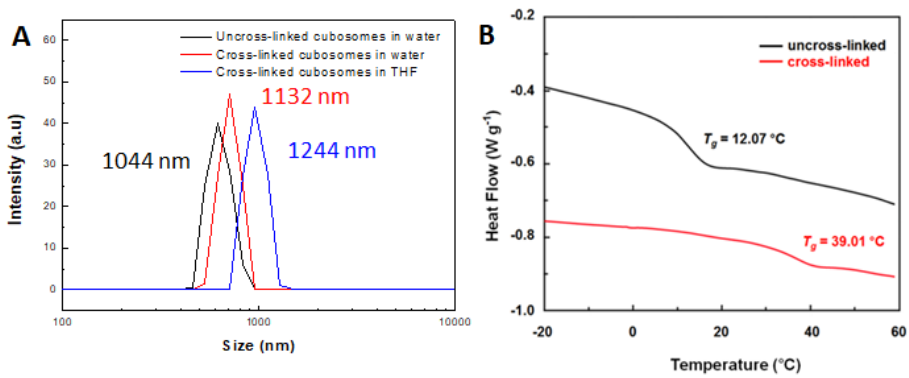

Figure 3-7. (A) DLS result of the cross-linked polymer cubosomes of PEG550$_3$-PI(*1,2*)(10K)$_2$ under exchanging the solvent from water to THF. (B) DSC traces of the uncross-linked particles (black) and cross-linked particles (red) of PEG550$_3$-PI(*1,2*)(10K)$_2$.

SEM images of the cross-linked polymer cubosomes (average diameter measured by DLS = ca. 1 μm) showed a presence of surface pores on the spherical particles. (Figure 3-8A and 3-8B). Although the cross-linking was effective to maintain the assembled morphology of BCPs having low T_g, we were unable to confirm the intact surface pore of inverse nanoparticles presumably due to structural damage during irradiation with the electron beam. Conventional TEM and cryo-TEM images showed that these polymer cubosomes possess internal cubic mesophases of BCP bilayers (Figure 3-8C and 3-8D).

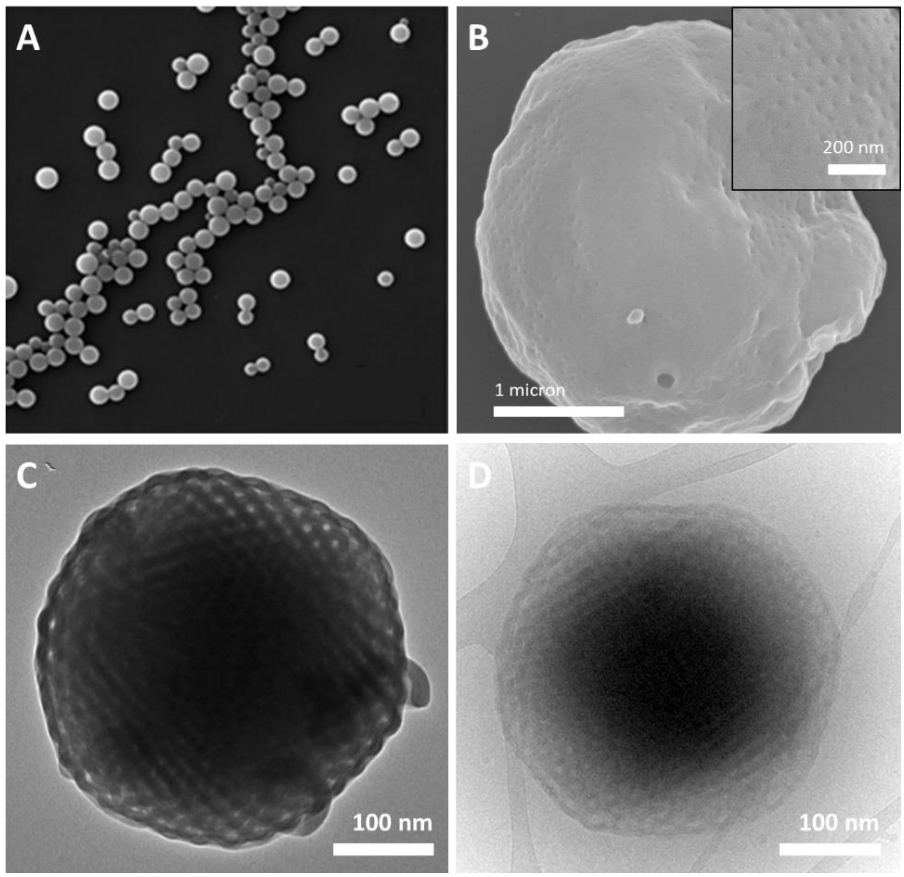

Figure 3-8. (A and B) SEM, (C) TEM, (D) cryo-TEM images of cross-linked polymer cubosomes of $PEG550_3$-PI(*1,2*)$(10K)_2$ after exchanging the solvent from water to THF.

TEM image of the polymer cubosomes of $PEG550_3$-PI(*1,2*)$(10K)_2$ dried from the THF solution showed well-defined periodic minimal surface structures (Figure 3-9A). According to the small-angle X-ray scattering (SAXS) result of the cross-linked polymer cubosomes, the peaks corresponding to double diamond structures ($Pn\bar{3}m$ space group, a = 43.8 nm) were observed, indicating that the cross-linking of vinyl pendants in PI chains could covalently stabilize the complex 3-D periodic structures (Figure 3-9B).

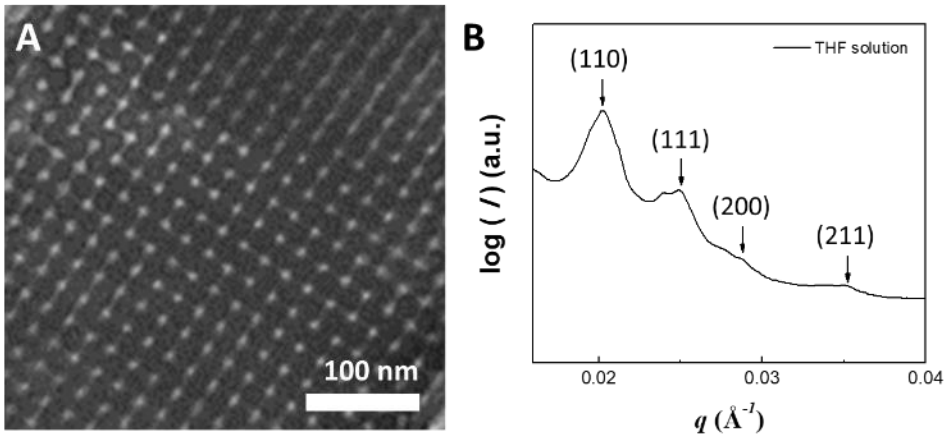

Figure 3-9. (A) TEM image of cross-linked polymer cubosomes (*Pn*$\bar{3}$*m)* viewed along the [100] direction. (B) small-angle X-ray scattering (SAXS) results obtained from the dried cross-linked polymer cubosomes of PEG550$_3$-PI(*1,2*)(10K)$_2$ after soaking in THF (*Pn*$\bar{3}$*m* symmetry, a = 43.8 nm).

3.4 Conclusion

In summary, we synthesized a series of BCPs by adopting the modular synthesis of branched PEG hydrophilic and linear/ branched PI hydrophobic structural modules. The PI chains were used for their low T_g and the ability to form covalent bonds between the PI chains by radical-mediated coupling of their pendant vinyl groups. Structural factors of the BCPs such as the block ratio and the length of the hydrophobic polymer chains were investigated in order to form inverse mesophases by solution self-assembly. At the same block ratio, the direct reduction of the hydrophobic polymer chain length by adopting a branched architecture confirmed that this structural parameter plays a crucial role in determining the phase of self-assembled structures from polymersomes to inverse mesophases. We also showed morphological changes in self-assembled structures by controlling the block ratio of

BCPs by adopting various PI chains with different molecular weight. In particular, we found the formation of polymer cubosomes by the solution self-assembly of $PEG550_3$-PI(*1,2*)$(10K)_2$.The change of the microstructure of the PI chains reduced the chain length without altering the molecular weight and the volume of the hydrophobic block. Overall, these results indicate that the structural parameters of PEG-PI BCPs could be adjusted to favor the formation of inverse cubic mesophases in solution. The pendant vinyl groups of the PI chains having a 1,2-rich microstructure allowed the self-assembled mesophases to be covalently stabilized by photo-induced cross-linking of the PI chains. After irradiation by UV light (365 nm), the resulting nanostructures maintained their structural integrity in organic solvents. Our study is likely to should contribute to the development of well-defined porous polymers of which their mechanical properties such as toughness and elasticity could be optimized for various applications such as ultrafiltration and separation.

3.5 References

1. Wu, D.; Xu, F.; Sun, B.; Fu, R.; He, H.; Matyjaszewski, K. Design and Preparation of Porous Polymers. *Chem. Rev.* **2012,** *112,* 3959−4015.
2. Shannon, M. A.; Bohn, P. W.; Elimelech, M.; Georgiadis, J. G.; Mariñas, B. J.; Mayes, A. M. Science and technology for water purification in the coming decades. *Nature* **2008,** *452,* 301−310.
3. Tokarev, I.; Minko, I. Multiresponsive, hierarchically structured membranes: new, challenging, biomimetic materials for biosensors, controlled release, biochemical gates, and nanoreactors. *Adv. Mater.* **2009,** *21,* 241−247.

4. Svec, F. Porous polymer monoliths: amazingly wide variety of techniques enabling their preparation. *J. Chromatogr. A* **2010,** *1217,* 902−924.
5. Nischang, I.; Teasdale, I; Brüggemann, O. Porous polymer monoliths for small molecule separations: advancements and limitations. *Anal. Bioanal. Chem.* **2011,** *400,* 2289−2304.
6. Salentinig, S.; Phan, S.; Hawley, A.; Boyd, B. J. Self-Assembly Structure Formation during the Digestion of Human Breast Milk. *Angew. Chem. Int. Ed.* **2015,** *127,* 1620−1623.
7. Sun, Q.; Dai, Z.; Meng, X.; Xiao, F. -S. Porous polymer catalyst with hierarchical structures. *Chem. Soc. Rev.* **2015,** *44,* 6018−6034.
8. Allen, S. D.; Bobbala, S.; Karabin, N. B.; Scott, E. A. On the advancement of polymeric bicontinuous nanospheres toward biomedical applications. *Nanoscale Horiz.* **2019,** *4,* 258−272.
9. Phillip, W. A.; Dorin, R. M.; Werner, J.; Hoek, E. M.; Wiesner, U.; Elimelech, M. Tunning structure and properties of graded triblock terpolymer-based mesoporous and hybrid films. *Nano Lett.* **2011,** *11,* 2892−2900.
10. McKenzie, B. E.; Friedrich, H.; Wirix, M. J.; de Visser, J. F.; Monaghan, O. R.; Bomans, P. H.; Nudelman, F.; Holder, S. J.; Sommerdijk, N. A. J. M. Controlling Internal Pore Sizes in Bicontinuous Polymeric Nanospheres. *Angew. Chem. Int. Ed.* **2015,** *54,* 2457−2461.
11. Groschel, A. H.; Walther, A. Block Copolymer Micelles with Inverted Morphologies. *Angew. Chem. Int. Ed.* **2017,** *56,* 10992−10994.
12. La, Y.; Song, J.; Jeong, M. G.; Cho, A.; Jin, S.; Lee, E.; Kim, K. T. Templated synthesis of cubic crystalline single networks having large open-space lattices by polymer cubosomes. *Nat. Commun.* **2018,** *9,* 5327−5335.

13. Holder, S. J.; Woodward, G.; McKenzie, B.; Sommerdijk, N. A. J. M. Semi-crystalline block copolymer bicontinuous nanospheres for thermoresponsive controlled release. *RSC Adv.* **2014,** *4,* 26354−26358.
14. Peinemann, K. -V.; Abetz, V.; Simon, P. F. W. Asymmetric superstructure formed in a block copolymer via phase separation. *Nat. Mater.* **2007,** *6,* 992−996.
15. Jung, A.; Rangou, S.; Abetz, C.; Filiz, V.; Abetz, V. Structure Formation of Integral Asymmetric Composite Membrane of Polystyrene-*block*-Poly(2-vinylpyridine) on a Nonwoven. *Macromol. Mater. Eng.* **2012,** *297,* 790−798.
16. Hahn, J.; Filiz, V.; Rangou, S.; Clodt, J.; Jung, A.; Buhr, K.; Abetz, C.; Abetz, V. Structure formation of integral-asymmetric membranes of polystyrene-*block*-poly(ethylene oxide). *J. Polym. Sci., Part B: Polym. Phys.* **2013,** *51,* 281−290.
17. Sai, H.; Tan, K. W.; Hur, K.; Asenath-Smith, E.; Hovden, R.; Jiang, Y.; Riccio, M.; Muller, D. A.; Elser, V.; Estroff, L. A.; Gruner, S. M.; Wiesner, U. Hierarchical Porous Polymer Scaffolds from Block Copolymers. *Science* **2013,** *341,* 530−534
18. Jackson, E. A.; Hillmyer, M. A. Nanoporous Membranes Derived from Block Copolymers: From Drug Delivery to Water Filtration. *ACS nano* **2010,** *4,* 3548−3553.
19. Querelle, S. E.; Jackson, E. A.; Cussler, E. L.; Hillmyer, M. A. Ultrafiltration
    Membranes with a Thin Poly(styrene)-*b*-poly(isoprene) Selective Layer. *ACS appl. Mater. Interfaces* **2013,** *5,* 5044−5050.
20. Lee, H.-C.; Hsueh, H.-Y.; Jeng, U.-S.; Ho, R.-M. Functionalized Nanoporous Gyroid SiO_2 with Double-Stimuli-Responsive Properties as Environment-Selective Delivery systems. *Macromolecules* **2014,** *47,* 3041−3051.

21. La, Y.; Park, C.; Shin, T. J.; Joo, S. H.; Kang, S.; Kim, K. T. Mesoporous monoliths of inverse bicontinuous cubic phases of block copolymer bilayers. *Nat. Chem.* **2014,** *6,* 534−541.
22. Park, C.; La, Y.; An, T. H.; Jeong, H. Y.; Kang, S.; Joo, S. H.; Kang, S.; Kim, K. T. Colloidal inverse bicontinuous cubic membranes of block copolymers with tunable surface functional groups. *Nat. Commun.* **2015,** *6,* 6392−6400.
23. An, T. H.; La, Y.; Cho, A.; Jeong, M. G.; Shin, T. J.; Park, C.; Kim, K. T. Solution Self-Assembly of Block Copolymers Containing a Branched Hydrophilic Block into Inverse Bicontinuous Cubic Mesophases. *ACS Nano* **2015,** *9,* 3084−3096.
24. La, Y.; An, T. H.; Shin, T. J.; Park, C.; Kim, K. T. A Morphological Transition of Inverse Mesophases of a Branched-Linear Block Copolymer Guided by Using Cosolvents. *Angew. Chem. Int. Ed.* **2015,** *54,* 10483−10487.
25. Cho, A.; La, Y.; Shin, T. J.; Park, C.; Kim, K. T. Structural Requirements of Block Copolymers for Self-Assembly into Inverse Bicontinuous Cubic Mesophases in Solution. *Macromolecules* **2016,** *49,* 4510−4519.
26. Cho, A.; La, Y.; Jeoung, S.; Moon, H. R.; Ryu, J, -H.; Shin, T. J.; Kim, K. T. Mix-and-Match Assembly of Block Copolymer Blends in Solution. *Macromolecules* **2017,** *50*, 3234−3243.
27. Larsson, K. Cubic lipid-water phases: structures and biomembrane aspects. *J. Phys. Chem.* **1989,** *93,* 7304−7314.
28. Gustafsson, J.; Ljusberg-Wahren, H.; Almgren, M.; Larsson, K. Cubic Lipid-Water Phase Dispersed into Submicron Particles. *Langmuir* **1996,** *12,* 4611−4613.
29. Gustafsson, J.; Ljusberg-Wahren, H.; Almgren, M.; Larsson, K. Submicron Particles of Reversed Lipid Phases in Water Stabilized by a Nonionic Amphiphilic Polymer. *Langmuir* **1997,** *13,* 6964−6971.

30. Spicer, P. T. Progress in liquid crystalline dispersions: Cubosomes. *Curr. Opin. in Colloid Interface Sci.* **2005,** *10,* 274−279.
31. Barauskas, J.; Johnsson, M; Tiberg, F. Self-Assembled Lipid Superstructures: Beyond Vesicles and Liposomes. *Nano lett.* **2005,** *5,* 1615−1619.
32. Barauskas, J.; Johnsson, M.; Joabsson, F.; Tiberg, F. Cubic Phase Nanoparticles: Principles for Controlling Size, Structure, and Stability. *Langmuir* **2005,** *21,* 2569−2577.
33. Almsherqi, Z. A.; Kohlwein, S. D.; Deng, Y. Cubic membranes: a legend beyond the Flatland* of cell membrane organization. *J. Cell Biol.* **2006,** *173,* 839−844.
34. Jeong, M. G.; Kim, K. T. Covalent Stabilization of Inverse Bicontinuous Cubic Structures of Block Copolymer Bilayers by Photodimerization of Indene Pendant Groups of Polystyrene hydrophobic Blocks. *Macromolecules* **2017,** *50,* 223−234.
35. Kanai, T.; Yamamoto, S.; Sawada, T. Swelling of Gel-Immobilized Colloidal Photonic Crystals in Ionic Liquids. *Macromolecules* **2011,** *44,* 5865−5867.
36. Smith, L. C.; Lind, J. U.; Nielsen, C. H.; Christiansen, M. B.; Buss, T.; Larsen, N. B.; Kristensen, A. Enhanced transduction of photonic crystal dye lasers for gas sensing via swelling polymer film. *Opt. Lett.* **2012,** *36,* 1392−1394.
37. Zhang, Y.; Fu, Q.; Ge, J. Photonic sensing of organic solvents through geometric study of dynamic reflection spectrum. *Nat. Commun.* **2015,** *6,* 7510−7516.
38. Lencki, R. W.; Williams, S. Effect of nonaqueous solvents on the flux behavior of ultrafiltration membranes. *J. Memb. Sci.* **1995,** *101,* 43−51.

39. Jeong, M. G.; van Hest, J. C. M.; Kim, J. T. Self-assembly of dendritic-linear block copolymers with fixed molecular weight ratio. *Chem. Commun.* **2012,** *48,* 3590−3592.
40. Percec, V.; Peterca, M.; Tadjiev, T.; Zeng, X.; Ungar, G.; Leowanawat, P.; Aqad, E.; Imam, M. R.; Rosen, B. M.; Akbey, U.; Graf, R.; Sekharan, S.; Sebastiani, D.; Spiess, H. W.; Heiney, P. A.; Hudson, S. D. Self-Assembly of Dendronized Perylene Bisimides into Complex Helical Columns. *J. Am. Chem. Soc.* **2011,** *133,* 12197−12219.
41. Touris, A.; Mays, J. W.; Hadjichristidis, N. Acetylene-Functionalzed Lithium Initiators for Anionic Polymerization. Powerful Precursors for "Click" Chemistry. *Macromolecules* **2011,** *44,* 1886−1893.
42. Israelachvili, J. N.; Mitchell, J.; Ninham, B. W. Theory of self-assembly of hydrocarbon amphiphiles into micelles and bilayers. *J. Chem. Soc., Faraday Trans. 2* **1976,** *72,* 1525−1568.
43. Zhang, L.; Eisenberg, A. Multiple Morphologies of "Crew-Cut" Aggregates of Polystyrene-*b*-poly(acrylic acid) Block Copolymers. *Science* **1995,** *268*, 1728−1731.
44. Mai, Y.; Eisenberg, A. Self-assembly of block copolymers *Chem. Soc. Rev.* **2012,** *41,* 5969−5985.
45. McKenzie, E.; Nudelman, F.; Bomans, P. H. H.; Holder, S. J.; Sommerdijk, N. A. J. M. Temperature-Responsive Nanospheres with Bicontinuous Internal Structures from a Semicrystalline Amphiphilic Block Copolymer. *J. Am. Chem. Soc.* **2010,** *132*, 10256−10259.
46. Demurtas, D.; Guichard, P.; Martiel, I.; Mezzenga, R.; Hébert, C.; Sagalowicz, L. Direct visualization of dispersed lipid bicontinuous cubic phases by cryo-electron tomography. *Nat. Commun.* **2015,** *6*, 8915.

47. Ohsuna, T.; Sakamoto, Y.; Terasaki, O.; Kuroda, K. TEM image simulation of mesoporous crystals for structure type identification. *Solid State Sciences* **2011,** *13,* 736−744.

Chapter 4. Block Copolymers Composed of Main-Chain Cyclic Polymers: Morphology Transition and Covalent Stabilization of Self-Assembled Nanostructures via Intra- and Interchain Cyclization of Styrene-*co*-Isoprene Blocks

4.1 Abstract

Amorphous saturated hydrocarbon polymers containing main-chain cyclic units have potential as novel optoelectronic materials for plastic lenses and optical storage media owing to their high glass transition temperature, nonhygroscopic nature, transparency, and low birefringence. Here, we report the synthesis of block copolymers (BCPs) incorporating a branched polyethylene glycol (PEG) hydrophilic block and randomly copolymerized styrene and isoprene units (p(St-*co*-Ip)) of different molecular weights as the hydrophobic component. Amorphous polymers bearing cyclic structures along hydrophobic chains were prepared via the cationic cyclization of the unsaturated hydrocarbon polymers under acidic conditions. We suggest that the morphological transitions of self-assembled BCP structures are dependent on changes in the chain length of the hydrophobic block, which is determined by the regiospecificity of the isoprene units. The self-assembled structures could be covalently stabilized via intermolecular cyclization between the hydrophobic blocks. Notably, the cross-linked structures displayed a reversible swelling/deswelling ability in response to the type of solvent medium.

4.2 Introduction

Amorphous hydrocarbon polymers with cyclic structures along their main chains have received significant attention as optical materials because of their nonhygroscopic nature, good thermal properties, and transparency.[1,2] In addition, compared with conventional materials such as poly(methyl methacrylate) and polycarbonate, amorphous saturated hydrocarbon polymers containing main-chain cyclic units can potentially be employed as novel optoelectronic materials for plastic lenses and optical storage media owing to their excellent properties such as a high glass transition temperature (T_g) and low birefringence.[3]

One of widely used methods for producing amorphous polymers consisting of cyclic units is the cationic cyclization of unsaturated hydrocarbon polymers under acidic conditions via carbocationic intermediates.[4-8] Kamigaito and co-workers reported that a styrene-diene copolymer can be treated with a strong Brönsted acid (CF_3SO_3H) to induce Friedel–Crafts alkylation between adjacent diene–styrene units to form a rigid tetrahydronaphthyl bicyclic main-chain structure.[9-11] This intramolecular cyclization in the main chain leads to a high T_g and robust mechanical properties for the random copolymer. The synthesis of thermally and optically high-performance plastics from styrene (St) and isoprene (Ip) through the intramolecularly cyclized random St-Ip polymers have been studied.[12-16] Furthermore, postpolymerization modification reactions that change the main-chain structures of existing polymers can lead to new applications.[17-20]

The control of the structures of nanomaterials allow the fine-tuning of their physical and chemical properties.[21-28] The self-assembly of block copolymers in solutions has been a method to generate soft nanostructures of controlled size, morphology, and chemical functionalities via the synthesis of building block BCPs with controlled structural parameters such as

chemistries and molecular weights of constituent polymer blocks.[29-43] To the best of our knowledge, nanostructures constructed via the self-assembly of amphiphilic block copolymers (BCPs) consisting of amorphous hydrocarbon polymers with main-chain cyclic units have not been investigated. The controlled construction of nanostructures possessing excellent optoelectronic properties could provide novel physical properties and improve device performance for potential optoelectronic applications.

Here, we report the synthesis of BCPs composed of identical branched hydrophilic polyethylene glycol (PEG) blocks and a series of randomly copolymerized styrene and isoprene (p(St-*co*-Ip)) hydrophobic blocks with different molecular weights. Cationic cyclization of the unsaturated hydrocarbon polymers under acidic conditions via Friedel–Crafts alkylation produced amorphous polymers containing main-chain cyclic units as hydrophobic blocks. A variety of nanostructures such as polymer vesicles, sponge structures, and polymer cubosomes were prepared from BCPs with different molecular ratios between the hydrophobic and hydrophilic blocks. We found that reducing the length of the hydrophobic blocks via Friedel–Crafts cyclization induced morphological transitions of the self-assembled structures. In addition, we discovered that intermolecular cyclization covalently stabilized the self-assembled structures. Moreover, the cross-linked nanoparticles retained their structural integrity in response to external stimuli such as solvents.

4.3 Results and Discussion

Design and synthesis of block copolymers

As hydrophobic blocks, random copolymers of styrene and isoprene, p(St-*co*-Ip), were prepared via living anionic copolymerization using *n*-butyllithium as an initiator. To obtain a random and less blocky monomer sequence, the premixed styrene and isoprene monomers were slowly added to cyclohexane (20 mL) containing a small amount of THF (15 μL) as a randomizer.[44-46] After stirring the reaction mixture for 1 h at 40°C, the polymerization was quenched with 1-chloro-5-triethylsilyl-4-pentyne to provide a protected acetylene group at each chain end, thus affording the random copolymer p(St-*co*-Ip)(1,4) (Scheme 4-1). The polymer was purified by precipitation in methanol. ^{1}H NMR analysis showed that the comonomer composition ratio in the obtained copolymer was consistent with the initial feed ratio (styrene content = ~54%). The isoprene units in p(St-*co*-Ip) displayed microstructures predominantly composed of 1,4-polymerized repeating units (1,4:1,2:3,4 = 70–73:0:27–30) along the copolymer chain (Table 4-1), which was identified and quantified by integrating the peaks in the ^{1}H and ^{13}C NMR spectra (Figure S8). In C^{13} NMR, a decrease in the peaks (41–42 ppm) corresponding to the main-chain α-carbon of the mid-styrene unit in the styrene sequence indicated fewer consecutive styrene units in the random copolymers (Figure 4-1).

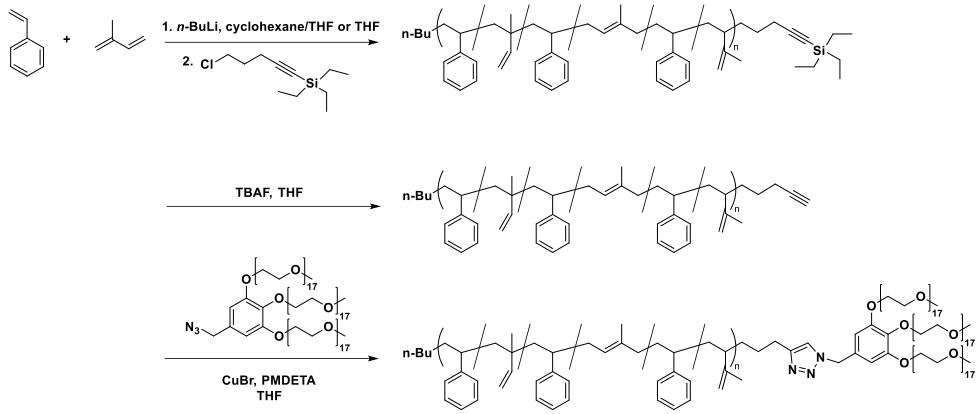

Scheme 4-1. Synthesis of p(St-*co*-Ip)-*b*-PEG750$_3$ random block copolymers composed of branched hydrophilic PEG blocks and linear hydrophobic random copolymer blocks. Polymerization conditions: cyclohexane/THF for p(St-*co*-Ip)(1,4) and THF for p(St-*co*-Ip)(3,4).

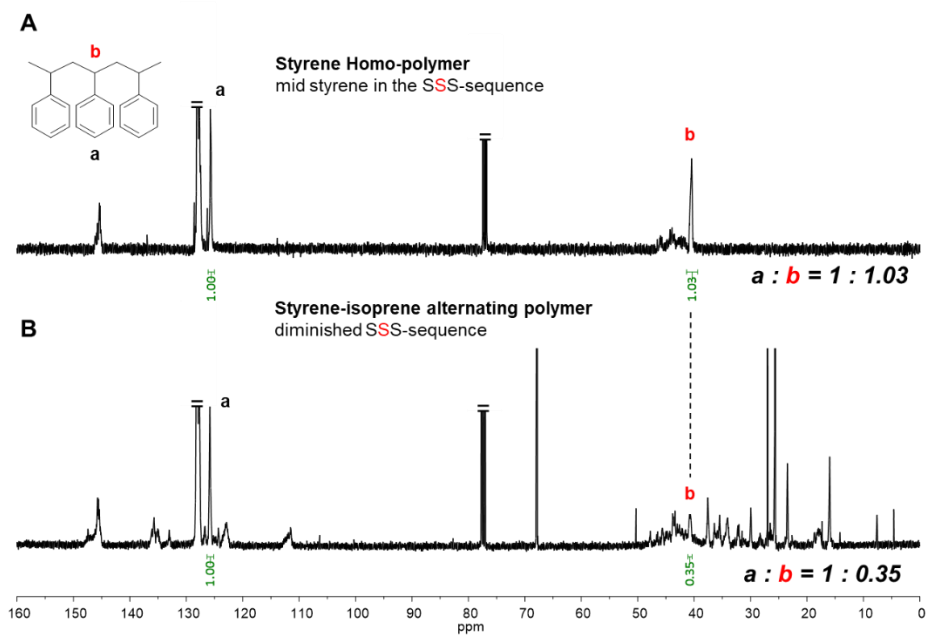

Figure 4-1. ^{13}C NMR spectra of (A) polystyrene and (B) random copolymer p(St-*co*-Ip)(1,4). The signals (a) at 125.0-126.3 ppm were assigned to para-positioned carbons of the styrene unit, while the signals (b) at 40.2-41.4 ppm was to the main chain α-carbon of the mid-styrene unit un the SSS-sequence.

Table 4-1. Characteristics of hydrophobic and amphiphilic block copolymers.

Entry	Dominant microstructure	p(St-*co*-Ip)				p(St-*co*-Ip)-*b*-PEG750$_3$		
		M_n (g mol^{-1})[a]	$Đ$ [a]	1,4:1,2:3,4[b]	f_{St} (%)[c]	M_n (g mol^{-1})[a]	$Đ$ [a]	f_{PEG} (%)[d]
1	p(St-*co*-Ip)(1,4)	14500	1.036	70:0:30	54	15300	1.044	16.0
2		20700	1.038	69:0:31	52	21200	1.045	11.2
3		24200	1.034	73:0:27	49	25000	1.039	9.8
4	p(St-*co*-Ip)(3,4)	13100	1.159	0:29:71	48	14200	1.162	16.2
5		18300	1.133	0:28:72	50	19200	1.132	12.8
6		22800	1.166	0:25:75	51	23600	1.184	10.4

[a]Number average molecular weight (M_n) and molecular weight distribution ($Đ$) determined by GPC using polystyrene (PS) standards. Elution was performed with THF at a flow rate of 1 mL min^{-1} at 30 °C. [b]DP_n determined by ^{1}H NMR integration. [c]Molecular weight fraction of the PS domain relative to the hydrophobic block. [d]Molecular weight fraction of the PEG domain relative to the amphiphilic block copolymer.

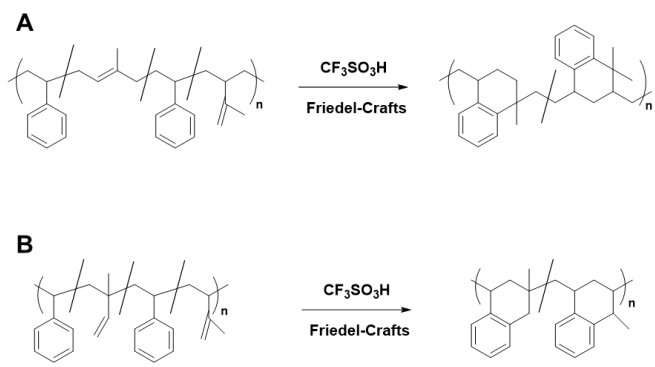

Scheme 4-2. Intramolecular Friedel–Crafts cyclization of random copolymers (A) p(St-*co*-Ip)(1,4) and (B) p(St-*co*-Ip)(3,4) under a strong acid (CF_3SO_3H).

To investigate intramolecular Friedel–Crafts cyclization, the well-controlled cyclization of random copolymers was used to obtain cycloolefin copolymer analogues. A strong Brönsted acid (CF_3SO_3H) was employed as a catalyst for the intramolecular cyclization of p(St-*co*-Ip) (Scheme 4-2). Under

acidic conditions, the protonated isoprene units can react with the *ortho*-position of the benzene ring in an adjacent styrene unit to form a rigid tetrahydronaphthyl bicyclic structure. The thus-formed polymers were obtained as powdery compounds (Figure S10). ^{1}H NMR analysis showed that the signals for the olefin protons of the isoprene units in the random copolymers (4.3–5.3 ppm for 1,4- and 3,4-microstructure, and 5.5–6.0 ppm for 1,2-microstructures) dramatically decreased in the corresponding cyclized products, and the peaks of the aromatic protons (6.0–7.4 ppm) became broader (Figure S11A). In addition, the molecular weight of the polymer slightly decreased and the peaks broadened after cyclization owing to a reduction in hydrodynamic volume (Figure S11B).

Branched hydrophilic block, PEG750$_3$-N$_3$ was prepared by the previously reported procedure.[47,48] To synthesize BCPs composed of branched hydrophilic PEG blocks and hydrophobic p(St-*co*-Ip) blocks, the triethylsilyl protecting group was removed from the random copolymers using tetrabutylammonium fluoride, thus providing the hydrophobic chain with an acetylene end group. BCPs containing p(St-*co*-Ip)-*b*-PEG750$_3$ with varying isoprene microstructures were synthesized by a Cu(I)-catalyzed click reaction between the hydrophilic and hydrophobic components in THF (Scheme 4-1). ^{1}H NMR analysis confirmed the successful synthesis of the expected BCP (Figure 4-2A). Additionally, for the resulting BCP showed, GPC revealed a unimodal peak with a narrow distribution (Figure 4-2B). Subsequently, the CF_3SO_3H-catalyzed intramolecular cyclization of p(St-*co*-Ip)-*b*-PEG750$_3$ was performed, similar to that of p(St-*co*-Ip). A comparison of the ^{1}H NMR spectra of the amphiphilic BCP, p(St-*co*-Ip)-*b*-PEG750$_3$, and the corresponding cyclized product showed that cyclization resulted in the complete consumption of the signals corresponding to the olefin protons of isoprene (Figure S15).

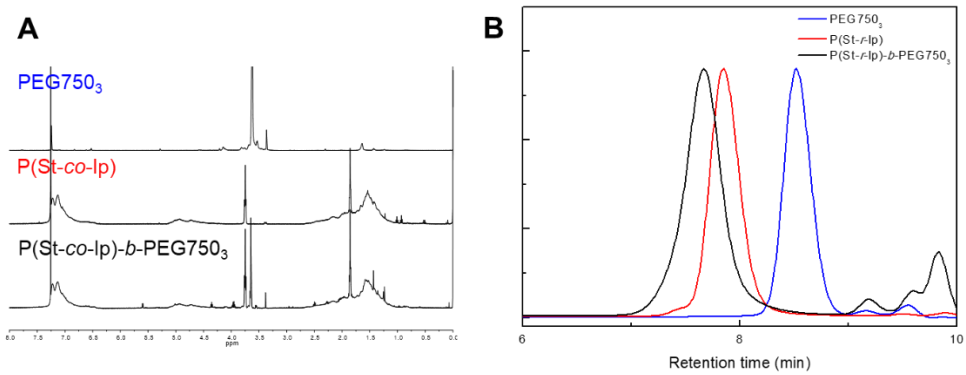

Figure 4-2. (A) ^{1}H NMR spectra and (B) GPC spectra of the block copolymer p(St-*co*-Ip)(1,4)-*b*-PEG750$_3$ (black) synthesized by click chemistry between PEG (blue) and p(St-*co*-Ip) (red).

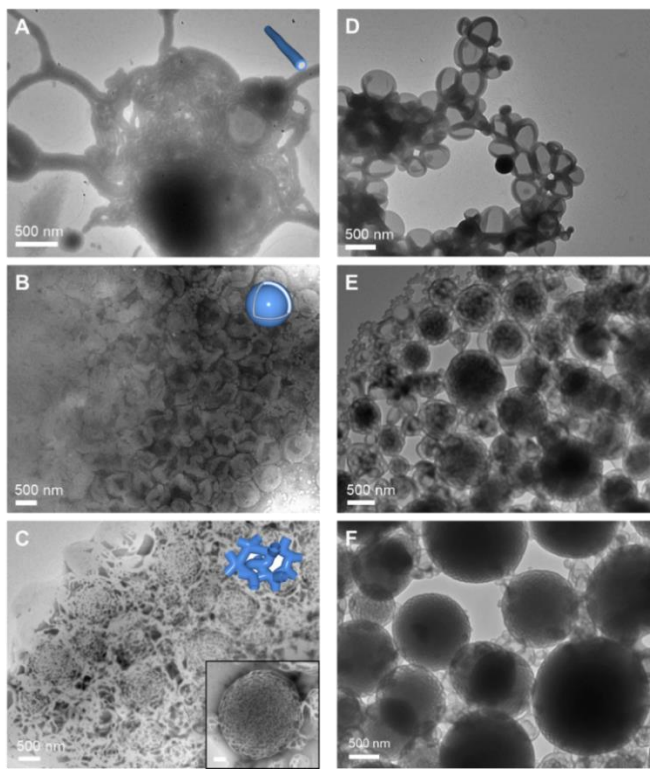

Figure 4-3. TEM images of the self-assembled structures of (A, B, and C) p(St-*co*-Ip)(1,4)-*b*-PEG750$_3$ (M_n = 15.3k, 21.2k, and 25.0k) and (D, E, and F) their cyclized products. The structures of p(St-*co*-Ip)(1,4)-*b*-PEG750$_3$ (A to C) were treated with phosphotungstic acid solution for negative staining.

Morphologies of the self-assembled structures of p(St-*co*-Ip)(1,4)-*b*-PEG750$_3$ and the corresponding cyclized products

The BCPs were composed of identical hydrophilic blocks and a series of p(St-*co*-Ip) blocks with different molecular weights. The prepared BCPs were dissolved in dioxane as a common solvent at a concentration of 5 mg mL^{-1}. Then, to construct nanostructures, distilled water as a selective solvent was slowly added at a rate of 0.5 mL h^{-1} via a syringe pump. The TEM images of the self-assembled structures revealed that p(St-*co*-Ip)(1,4)-*b*-PEG750$_3$ (M_n = 15.3k, 21.2k, and 25.0k) self-assembled into cylindrical micelles, vesicles, and sponge phases respectively (Figure 4-3A to 4-3C). In addition, the morphologies of the self-assembled structures were confirmed by cryo-TEM (Figure S16).

Table 4-2. Characteristics of p(St-*co*-Ip)-*b*-PEG750$_3$ random copolymers and their cyclized products.

Entry	Before Friedel–Crafts cyclization			After Friedel–Crafts cyclization		
	M_n (g mol^{-1})[a]	$Đ$ [a]	Morphology	M_n (g mol^{-1})[a]	$Đ$ [a]	Morphology
1	15300	1.044	Cylindrical micelles	13800	1.128	Vesicles
2	21200	1.045	Vesicles	18200	1.125	Sponge phase
3	25000	1.039	Sponge phase	22200	1.133	Cubosomes
4	14200	1.162	Spherical micelles	13600	1.232	Spherical micelles
5	19200	1.132	Vesicles	18700	1.233	Vesicles
6	23600	1.184	Cubosomes	22900	1.263	Cubosomes

[a]Number average molecular weight (M_n) and molecular weight distribution ($Đ$) determined by GPC using polystyrene (PS) standards. Elution was performed with THF at a flow rate of 1 mL min^{-1} at 30 °C. [b]DP_n determined by ^{1}H NMR integration.

We discovered that intramolecular Friedel–Crafts cyclization induced morphological transitions of the self-assembled structures (Figure 4-4). For intramolecularly cyclized p(St-*co*-Ip)(1,4)-*b*-PEG750$_3$, nanostructures were constructed using the cosolvent method. At the early stage of self-assembly, the hydrophobic chains are surrounded with dioxane molecules and the compartment is in a swollen-state at this point. Under this experiment condition, the rigidity of polymers after cyclization of the unsaturated hydrocarbon polymers does not significantly affect the morphology of the self-assembled structures of BCPs. After dialysis against water, the self-assembled BCP structures were observed by TEM (Figure 4-3D to 4-3F). After cyclization, the cylindrical micelles of p(St-*co*-Ip)-*b*-PEG750$_3$ (M_n = 15.3k) became polymer vesicles, the vesicles of p(St-*co*-Ip)-*b*-PEG750$_3$ (M_n = 21.2k) transformed into sponge structures, and the sponge structures of p(St-*co*-Ip)-*b*-PEG750$_3$ (M_n = 25.0k) became polymer cubosomes. The morphological transitions of the self-assembled structures of p(St-*co*-Ip)(1,4)-*b*-PEG750$_3$ and their cyclized products are summarized in Table 4-2.

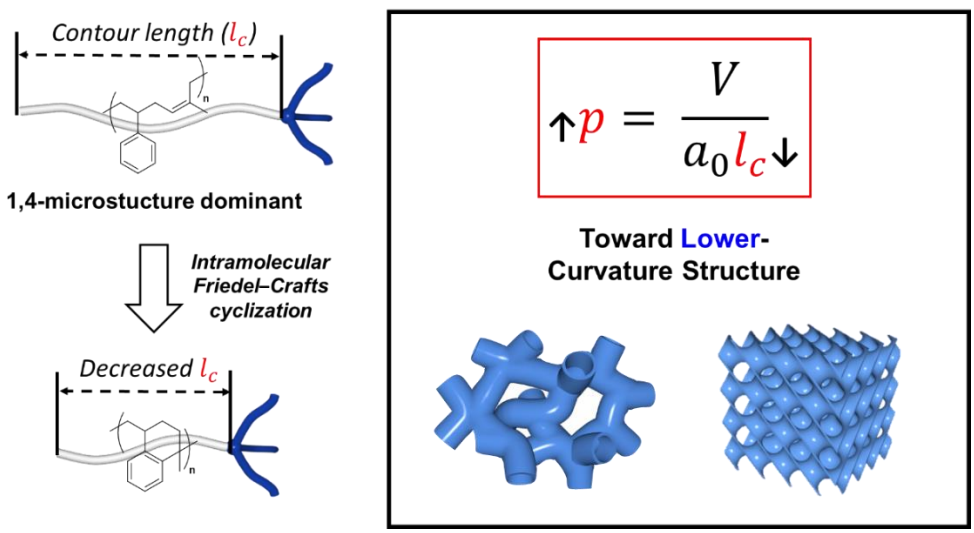

Figure 4-4. Schematic representation of the morphological transitions of self-assembled structures of p(St-*co*-Ip)-*b*-PEG750$_3$ random block copolymer after cyclization.

To explain this phenomenon, we suggest that the tetrahydronaphthyl bicyclic structures caused by Friedel–Crafts cyclization led to a decrease in the chain length (l_c) of the hydrophobic block. The chain length change after complete cyclization was theoretically calculated (Table 4-3). As the volume of the hydrophobic polymer block (V) and the interfacial area at the junction between the two polymer blocks (a_0) remain constant, the architectural effect of decreasing l_c is an increased packing parameter (p) for the BCP.[49-53] Therefore, the Friedel–Crafts cyclization of p(St-*co*-Ip)(1,4)-*b*-PEG750$_3$ induces morphological transitions of the self-assembled structures toward lower-curvature nanostructures.

Furthermore, we measured the thicknesses of the bilayer membranes of the self-assembled structures before and after the cyclization process. The TEM image of the sponge structures of p(St-*co*-Ip)(1,4)-*b*-PEG750$_3$ (M_n = 25.0k) reveals a bilayer membrane with a thickness of ~34 nm (Figure 4-5A). In comparison, the TEM image of the polymer cubosomes of its cyclized polymer exhibit a bilayer consisting of inverse cubic mesophases with a thickness of ~19 nm (Figure 4-5B). In the self-assembled structures, the thickness of the bilayer membrane was obviously decreased after intramolecular Friedel–Crafts cyclization, which can be attributed to the reduced chain length of the hydrophobic block.

Table 4-3. Theoretical calculation of chain length change after intramolecular cyclization.

Entry	M_n (g/mol)[a]	1,4-:1,2-:3,4-[b]	Δl^c *(nm)*
1	14500	70:0:30	5.35
2	20700	69:0:31	7.53
3	24200	73:0:27	9.32
4	13100	0:29:71	0
5	18300	0:28:72	0
6	22800	0:25:75	0

[a]Number average molecular weight (M_n) and molecular weight distribution (D) determined by GPC using polystyrene (PS) standards. Elution was performed with THF at a flow rate of 1 mL/min at 30 °C. [b]DP_n determined by ^{1}H NMR integration. [c]Theoretical calculation of chain length change after complete cyclization.

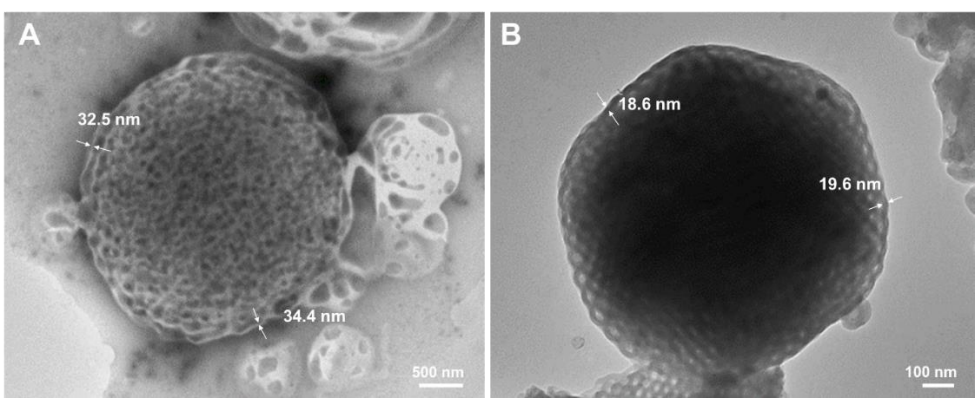

Figure 4-5. TEM images of self-assembled structures showing the thickness of the bilayer membrane: (A) sponge structures of p(St-*co*-Ip)(1,4)-*b*-PEG750$_3$ (M_n = 25.0k) (negatively stained) and (B) polymer cubosomes of its cyclized product.

Morphologies of the self-assembled structures of p(St-*co*-Ip)(3,4)-*b*-PEG750$_3$ and the corresponding cyclized products

We suggested that the morphological change observed for p(St-*co*-Ip)(1,4)-*b*-PEG750$_3$ is driven by a change in the length of the p(St-*co*-Ip) chains via intramolecular cationic cyclization. However, Friedel–Crafts alkylation between 1,2- or 3,4-isoprene units and the benzene ring of an adjacent styrene unit is not expected to change the length of the hydrophobic block. Therefore, as a control experiment to confirm our hypothesis, we synthesized p(St-*co*-Ip)(3,4) random copolymers, which were composed of 1,2- and 3,4-microstuctures with pendant vinyl groups (1,4:1,2:3,4 = 0:25–29:71–75) (Table 4-1). Subsequently, the corresponding BCPs and their cyclized products were self-assembled. The TEM images of the self-assembled structures revealed that p(St-*co*-Ip)(3,4)-*b*-PEG750$_3$ (M_n = 14.2k and 19.2k) self-assembled into spherical micelles and vesicles, respectively (Figure 4-5A and 4-5B), whereas p(St-*co*-Ip)(3,4)-*b*-PEG750$_3$ (M_n = 23.6k) formed polymer cubosomes (Figure 4-5C). After intramolecular cyclization, no changes in morphology were observed (Figure 4-5D to 4-5F). In addition, TEM imaging showed that the thickness of the bilayer membranes of the polymer vesicles did not change dramatically after intramolecular cyclization (Figure S17), which suggests that the chain length of the hydrophobic block barely changed.

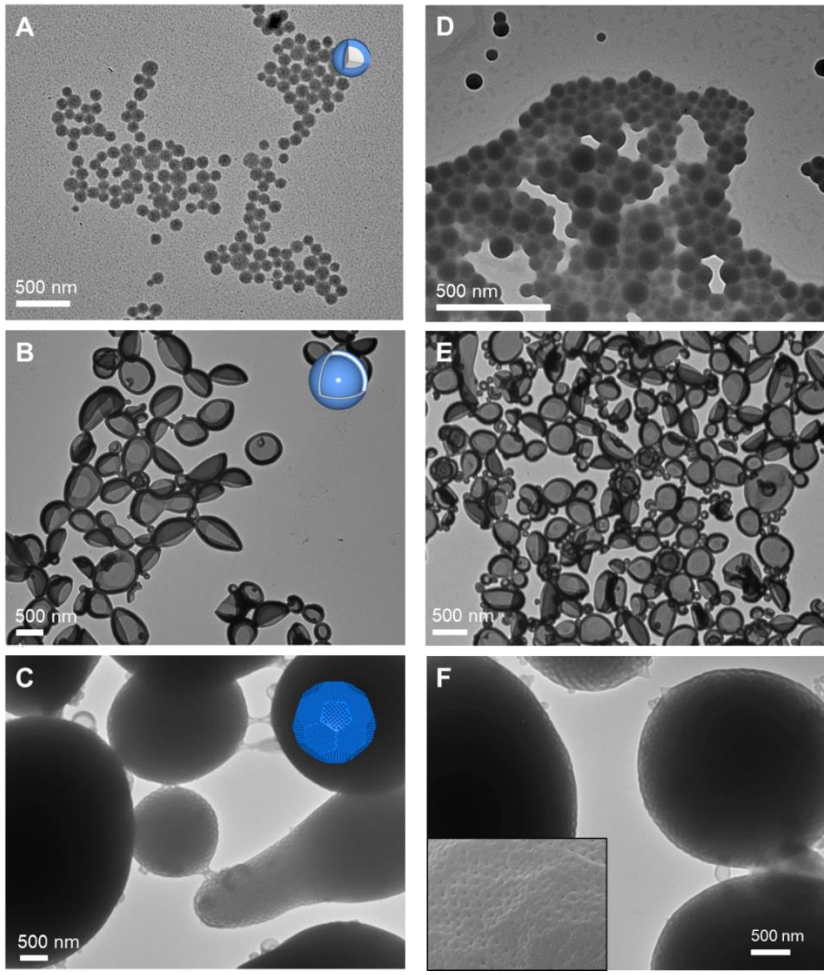

Figure 4-6. TEM images of the self-assembled structures of (A, B, and C) p(St-*co*-Ip)(3,4)-*b*-PEG750$_3$ (M_n = 14.2k, 19.2k, and 23.6k) and (D, E, and F) their cyclized products.

Cross-linking of the self-assembled structures of p(St-*co*-Ip)-*b*-PEG750$_3$ via intermolecular alkylation

In order to increase the mechanical stability of self-assembled nanoparticles, the cross-linking the membrane is a viable option, making them well suited as nanoreactors.[54-60] We hypothesized that the Friedel–Crafts reaction between diene and styrene units could be performed intermolecularly when the hydrophobic blocks were condensed in the core of the self-assembled structures. We discovered that intermolecular cyclization

covalently stabilized the self-assembled structures, which were maintained in organic solvents such as THF (Figure 4-7). The Brönsted acid-catalyzed alkylation could not be performed in protic media such as water and methanol. The solvent should be exchanged for an aprotic solvent that is also sufficiently polar to retain the self-assembled structures before intermolecular cyclization. Therefore, after the polymer vesicles of p(St-*co*-Ip)-*b*-PEG750$_3$ (M_n = 21.2k) were constructed, the solvent was exchanged from water to acetonitrile, which is a polar aprotic solvent, via dialysis for 24 h. TEM imaging showed that the polymer vesicles were able to retain their structures upon exchange of the medium (Figure 4-8A).

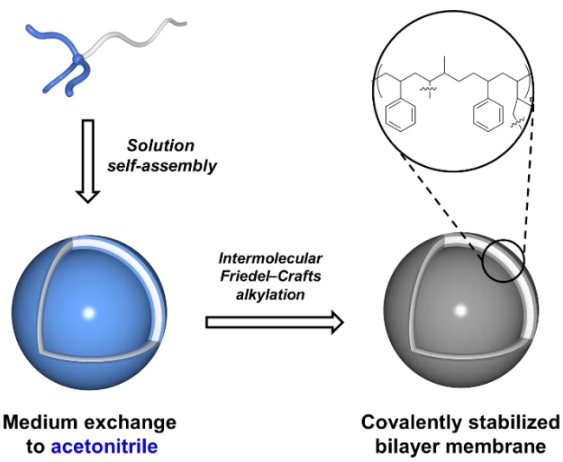

Figure 4-7. Schematic representation of the self-assembly of p(St-*co*-Ip)-*b*-PEG750$_3$ and cross-linking of the hydrophobic compartment by intermolecular alkylation.

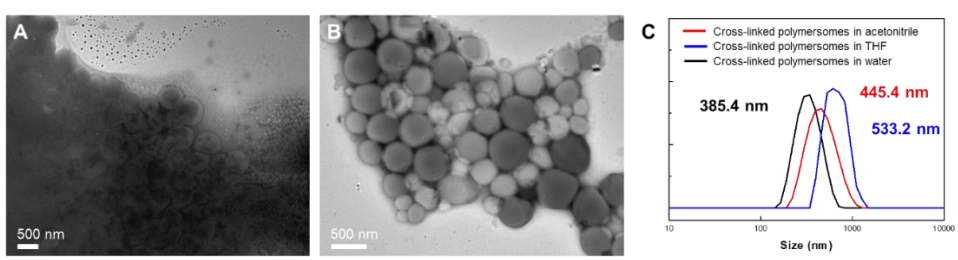

Figure 4-8. TEM images of (A) polymer vesicles of p(St-*co*-Ip)(1,4)-*b*-PEG750$_3$ (M_n = 21.2k) in acetonitrile and (B) the corresponding cross-linked polymer vesicles in THF. (C) Dynamic light scattering (DLS) size plots of the cross-linked polymer vesicles in different solvents.

To impart structural robustness to the self-assembled BCP structures, we performed covalent cross-linking of the hydrophobic chains by intermolecular cyclization. The cross-linked polymersomes of p(St-*co*-Ip)(1,4)-*b*-PEG750$_3$ (M_n = 21.2k) maintained their structures upon exchange of the medium from acetonitrile to THF (Figure 4-8B), indicating that the compartmentalizing membrane of the polymersomes was covalently stabilized by cross-linking of the hydrophobic domain in the bilayer membrane. The average diameter of the cross-linked polymer vesicles, as measured by dynamic light scattering (DLS) analysis, increased from 445.4 nm in acetonitrile to 533.2 nm in THF, suggesting swelling of the cross-linked p(St-*co*-Ip) chains (Figure 4-8C). Upon exchange of the medium from THF to water, the cross-linked polymersomes returned to their original diameter (385.4 nm).

For comparison, the cross-linking of the polymer vesicles of cyclized p(St-*co*-Ip)(1,4)-*b*-PEG750$_3$ (M_n = 13.8k) was also investigated in acetonitrile under acidic conditions. Because the double bonds in the isoprene units were already consumed during intramolecular cyclization, the compartmentalizing membrane of these polymersomes was not covalently stabilized by cross-linking, leading to a collapse of the self-assembled structure of cyclized p(St-*co*-Ip)(1,4)-*b*-PEG750$_3$ (M_n = 13.8k) in THF (Figure S19).

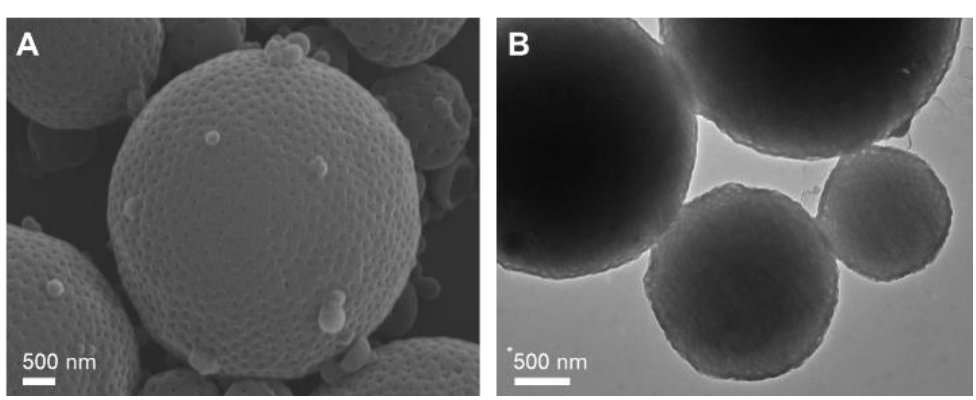

Figure 4-9. (A) SEM and (B) TEM images of the cross-linked polymer cubosomes of p(St-*co*-Ip)(3,4)-*b*-PEG750$_3$ (M_n = 23.6k) in THF.

Furthermore, we demonstrated that 3-D complex inverse bicontinuous bilayers of p(St-*co*-Ip)(3,4)-*b*-PEG750$_3$ (M_n = 23.6k) containing diene and styrene units as the hydrophobic core could covalently cross-linked in acetonitrile via intermolecular alkylation. The cross-linked cubosomes retained their structure upon exchange of the medium from acetonitrile to THF. The covalently fixed cubic mesophases of this BCP showed enhanced stability under chemical stress (i.e., exposure to THF) (Figure 4-9). Thus, the triply periodic minimal surfaces of BCPs can be directly used as mesoporous materials without losing their structural integrity in response to external stimuli such as solvents and physical force.

4.4 Conclusion

In summary, we synthesized a series of p(St-*co*-Ip)-*b*-PEG750$_3$ BCPs with different molecular weights. Amorphous polymers consisting of cyclic units along the main chain were prepared via cationic cyclization of the unsaturated hydrocarbon polymers under acidic conditions. We found that the Friedel–Crafts cyclization of p(St-*co*-Ip)(1,4)-*b*-PEG750$_3$ induced morphological transitions of the self-assembled structures toward lower-curvature nanostructures because the lengths of the polymer chains constituting the hydrophobic block were decreased by intramolecular cyclization. Furthermore, we performed covalent cross-linking of the hydrophobic chains in the core of self-assembled structures via intermolecular cyclization to stabilize the self-assembled structures. Because the hydrophobic chains were compacted in the bilayer membrane, intermolecular alkylation was favored over intramolecular cyclization. The controlled construction of nanostructures possessing excellent optoelectronic properties could provide novel physical properties and improved device

performance for optoelectronic applications.

4.5 References

1. Butler, G. B. Cyclopolymerization. *J. Polym. Sci. Part A: Polym. Chem.* **2000,** *38,* 3451−3461.
2. Dragutan, V.; Streck, R. *Catalytic Polymerization of Cycloolefins, Studies in Surface Science and Catalysis*; Elsevier Science: Amsterdam, The Netherlands, 2000**.**
3. Satoh, K. Nakahara, A.; Mukunoki, K.; Sugiyama, H.; Saito, H.; Kamigaito, M. Sustainable cycloolefin polymer from pine tree oil for optoelectronics material: living cationic polymerization of β-pinene and catalytic hydrogenation of high-molecular-weight hydrogenated poly(β-pinene). *Polym. Chem.* **2014,** *5,* 3222−3230.
4. Van Veersen, G. J. Preparation of Cyclized Rubber from Natural Rubber Latex. *J. Polym. Sci.* **1951,** *6,* 29−32.
5. Riyajan, S.; Liaw, D. J.; Tanaka, Y.; Sakdapipanich, J. T. Cationic cyclization of purified natural rubber in latex form with a trimethylsilyl triflate as a novel catalyst. *J. Appl. Polym. Sci.* **2007,** *105,* 664−672.
6. Abdel-Razik, E. A. Cyclization of butadiene rubber with lewis acid/cocatalyst systems. *Polymer* **1988,** *29,* 1704−1708.
7. Wang, C.; Huang, X.; Yang, J. Cationic cyclization of styrene-butadiene rubber. *Eur. Polym. J.* **2001,** *37,* 1895−1899.
8. Qi, X. Xie, F.; Zhang, J.; Zhang, L.; Yue, D. Bio-based cyclized *Eucommia ulmoides* gum elastomer for promising damping applications. *RSC Adv.* **2019,** *9,* 42367−42374.
9. Nakahara, A.; Satoh, K.; Kamigaito, M. Cycloolefin Copolymer Analogues from Styrene and Isoprene: Cationic Cyclization of the Random Copolymers Prepared by Living Anionic Polymerization.

Macromolecules **2009,** *42,* 620−625.

10. Nakahara, A.; Satoh, K.; Saito, H.; Kamigaito, M. Intramolecular Friedel-Crafts Cyclization and Subsequent Hydrogenation of Styrene-Isoprene Random Copolymers Prepared by Anionic Polymerization for Thermally-Resistant and Optical Applications. *J. Polym. Sci. Part A: Polym. Chem.* **2012,** *50,* 1298−1307.
11. Nakahara, A.; Satoh, K.; Kamigaito, M. Random copolymer of styrene and diene derivatives via anionic living polymerization followed by intramolecular Friedel-Crafts cyclization for high-performance thermoplastics. *Polym. Chem.* **2012,** *3,* 190−197.
12. Cai, Y.; Lu, J.; Jing, G.; Yang, W.; Han, B. High-Glass-Transition-Temperature Hydrocarbon Polymers Produced through Cationic Cyclization of Diene Polymers with Various Microstructures. *Macromolecules* **2017,** *19,* 7498−7508.
13. Cai, Y.; Lu, J.; Zuo, D.; Li, S.; Cui, D.; Han, B.; Yang, W. Extremely High Glass Transition Temperature Hydrocarbon Polymers Prepared though Cationic Cyclization of High 3,4-Regulated Poly(Phenyl-1,3-Butadiene). *Macromol. Rapid Commun.* **2018,** *39,* 1800298.
14. Iwata, S.; Tsukahara, H.; Nihei, E.; Koike, Y. Transoparent zero-birefringence copolymer and its optical properties. *Appl. Opt.* **1997,** *36,* 4549−4555.
15. Tagaya, A.; Ohkita, H.; Harada, T.; Ishibashi, K.; Koike, Y. Zero-Birefringence Optical Polymers. *Macromolecules* **2006,** *39,* 3019−3023.
16. Ban, H. T.; Hagihara, H.; Nishii, K.; Tsunogae, Y.; Nojima, S.; Shiono, T. A New Approach for Controlling Birefringent Property of Cyclic Olefin Copolymers. *J. Polym. Sci. Part A: Polym. Chem.* **2008,** *46,* 7395−7400.

17. Tanaka, K.; Ando, S.; Ishige, R. Spontaneous Chain Orientation of Aromatic Polyimides Evolved during Thermal Imidization from Shear-Oridented Glassy Liquid Crystalline Precursors. *Macromolecules* **2019,** *52,* 5054−5066.
18. Chen, Z.; Mercer, J. A. M.; Zhu, X.; Romaniuk, J. A. H.; Pfattner, R.; Cegelski, L.; Martinez, T.; Burns, N. Z.; Xia, Y. Mechanochemical unzipping of insulating polyladderene to semiconducting polyacetylene. *Science* **2017,** *357,* 475−479.
19. Mauldin, T. C.; Wertz, J. T.; Boday, D. J. Acrylic Platform from Renewable Resources via a Paradigm Shift in Lactide Polymerization. ACS *Macro Lett.* **2016,** *5,* 544−546.
20. Moon, S.; Masada, K.; Nozaki, K. Reversible Polymer-Chain Modification: Ring-Opening and Closing of Polyactone. *J. Am. Chem. Soc.* **2019,** *141*, 10938−10942.
21. van Hest, J. C. M.; Delnoye, D. A. P.; Baars, M. H. P.; van Genderen, M. H. P.; Meijer, E. W. Polystyrene-dendrimer amphiphilic block copolymers with a generation-dependent aggregation. *Science* **1995,** *268,* 1592−1595.
22. Zhang, L.; Eisenberg, A. Multiple morphologies of "crew-cut" aggregates of polystyrene-b-poly(acrylic acid) block copolymers. *J. Am. Chem. Soc.* **1996,** *118,* 3168−3181.
23. Kim, K. T.; Meeuwissen, S. A.; Nolte, R. J. M.; van Hest, J. C. M. Smart nanocontainers and nanoreactors. *Nanoscale* **2010,** *2,* 844−858.
24. Zhang, W. B.; Yu, X.; Wang, C. L.; Sun, H. J.; Hsieh, I. F.; Li, Y.; Dong, X. H.; Yue, K.; Horn, R. V.; Cheng, S. Z. D. Molecular nanoparticles Are Unique Elements for Macromolecular Science: From "Nanoatoms" to Giant Molecules. *Macromolecules* **2014**, *45*, 1221−1239.
25. Renggli, K.; Baumann, P.; Langowska, K.; Onaca, O.; Bruns, N.; Meier, W. Selective and Responsive Nanoreactors. *Adv. Funct. Mater.* **2011,** *21,* 1241−1259.

26. Brinkhuis, R. P.; Rutjes, F. P. J. T.; van Hest, J. C. M. Polymeric vesicles in biomedical applications. *Polym. Chem.* **2011,** *2,* 1449−1462.
27. An, T. H.; La, Y.; Cho, A.; Jeong, M. G.; Shin, T. J.; Park, C.; Kim, K. T. Solution Self-Assembly of Block Copolymers Containing a Branched Hydrophilic Block into Inverse Bicontinuous Cubic Mesophases. *ACS Nano* **2015,** *9,* 3084−3096.
28. Massignani, M.; Lopresti, C.; Blanazs, A.; Madsen, J.; Armes, S. P.; Lewis, A. L.; Battaglia, G. Controlling Cellular Uptake by Surface Chemistry, Size, and Surface Topology at the Nanoscale. *Small* **2009,** *5,* 2424−2432.
29. Hamley, I. W. *Block Copolymers in Solutions: Fundamentals and Applications;* Wiley: Chichester, 2005.
30. Mai, Y.; Eisenberg, A. Self-assembly of block copolymers. *Chem. Soc. Rev.* **2012,** *41,* 5969−5985.
31. D. E. Discher, A. Eisenberg. Polymer Vesicles. *Science* **2002,** *297,* 967−973.
32. U. Tritschler, S. Pearce, J. Gwyther, G. R. Whittell, I. Manners. Functional Nanoparticles from the Solution Self-Assembly of Block Copolymers. *Macromolecules* **2017,** *50,* 3439−3463.
33. Huang, J.; Bonduelle, C.; Thevenot, J.; Lecomandoux, S.; Heise, A. Biologically Active Polymersomes from Amphiphilic Glycopeptides. *J. Am. Chem. Soc.* **2012**, *134*, 119−122.
34. Jeong, M. G.; Kim, J.; Kwon, J. H.; Kim, K. T. Morphological transition of nanostructures of self-assembled block copolymers by stimuli-induced conformational changes in the hydrophilic block. *J. Polym. Sci.* **2020,** *58,* 1153−1162.
35. Gota, C.; Okabe, K.; Funatsu, T.; Harada, Y.; Uchiyama, S. Hydrophilic Fluorescent Nanogel Thermometer for Intracellular Thermometry. *J. Am. Chem. Soc.* **2009,** *131,* 2766−2767.

36. Jiang, X.; Lavender, C. A.; Woodcock, J. W.; Zhao, B. Multiple Micellization and Dissociation Transitions of Thermo- and Light-Sensitive Poly(ethylene oxide)-*b*-poly(ethoxytri(ethylene glycol) acrylate-*co*-*o*-nitrobenzyl acrylate) in Water. *Macromolecules* **2008,** *41,* 2632−2643.
37. Qiao, J.; Qi, L.; Shen, Y.; Zhao, L.; Qi, C.; Shangguan, D.; Mao, L.; Chen, Y. Thermal responsive fluorescent block copolymer for intracellular temperature sensing. *J. Mater. Chem.* **2012,** *22,* 11543−11549.
38. Jiang, J.; Tong, X.; Morris, D.; Zhao, Y.Toward Photocontrolled Release Using Light-Dissociable Block Copolymer Micelles. *Macromolecules* **2006,** *39,* 4633−4640.
39. Sulistio, A.; Widjaya, A.; Blencowe, A.; Zhang, X.; Qiao, G. G. Star polymers composed entirely of amino acid building blocks: a route towards stereospecific, biodegradable and hierarchically functionalized stars. *Chem. Commun.* **2011,** *47,* 1151−1153.
40. Liu, G.; Zhou, L.; Guan, Y.; Su, Y.; Dong, C. M. Multi-Responsive Polypeptidosome: Characterization, Morphology Transformation, and Triggered Drug Delivery. *Macromol. Rapid Commun.* **2014,** *35,* 1673-1678.
41. Ratchliffe, L. P. D.; Couchon, C.; Armes, S. P.; Paulusse, J. M. Inducing an Order-Order Morphological Transition via Chemical Degradation of Amphiphilic Diblock Copolymer Nano-Objects. *Biomacromolecules* **2016,** *17,* 2277−2283.
42. Machado, C. A.; Tran, R.; Jenkins, T. A.; Pritzlaff, A. M.; Sims, M. B.; Sumerlin, B. S.; Savin, D. A. UV-induced vesicle to micelle transition: a mechanistic study. *Polym. Chem.* **2019,** *10,* 6037−6046.
43. Busatto, N.; Keddie, J.; Roth, P. J. Sphere-to-worm morphological transitions and size changes through thio-para-fluoro core modification of PISA-made nano-objects. *Polym. Chem.* **2020,** *11,* 704−711.

44. Johnson, A. F.; Worsfold, D. J. Anionic Polymerization of Butadiene and Styrene. *J. Polym. Sci., Part A: Gen. Pap.* **1965,** *3,* 449−455.
45. Hsieh, H. L. Kinetics of Polymerization of Butadiene, Isoprene, and Styrene with Alkyllithiums. Part I. Rate of polymerization. *J. Polym. Sci., Part A: Gen. Pap.* **1965,** *3,* 153−161.
46. Worsfold, D. J.; Bywater, S. Anionic Polymerization of Isoprene. *Can. J. Chem.* **1964,** *2,* 2884−2892.
47. Jeong, M. G.; van Hest, J. C. M.; Kim, K. T. Self-assembly of dendritic-linear block copolymers with fixed molecular weight and block ratio. *Chem. Commun.* **2012,** *48,* 3590−3592.
48. Percec, V.; Peterca, M.; Tadjiev, T,; Zeng, X.; Ungar, G.; Leowanawat, P.; Aqad, E.; Imam, M. R.; Rosen, B. M.; Akbey, U.; Graf, R.; Sekharan, S.; Sebastiani, D.; Spiess, H. W.; Heiney, P. A.; Hudson, S. D. Self-Assembly of Dendronized Perylene Bisimides into Complex Helical Columns. *J. Am. Chem. Soc.* **2011,** *133,* 12197−12219.
49. Zhang, L. Yu, K.; Eisenberg, A. Ion-Induced Morphological Changes in "Crew-Cut" Aggregates of Amphiphilic Block Copolymers. *Science* **1996,** *272,* 1777−1779.
50. Cho, A.; La, Y.; Shin, T. J.; Park, C.; Kim, K. T. Structural Requirements of Block Copolymers for Self-Assembly into Inverse Bicontinuous Cubic Mesophases in Solution. *Macromolecules* **2016,** *49,* 4510−4519.
51. Nagarajan, R. Molecular Packing Parameter and Surfactant Self-Assembly: The Neglected Role of the Surfactant Tail. *Langmuir* **2002,** *18,* 31−38.
52. Kim, J.; Yoon, M.; Jin, S-M.; Lee, E.; Kim, K. T. Polymer Cubosomes of Block Copolymers Having Cross-linkable Soft Hydrophobic Blocks. *Polym. Chem.* **2019,** *10,* 3778−3785.

53. Discher, B. M.; Bermudez, H.; Hammer, D. A.; Discher, D. E.; Won, Y.-y.: Bates, F. S. Cross-linked Polymersome Membranes: Vesicles with Broadly Adjustable Properties. *J. Phys. Chem. B* **2002,** *106*, 2848−2854.
54. Ahmed, F.; Hategan, A.; Discher, D. E.; Discher, B. M. Block Copolymer Assemblies with Cross-link Stabilization: From Single-Component Monolayers to Bilayer Blends with PEO-PLA. *Langmuir* **2003,** *19*, 6505−6511.
55. Che, H.; Cao, S.; van Hest, J. C. M. Feedback-induced temporal control of "breathing" polymersomes to create self-adaptive nanoreactors. *J. Am. Chem. Soc.* **2018,** *140*, 5356−5359.
56. Che, H.; van Hest, J. C. M. Stimuli-responsive polymersomes and nanoreactors. *J. Mater. Chem. B* **2016,** *4*, 4632−4647.
57. Jeong, M. G.; Kim, K. T. Covalent Stabilization of Inverse Bicontinuous Cubic Structures of Block Copolymer Bilayers by Photodimerization of Indene Pendant Groups of Polystyrene Hydrophobic Blocks. *Macromolecules* **2017,** *50*, 223−234.
58. Peters, R. J. R. W.; Marguet, M.; Marais, S.; Fraaije, M. W.; van Hest, J. C. M.; Lecommandoux, S. Cascade reactions in multicompartmentalized polymersomes. *Angew. Chemie. Inter. Ed.* **2014,** *53*, 146−150.
59. Kim, J.; Jeong, S.; Korneev, R.; Shin, K.; Kim, K. T. Cross-linked Polymersomes with Reversible Deformability and Oxygen Transportability. *Biomacromolecules* **2019,** *20*, 2430−2439.
60. Feng, A.; Yuan, J. Smart nanocontaininers: progress on novel stimuli-responsive polymer vesicles. *Macromol. Rapid Commun.* **2014,** *35*, 767−779.

Chapter 5. Shape Transformation of Nanoparticles Driven by Light-Induced Conformational Change of Hydrazone-Based Photoswitches

5.1 Abstract

The hydrazone framework is the basis of molecular switches, and is the most promising in the development of molecular machines owing to a bistable system that can permanently lock the actuation of dynamic molecules. We synthesized block copolymers composed of hydrophilic polyethylene glycol (PEG) blocks and discrete poly(phenyllactic acid) (dPPLA) blocks possessing hydrazone-based photoswitches in specific positions. This system allowed us to investigate the effect of the light-induced configurational switching of photoswitches on the self-assembled structures of BCPs. We found that the isomerization of the hydrazone-based photoswitch was amplified to change the self-assembled morphologies, indicating that the position of the switch along the hydrophobic dPPLA chains determines the shape transformation of nanostructures. In addition, the release of rhodamine B from the bilayer membranes of nanoparticles under blue-light irradiation indicated that the light-induced shape transformation can be potentially applied in smart nanocapsules with various guest molecules.

5.2 Introduction

Photoresponsive nanoplatforms that are sensitive to external light sources have received significant attention as novel materials owing to the advantages of no contact, no pollution, and adjustable performance parameters.[1-2] Polymeric systems have been used successfully in this context, and it is expected that the development of the materials into shape-shifting actuators will lead to innovation in a broad range of applications. Numerous challenges such as integrating switches with bulk materials and controlling the directionality of their motion have been investigated to yield various molecular architectures that work as muscles, ratchets, and walkers.[3-4] Common switchable moieties such as azobenzenes,[5] spiropyrans,[6] rotaxanes,[7] and diarylethenes[8] have been investigated since the past few decades. A photoresponsive system embedded within nanoparticles undergoes structural changes in response to external light, allowing them to be used in various fields such as medicinal and supramolecular chemistry.[9-16]

Among the photoresponsive systems, the hydrazone framework is the basis of molecular switches, and shows the most promise toward developing molecular machines. The light-induced activation of hydrazone-based photoswitches has been studied in molecular-level motion by the Aprahamian group.[17-21] Compared to other photoswitches that lack light-induced shape stability, hydrazone-based photoswitches are a bistable system that can permanently lock the actuation of dynamic molecules, making the hydrazone group particularly suitable for switching applications. Therefore, the hydrazone framework was chosen as the basis of molecular switches in polymer networks, enabling the utilization of hydrazone-based photoswitches in macroscopic-level studies by many groups.[22-25]

Here we report the synthesis of block copolymers (BCPs) composed of hydrophilic polyethylene glycol (PEG) blocks and discrete

poly(phenyllactic acid) (dPPLA) blocks with hydrazone-based photoswitches in specific positions. To observe the effect of the light-induced configurational switching of photoswitches, they were embedded in two different positions within the BCP chains: (1) in the middle of hydrophobic PPLA chains and (2) at the junction of amphiphilic chains. The BCPs self-assembled into nanostructures via a co-solvent method and direct hydration respectively. The nanostructures were placed under a light source (wavelength = 405 nm) to induce the *E/Z* isomerization of the hydrazone-based photoswitches. We found that the configurational switching of this system can be attributed to the reduced hydrodynamic volume of hydrophobic chains, leading to the shape transformations of the self-assembled nanoparticles (Figure 5-1). In addition, the light-induced shape transformation allowed the self-assembled nanostructures to be used as polymer nanocapsules that can transport guest molecules within a nanoscale compartment.

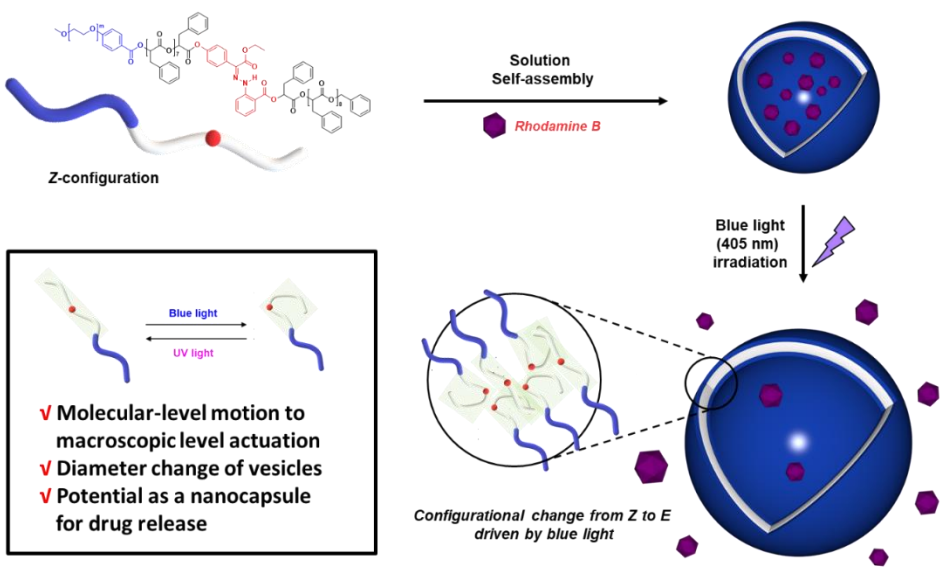

Figure 5-1. Schematic representation of the drug-release ability of self-assembled structures of PEG-*b*-dPPLA containing hydrazone-based photoswitches under blue light.

5.3 Results and discussion

The hydrazone-based photoswitch **H1** was synthesized using a previously reported procedure (Scheme S6).[22] The prepared **H1** was studied using ^{1}H NMR in DMSO (Figure S20). Irradiating a sample of *Z*-**H1** (>99%) with λ = 405 nm light yields a photostationary state (PSS) consisting of 90% *E*-**H1**, while irradiating the resulting solution with UV light (365 nm) yields a mixture of 70% of the *Z* isomer at the PSS (Figure 5-2A and 5-2B). In addition, UV-Vis spectroscopy was employed for photoisomerization studies (Figure 5-2C). Hydrazone solutions in DMSO were prepared for the UV-Vis absorption measurements. Switching was accomplished by irradiation with 405 nm light until the PSS was reached, followed by irradiation with 365 nm light to reach the reverse PSS. The switching cycles of **H1** in DMSO upon alternating irradiation were confirmed by the absorbance change at 373 nm that was monitored using UV-Vis spectroscopy (Figure 5-2D).

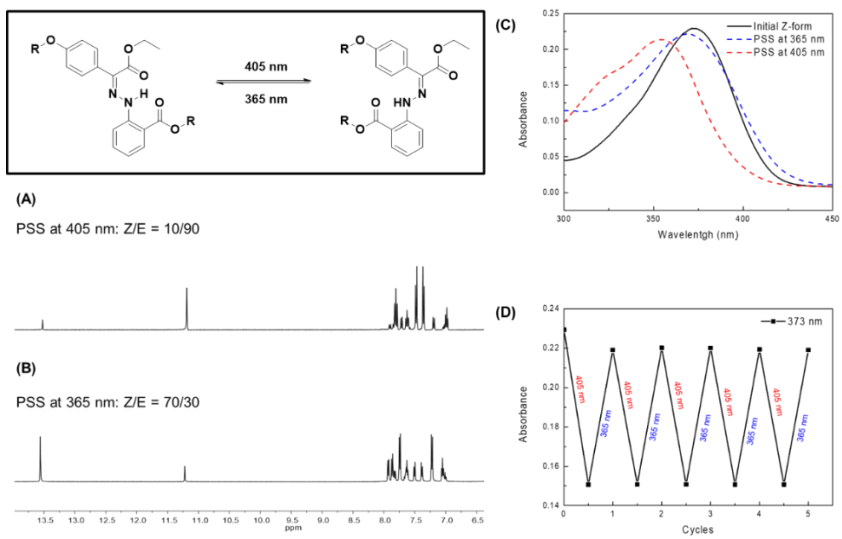

Figure 5-2. ^{1}H NMR spectra in DMSO of hydrazone-based photoswitches (A) after 405 nm, followed by (B) 365 nm photoirradiation to reach the PSS. (C) UV-Vis absorption spectra of hydrazone-based photoswitches in DMSO. (D) Switching cycles of hydrazone-based photoswitches in DMSO upon alternating irradiation using 405 nm and 365 nm light sources.

As hydrophobic blocks, dPPLAs of different molecular weights were prepared via iterative convergent methods (Scheme S7 and S8).[26,27] The monodispersities of dPPLAs containing **H1** were confirmed by ^{1}H NMR and Matrix-assisted laser desorption/ionization time-of-flight (MALDI-TOF) analyses (Figure 5-3A). Owing to the low efficiency of the Mitsunobu reaction between **H1** and high-molecular-weight PPLA, phenyllactic acid was employed as a spacer and the *N*-(3-dimethylaminopropyl)-*N*'-ethylcarbodiimide (EDC) reaction was the primary mechanism of coupling the ester bonds to prepare the amphiphilic chains embedding the prepared photoswitch **H1** at the specific positions (Scheme S9 and S10). The synthesis of BCPs with different positions of **H1** was confirmed by ^{1}H NMR and MALDI-TOF analyses (Figure 5-3C, 5-3D, S26C and S26D) and is summarized in Table 5-1.

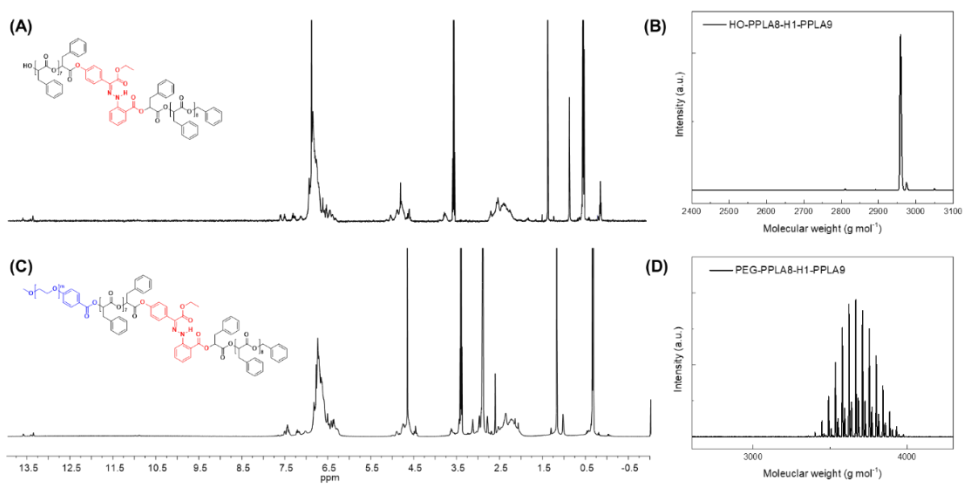

Figure 5-3. (A and C) ^{1}H NMR spectra in $CDCl_3$ and (B and D) MALDI-TOF spectra of monodisperse hydrophobic block (HO-PPLA$_8$-H1-PPLA$_9$) and amphiphilic block copolymer (PEG-PPLA$_8$-H1-PPLA$_9$) respectively.

The photoisomerization of the prepared **BCP 1** was studied using ^{1}H NMR in $CDCl_3$ (Figure 5-4). The actual PSS values were determine using ^{1}H NMR spectroscopy upon continuous irradiation of the samples until no further isomerization was observed. Irradiating BCP containing *Z*-**BCP1** (>99%) with blue light (λ = 405 nm) yields a PSS consisting of 85% *E*-**BCP1**, while irradiating the resulting solution with UV light (365 nm) yields a mixture containing 95% of the *Z* isomer at the PSS (Figure 5-4B and 5-4C).

Shape transformation of BCPs containing photoswitches in different positions

The BCPs composed of the hydrophilic PEG block and hydrophobic blocks with different positions of **H1** were dissolved in dioxane as a common solvent at a concentration of 5 mg mL^{-1}. Subsequently, to construct nanostructures, distilled water as a selective solvent was slowly added at a rate of 0.5 mL h^{-1} using a syringe pump. The prepared **BCP1**, PEG550-*b*-$PPLA_8$-H1-$PPLA_9$, self-assembled into cylindrical micelles. To induce the configuration change of **H1** embedded in the nanoparticles, the self-assembled nanoparticles were subjected to 405 nm light irradiation for 2 h at room temperature. After blue-light irradiation, the cylindrical micelles of **BCP 1** became spherical micelles (Figure 5-5A and 5-5B).

Table 5-1. Characteristics of amphiphilic block copolymers containing photoswitch.

Sample	Name	Position of H1	M_n (g mol^{-1})[a] of hydrophobic block	M_n (g mol^{-1})[a] of hydrophilic block	$Đ$ [a] of BCPs	f_{PEG} (%)[b]
1	PEG550-*b*-dPPLA$_8$-H1-dPPLA$_9$	Center	2958	550	1.02	15.7
2	PEG550-*b*-H1-dPPLA$_{17}$	Junction	2958	550	1.02	15.7
3	PEG1000-*b*-dPPLA$_8$-H1-dPPLA$_9$	Center	2958	1000	1.02	25.2
4	PEG1000-*b*-H1-dPPLA$_{17}$	Junction	2958	1000	1.02	25.2

[a]Number average molecular weight (M_n) and molecular weight distribution ($Đ$) determined by GPC using polystyrene (PS) standards. Elution was performed with THF at a flow rate of 1 mL min^{-1} at 30 °C. [b]Molecular weight fraction of the PEG domain relative to the amphiphilic block copolymer.

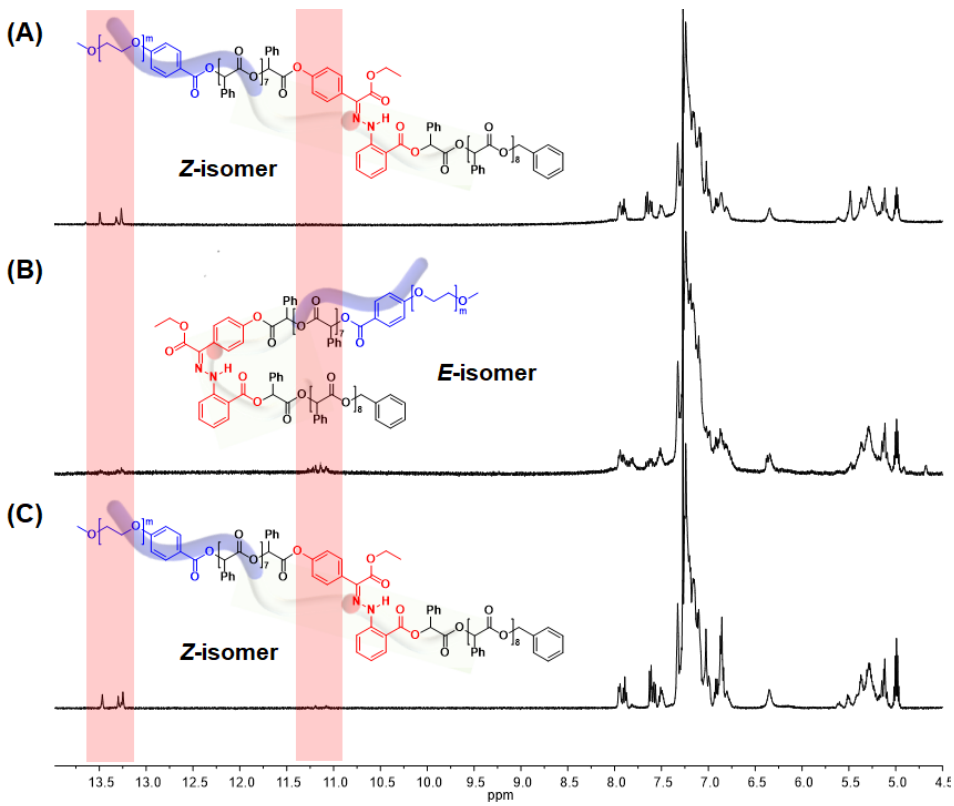

Figure 5-4. ^{1}H NMR spectra of amphiphilic block copolymer containing hydrazone-based photoswitches (A) before and (B) after 405 nm irradiation, followed by (C) 365 nm photoirradiation.

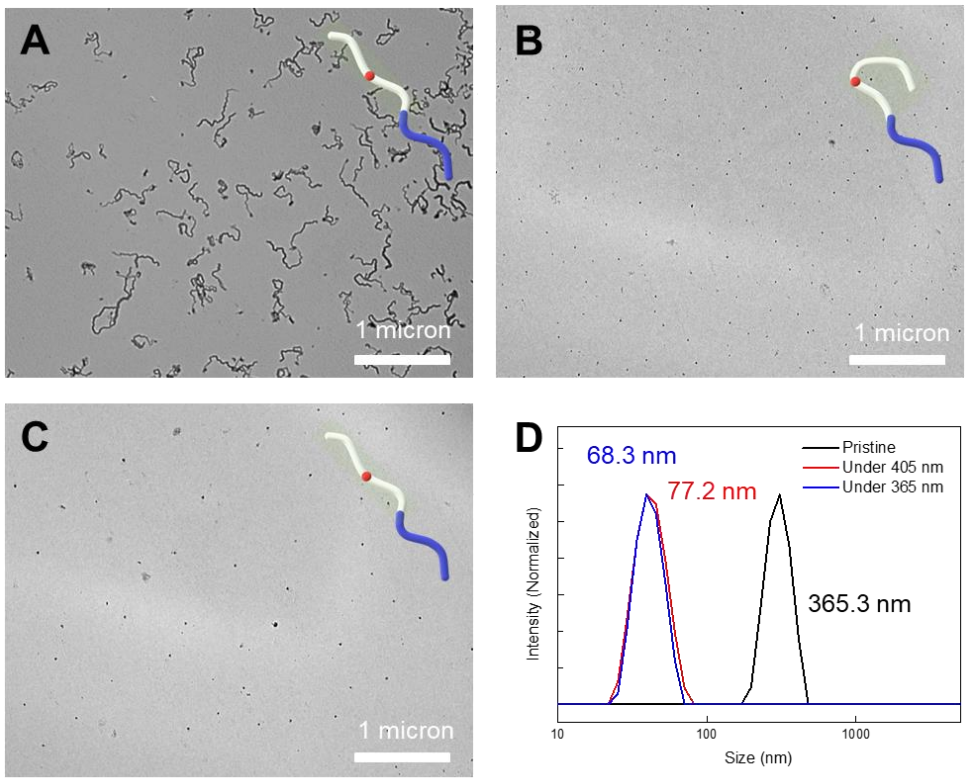

Figure 5-5. (A to C) TEM images and (D) dynamic light scattering (DLS) analysis of self-assembled structures of PEG550-*b*-dPPLA$_8$-H1-dPPLA$_9$ under different light sources. The morphologies were observed (A) before and (B) after blue-light irradiation, followed by (C) UV light irradiation.

The morphological change of the self-assembled nanoparticles was quantified by dynamic light scattering (DLS) analysis by measuring the hydrodynamic diameter of the nanoparticles suspended in water. Under blue-light irradiation, the average diameter of the cylindrical micelles changed from 365.3 nm to 77.2 nm (Figure 5-5D). The DLS results corresponded to the size change of the nanostructures observed in Transmission electron microscopy (TEM). We found that the configurational change driven by the isomerization of the hydrazone-based photoswitches was amplified to enable shape transformation, and that the position of the switch within the hydrophobic dPPLA chain determines the shape transformation of

nanostructures. Sequentially, the *E*-isomer was photochemically switched back to the *Z*-isomer upon 365 nm light irradiation to observe the reversibility of the shape transformation of nanostructures. Unfortunately, the diameter of the polymer vesicles did not change again, indicating that the process is not reversible. The morphologies and sizes of the self-assembled structures of the dPPLA-*b*-PEGs are summarized in Table 5-2.

Table 5-2. Morphological characteristics of self-assembled structures of dPPLA-*b*-PEG.

Sample	Name	Solvent used for self-assembly	Before 405 nm irradiation		After 405 nm irradiation	
			Morphology	Diameter (nm)	Morphology	Diameter (nm)
1	PEG550-*b*-dPPLA$_8$-H1-dPPLA$_9$	Dioxane	Cylindrical micelles	365.4	Spherical micelles	77.2
3	PEG1000-*b*-dPPLA$_8$-H1-dPPLA$_9$	Acetone	Vesicles	196.8	Vesicles	446.8

The **BCP3**, PEG1000-*b*-PPLA$_8$-H1-PPLA$_9$, self-assembled into polymer vesicles under the same co-solvent self-assembly condition except the fact that acetone was used as a common solvent instead of dioxane. After dialysis, the self-assembled polymer vesicles were also subjected to blue-light irradiation (405 nm). As expected, the hydrodynamic diameter of the nanoparticles significantly changed from 196.8 nm to 446.8 nm, while the morphologies of polymer vesicles did not drastically change (Figure 5-6A and 5-6B). We speculate that the expansion of the nanoparticles stems from swelling that is driven by the enhanced interactions between the aqueous solution and the hydrazone NH proton that becomes available for H-bonding in the E form. To observe the reversibility of the process, the size-increased vesicles were sequentially placed under UV light sources. Due to the poor physical properties of the nanoparticles of **BCP3**, it was hard to clearly

observe the shape-transformed structures whose transformation was driven by the configurational change of photoswitches from the *E*-isomer to *Z*-isomer. However, the decrease in particle size (446.8 nm to 270.3 nm) indicated the disruption of the nanoparticles via a light-triggered response.

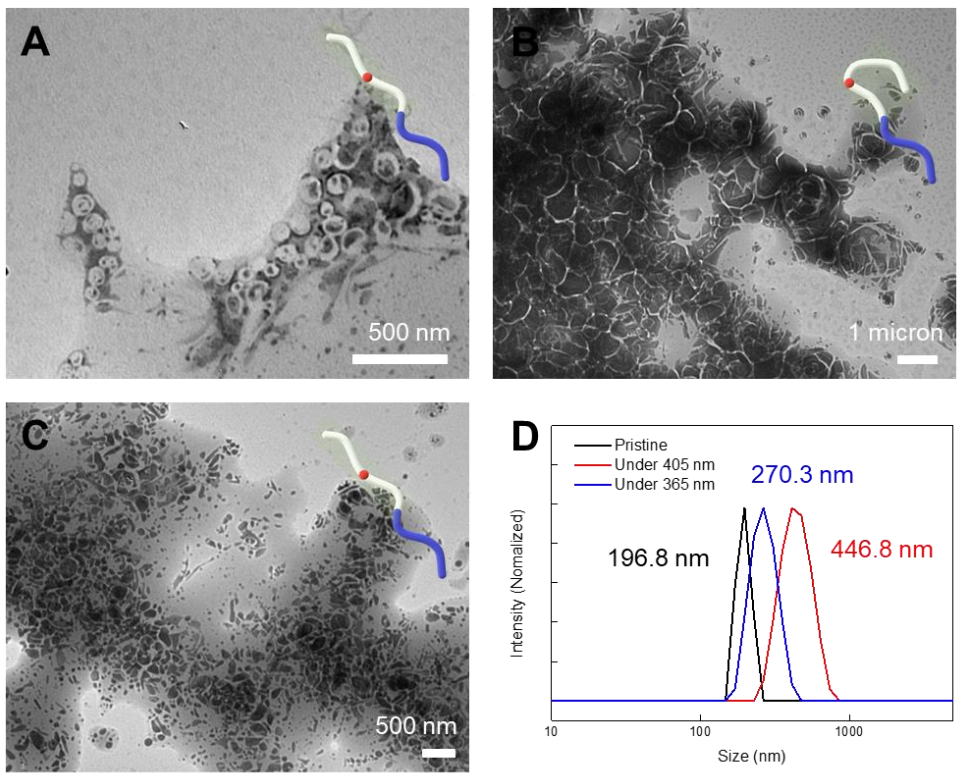

Figure 5-6. (A to C) TEM images and (D) dynamic light scattering (DLS) analysis of self-assembled structures of PEG1000-*b*-dPPLA$_8$-H1-dPPLA$_9$ under different light sources. The morphologies were observed (A) before and (B) after 405 nm light irradiation, followed by (C) 365 nm light irradiation.

Drug release triggered by light irradiation

The nanoparticles embedding the hydrazone-based photoswitches showed macroscopic-level changes such as shape transformation or diameter change of the nanoparticles under light irradiation. The significant increase in particle size due to blue-light irradiation highlighted the feasibility of using

polymer vesicles with photoswitches to deliver drugs in an on-demand and quantitative manner. We then investigated the release of guest molecules using rhodamine B-loaded nanoparticles of PEG1000-*b*-dPPLA. For encapsulation, distilled water containing rhodamine (0.1 mM) as a selective solvent was slowly added to the BCPs in acetone for solution self-assembly. The resulting dispersion was purified by dialysis (molecular weight cutoff 12-14 kDa, (SpectraPor, Ranco Dominguez, CA)) against water, followed by size exclusion chromatography (Sephadex G-200) to remove the unencapsulated rhodamine. The dye-encapsulated particles constructed by the self-assembly of BCPs were confirmed by TEM.

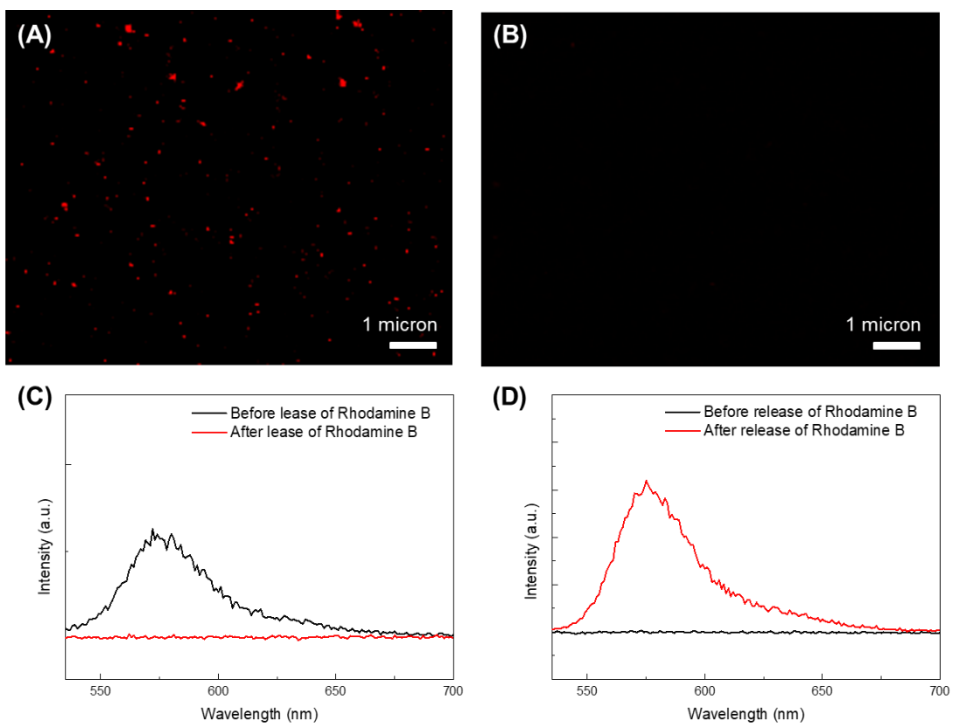

Figure 5-7. Confocal laser scanning microscopy (CLSM) images of rhodamine-loaded nanoparticles of PEG1000-*b*-dPPLA$_8$-H1-dPPLA$_9$ (A) before and (B) after blue-light irradiation, followed by centrifugation using an Amicon Ultra-Free-MC centrifugal filter. Determination of rhodamine B release by fluorometer: (C) dispersed solution and (D) filtered medium.

To evaluate the potential of drug release triggered by light irradiation in this system, the rhodamine-loaded nanoparticles were subjected to blue-light irradiation to induce the photo-isomerization of hydrazone switches. To remove the released dye molecules, centrifugation was performed using an Amicon Ultra-Free-MC centrifugal filter. The presence of rhodamine B encapsulated in the nanoparticles was determined by CLSM (Figure 5-7A and 5-7B). The nanoparticles constructed via the self-assembly of **BCP3** distinctly released the rhodamine dye from the inner compartment of the polymer vesicles after blue-light irradiation.

Furthermore, the release of the encapsulated guest molecules from the particles was confirmed by verifying the fluorescence of the dispersion and filtered medium after the release of rhodamine from the inner compartment. For the particle-dispersed solution, to eliminate the effect of nanoparticle-induced scatter on the observed emission, 1 mL of THF was added in the vial. The emission intensity of rhodamine B indicated that the nanoparticles with dominantly *E*-isomer switches completely released the dye molecules (Figure 5-7C). The dyes that spilled out of the particles were collected by centrifugation using an Amicon centrifugal filter and analyzed with a fluorophotometer (Figure 5-7D). The observed fluorescence intensity of rhodamine indicated that the configurational isomerization of hydrazone embedded in the hydrophobic block led to perforated particles and the release of guest molecules from the inner compartment. The proposed systems successfully demonstrated that the facile dye release of the particles afforded smart nanocapsules with various guest molecules.

5.4 Conclusion

In summary, we synthesized BCPs composed of hydrophilic PEG blocks and dPPLA blocks embedding hydrazone-based photoswitches in specific positions. The BCPs self-assembled into

nanostructures via cosolvent self-assembly. We found that the configurational change of the hydrazone-based photoswitches can be amplified to macroscopic motion such as shape transformations or a diameter change of the self-assembled nanoparticles. The nanoparticles constructed with BCPs possessing the photoswitch at the middle of the hydrophobic PPLA chains showed a diameter change of polymer vesicles under blue-light irradiation. To evaluate the potential of drug release triggered by light irradiation in this system, rhodamine-encapsulated nanostructures were prepared. Light-induced shape transformation allowed the encapsulated rhodamine within the compartment of the particles to be released. The release of dye molecules driven by the light-induced configurational change of hydrazone-based photoswitches successfully demonstrated that this facile system is promising as a smart nanocapsule with various guest molecules.

5.5 References

1. Sauvage, J. -P. *Molecular Machines and Motors;* Springer: New York, 2001.
2. Schilwa, W. *Molecular Motors;* Wiley-VCH: Weinheim, Germany, 2003.
3. Feringa, B. L. *Molecular switches,* 2nd ed.; Wiley-VCH: Weinheim, Germany, 2011.
4. Li, Q. *Intelligent Stimuli-Responsive Materials: From Well-Defined Nanostructures to Applications;* John Wiley & Sons: Hoboken, NJ, 2012.
5. Bandara, H. M. D.; Burdette, S. C. Photoisomerization in Different Classes of Azobenzene. *Chem. Soc. Rev.* **2012,** *41,* 1809−1825.
6. Klajn, R. Spiropyran-Based Dynamic Materials. *Chem. Soc. Rev.* **2013,** *43,* 148−184.
7. Coskunn, A.; Banaszak, M.; Astumian, R. D.; Stoddart, J. F.;

Grzybowski, B. A. Great Expectations: Can Artificial Molecular Machines Deliver on Their Promise. *Chem. Soc. Rev.* **2012,** *41,* 19−30.

8. Irie, M. Diarylethenes for Memories and Switches. *Chem. Rev.* **2000,** *100,* 1685−1716.
9. Kobayashi, S.; Mori, Y.; Fossey, J. S.; Salter, M. M. Catalytic enantioselective formation of C-C bonds by addition to imines and hydrazones: a ten-year update. *Chem. Rev.* **2011,** *111,* 2626−2704.
10. Vicini, P.; Incerti, M.; La Colla, P.; Loddo, R. Anti-HIV evaluation of benzo[d]isothiazole hydrazones. *Eur. J. Med. Chem.* **2009,** *44,* 1801−1807.
11. Lehn, J. -M. Perspectives in Chemistry-Steps towards Complex Matter. *Angew. Chem. Int. Ed.* **2013,** *52,* 2836−2850.
12. Zhou, X. -P.; Wu, Y.; Li, D. Polyhedral Metal-Imidazolate Cages: Control of Self-Assembly and Cage to Cage Transformation. *J. Am. Chem. Soc.* **2013,** *135,* 16062−16065.
13. Jin, Y.; Yu, C.; Denman, R. J.; Zhang, W. Recent advances in dynamic covalent chemistry. *Chem. Soc. Rev.* **2013,** *42,* 6634−6654.
14. Raue, R.; Brack, A.; Lange, K. H. Salt-free Synthesis of Azo and Hydrazone Dyes Under CO_2 Pressure. *Angew, Chem. Int. Ed.* **1991,** *30,* 1643−1644.
15. Lygaitis, R.; Getautis, V.; Grazulevicius, J. V. Hole-transporting hydrazones. *Chem. Soc. Rev.* **2008,** *37,* 770−788.
16. Serbutoviez, C.; Bosshard, C.; Knopfle, G.; Wyss, P.; Pretre, P.; Gunter, P.; Schenk, K.; Solari, E.; Chapuis, G. Hydrazone Derivatives, an Efficient Class of Crystalline Materials for Nonlinear Optics. *Chem. Mater.* **1995,** *7,* 1198−1206.
17. Su, X.; Aprahamian, I. Switching Around Two Axles: Controlling the Configuration and Conformation of a Hydrazone-Based Switch. *Org. Lett.* **2011,** *13,* 30−33.

18. Su, X.; Robbins, T. F.; Aprahamian, I. Switching Through Coordination-Coupled Proton Transfer. *Angew. Chem. Int. Ed.* **2011,** *50,* 1841−1844.
19. Su, X; Aprahamian, I. Hydrazone-based switches, metallo-assemblies and sensors. *Chem. Soc. Rev.* **2014,** *43,* 1963−1981.
20. Tatum, L.; Su, X.; Aprahamian, I. Simple Hydrazone Building Blocks for Complicated Functional Materials. *Acc. Chem. Res.* **2014,** *47,* 2141−2149.
21. Pramanik, S.; Aprahamian, I. Hydrazone Switch-Based Negative Feedback Loop. *J. Am. Chem. Soc.* **2016,** *138,* 15142−15145.
22. Ryabchun, A.; Li, Q.; Lancia, F.; Aprahamian, I.; Katsonis, N. Shape-Persistent Actuators from Hydrazone Photoswitches. *J. Am. Chem. Soc.* **2019,** *141,* 1196−1200.
23. Zheng, L. -Q.; Yang, S.; Lan, J.; Gyr, L.; Goubert, G.; Qian, H.; Aprahamian, I.; Zenobi, R. Solution Phase and surface photoisomerization of a hydrazone switch with long thermal half-life. *J. Am. Chem. Soc.* **2019,** *141,* 17637−17645.
24. Guo, X.; Shao, B.; Zhou, S.; Aprahamian, I.; Chen, Z. Visualizing intracellular particles and precise control of drug release using an emissive hydrazone photochrome. *Chem. Sci.* **2020,** *11,* 3016−3021.
25. Weyandt, E.; ter Huurne, G.; M. Vantomme, G.; Markvoort, A. J.; Palmans, A. R. A.; Meijer, E. W. Photodynamic Control of the Chain Length in Supramolecular Polymers: Switching an Intercalator into a Chain Capper. *J. Am. Chem. Soc.* **2020,** *142,* 6295−6303.
26. Lee, J. M.; Koo, M. B.; Lee, S. W.; Lee, H.; Kwon, J.; Shim, Y. H.; Kim, S. Y.; Kim, K. T. High-Density Information Storage in an Absolutely Defined Aperiodic Sequence of Monodisperse Copolyester. *Nat. Commun.* **2020,** *11,* 56.
27. Koo, M. B.; Lee, S. W.; Lee, J. M.; Kim, K. T. Iterative Convergent Synthesis of Large Cyclic Polymers and Block Copolymers with

Discrete Molecular Weights. *J. Am. Chem. Soc.* **2020,** *142*, 14028−14032.

Supporting Information

Chapter 2. Cross-linked Polymersomes with Reversible Deformability and Oxygen Transportability

1. Synthesis of hydrophilic modules

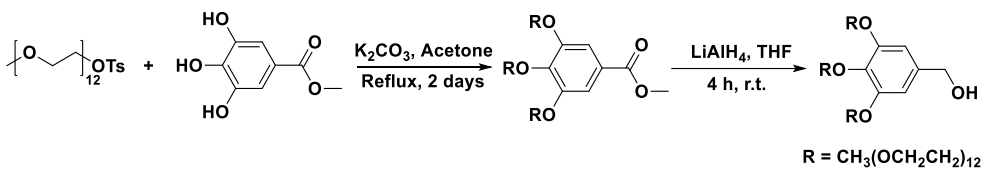

Scheme S1. Synthesis of PEG550$_3$-OH

PEG550$_3$-OH. PEG550$_3$-OH is synthesized in multi-gram quantity by following the literature methods.

^{1}H NMR (400 MHz, $CDCl_3$) 6.64(s, 2H), 4.58(d, *J*=5.6 Hz, 2H), 4.18(t, *J*=5.2 Hz, 4H), 4.14(t, *J*=5.2 Hz, 2H), 3.93-3.45 (m, -CH_2CH_2O-), 3.39(s, 9H), 2.52(t, *J*=5.6 Hz, 1H) ppm; **^{13}C NMR** (400 MHz, $CDCl_3$) 152.60, 137.49,137.22, 106.50, 72.29, 71.95, 70.77-70.57, 69.83, 68.79, 64.86, 59.07 ppm; **GPC** M_n = 2590 g mol^{-1}, $Đ$ = 1.03; **MALDI-TOF** M_n = 1811.34 g mol^{-1}.

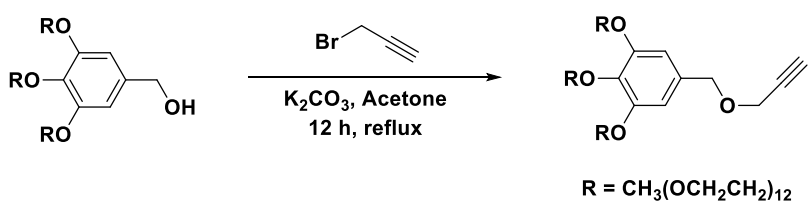

Scheme S2. Synthesis of PEG550$_3$-propargyl ether

PEG550$_3$-4-propargyl ether. A mixture of PEG550$_3$-OH (4 g, 2.22 mmol) and propargyl bromide (0.57 mL, 5.11 mmol, 2.3 eq., 80 wt% in toluene) was stirred for 10 min in acetone (100 mL). K_2CO_3 (5 g) was then added, and the reaction was stirred for 18 h under reflux. Thereafter, the solid was removed by filtration and acetone was evaporated. Water was added and the mixture was extracted with dichloromethane. The organic phase was dried over $MgSO_4$ and filtered. The solvent was removed by rotary evaporation and then mixture was purified by flash column chromatography using silica gel (dichloromethane : methanol = 95:5 v/v). The compound was obtained as yellow solid. **Yield**: 4.01 g, 93 %. **^{1}H NMR** (400 MHz, $CDCl_3$) 6.59(s, 2H), 4.49(d, *J*=5.2 Hz, 2H), 4.18(t, *J*=5.2 Hz, 4H), 4.14(t, *J*=5.2 Hz, 2H), 3.93-3.45 (m, -CH_2CH_2O-), 3.39(s, 9H), 2.49(t, *J*=5.6 Hz, 1H) ppm; **^{13}C NMR** (400 MHz, $CDCl_3$) 152.60, 137.49,137.22, 106.50, 72.29, 71.95, 70.77-70.57, 69.83, 68.79, 64.86, 59.9, 59.07, 78.7, 76.4 ppm.

2. Synthesis of hydrophobic modules

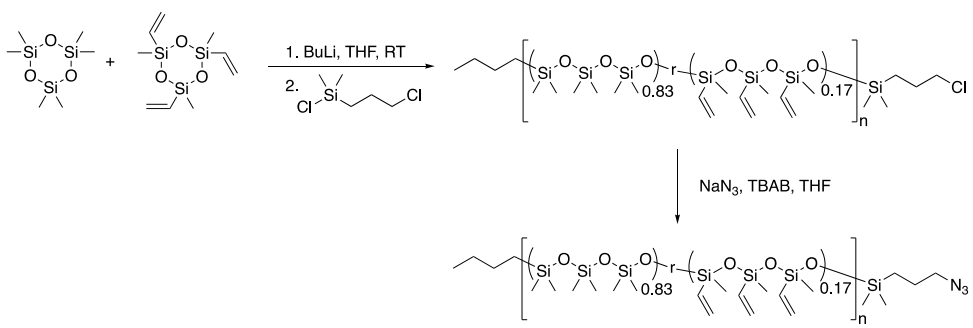

Scheme S3. Synthesis of ω-azido-PDMVS.

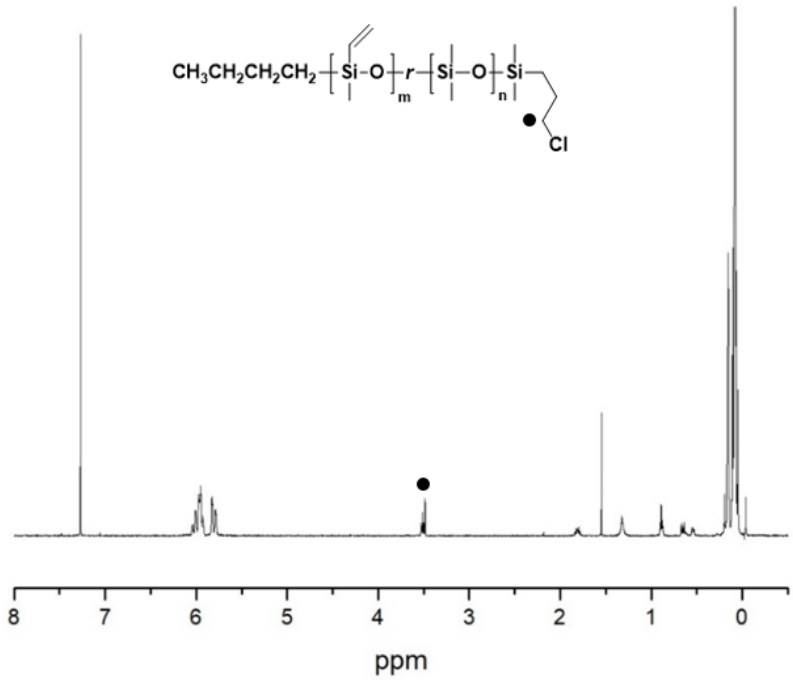

Figure S1. ^{1}H NMR (500 MHz, $CDCl_3$) spectrum of ω-chloro-PDMVS.

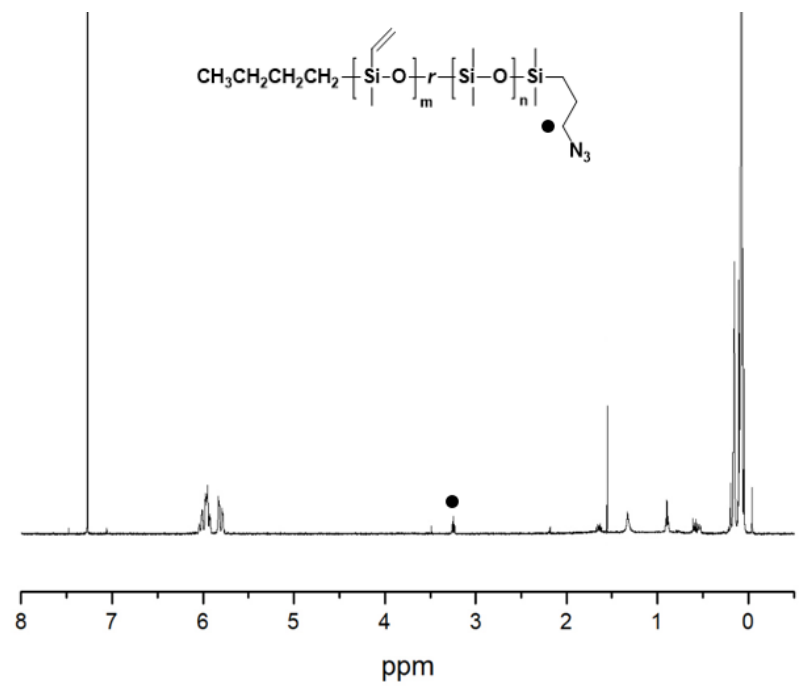

Figure S2. ^{1}H NMR (500 MHz, $CDCl_3$) spectrum of ω-azido-PDMVS.

4. Self-assembly and cross-linking

Solution self-assembly. These BCPs were allowed to self-assemble from a dioxane solution (2 mL, 1 wt %) by adding an equal volume of water at a controlled rate (1 mL h^{-1}) with stirring. To the solution (dioxane : water = 1 : 1 for volume ratio), 5 mg of 2-Hydroxy-4'-(2-hydroxyethoxy)-2-methylpropiophenone (Irgacure 2959) was added for cross-linking. The solution was stirred for 5 h under UV lamp (λ = 365 nm), followed by dialysis against water. All BCPs were self-assembled under identical conditions for comparison.

Direct hydration. These BCPs were dispersed to 500 μL of water. After 3 h, 100 μL of the solution was diluted with water (x 10). To the solution, 2-Hydroxy-4'-(2-hydroxyethoxy)-2-methylpropiophenone (Irgacure 2959) (5 mg) was added for cross-linking. The solution was stirred for 5 h under UV lamp (λ = 365 nm), followed by dialysis against water. All BCPs were self-assembled under identical conditions for comparison.

Difference of observed morphology of self-assembled structures. The BCPs with PDMVS having different molecular weights ($PEG550_3$-PDMVS15K and $PEG550_3$-PDMVS20K) formed polymersomes under different conditions. $PEG550_3$-PDMVS20K only formed polymersomes by the co-solvent method (dioxane/water). However, $PEG550_3$-PDMVS15K could directly self-assembled into polymersomes in water. We used $PEG550_3$-PDMVS20K for the morphological and physical characterization of the polymersomes because of their superior stability. In case of protein encapsulation, we used $PEG550_3$-PDMVS15K for preventing denaturation of hemoglobin. While the $PEG550_3$-PDMVS26K formed hexosomes, or nanoparticles composed of the inverse-hexagonal phase via solution self-assembly (Figure S4C), the BCP could not be directly dispersed in water due to its high-MW hydrophobic block.

Cross-linking procedure. Homopolymer, PDMVS (M_n = 14500 g mol^{-1}) was cross-linked by using 2-Hydroxy-4'-(2-hydroxyethoxy)-2-methylpropiophenone (Irgacure 2959, sigma) as a photoradical generator. Into 4 mL of co-solvent (dioxane/water), 100 mg of homopolymer and 10 mg of Irgacure 2959 were added. Under the illumination of UV (λ = 365 nm, 8 W) for 5 h, the resulting polymer solution (about 0.02 g mL^{-1}) yielded soft gel. The cross-linking of vinyl group in PMVS chain was confirmed by ^{1}H-NMR spectroscopy and differential scanning calorimetry (DSC) experiments. The soluble fraction of the cross-linked network was inspected by ^{1}H NMR, which resulted in the disappearance of the characteristic peaks of pendant vinyl groups at (δ = 5.5-6 ppm). DSC results of the cross-linked PDMVS showed a single peak (T_m = −50.3 °C) upon a heating scan, which are in contrast to the double melting peaks (T_{m1} = −47.3 °C and T_{m2} = −39.1 °C) for the pristine BCP. These results indicated the formation of covalent bonds between the PMVS chains in solution in the presence of photoradical generators.

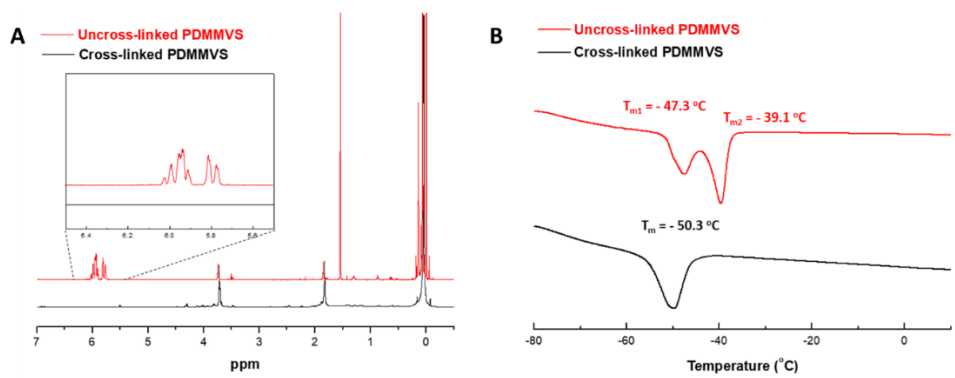

Figure S3. ^{1}H-NMR spectroscopy and differential scanning calorimetry (DSC) analysis for cross-linking of vinyl group in PMVS chain.

5. Micropipette aspiration experiments

Observation of microdeformed PEG-*b*-PDMVS polymersomes. For quantitative microdeformation experiments, the aspiration pressure P was controlled by adjusting the height of the oil-filled reservoir connected to the back of the pipette.Membrane tension σ was computed from $\sigma = K_a\alpha$ (eq 1). Here, σ represents the membrane tension. The area strain, α, is determined by A/A_0, where A_0 is the initial membrane area and A is the change in area due to application of pressure. Image analysis was performed using the public domain software ImageJ. A semi-automatic tracking procedure was implemented to monitor the tongue length position in time. Pipette and vesicle radii were measured separately for each set of experiments.

Capacity for polymersomes to undergo deflation-inflation cycles. The cross-linked polymersomes underwent the deflation-inflation cycle without losing structural integrity. In contrast, the unlinked polymersomes did not retain their structures under the same stresses. In other words, unlinked polymersomes failed to retain their structures by negative pressure into polymersomes.

6. Preparation of ZnTPP-loaded vesicles

Plot of calibration curve to determine ZnTPP loading amount. The ZnTPP loading amount within aqueous vesicles was determined by comparison of its vesicle absorption at 424 nm with the calibration of free ZnTPP. To 1 mL of ZnTPP loaded vesicles dispersion, addition of 1 mL of THF allowed to eliminate the effect of nanoparticle-induced scatter on the observed absorption by ZnTPP. According to the

calibration curve, the ZnTPP loading amount was approximately 0.19 wt% relative to the polymer mass.

7. Hemoglobin-Encapsulating Polymersomes

To prevent hemoglobin (Hb) from oxidizing to methemoglobin (metHb) during the preparation of hemoglobin-encapsulating polymersomes (HEPs), Hb was complexed with carbon monoxide (CO) before encapsulation. The bovine Hb was diluted with phosphate-buffered saline (PBS, pH 7.3) to 30 mg/mL. A few drops of sodium dithionite was added to the stock solution to form deoxyhemoglobin (deoxyHb) and then stabilized under a CO atmosphere to form deoxyhemoglobin and then stabilized under a CO atmosphere to generate CO-bound hemoglobin form (carboxyhemoglobin or COHb). The prepared carboxyhemoglobin stock solution was saturated with different gases were confirmed with UV-Vis spectroscopic analysis.

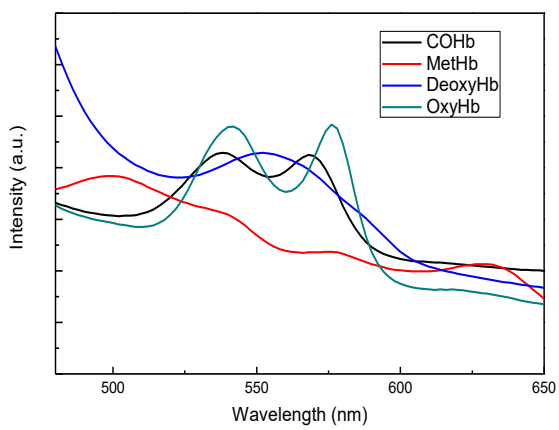

Figure S4. UV-Vis spectra of COHb, metHb, deoxyHb, and oxyHb. The commercially available bovine hemoglobin was reduced by Sodium dithionite, followed by saturation with CO gas to obtain COHb.

Preparation of Hemoglobin-encapsulating polymersome (HEP)

10 mg of $PEG550_3$-b-PDMVS15K was coated in 50 mL of a round bottom flask as a thin film. 500 μL of the prepared COHb stock solution was added for dispersion at 4ºC. After 16 h, any other aggregated particles were also removed by pipetting. The giant polymersomes were extruded through 200 nm polycarbonate membrane filter following Hb encapsulation to adjust their diameter to 200 nm. Unencapsulated Hb was removed from the aqueous suspension by dialysis against PBS (a 100 K cut off). After cross-linking of the polymersomes with Irgacure 2959 under UV light (365 nm).

Oxygen-nitrogen cycling experiments with HEP

To investigate the oxygen binding of HEP, UV-Vis spectrometry was used. The solution containing HEP was sealed off from the surrounding air and deoxygenated by repeated evacuation and flushing with pure N_2 for 150 min. 2 mL of suspension was analyzed by UV-Vis spectrometry to observe the characteristic peaks of deoxyHb. Introducing oxygen to the suspension was performed by pure O_2 saturation for 60 min. The oxygen-nitrogen exchange process was repeated at least three times.

Chapter 3. Polymer Cubosomes of Block Copolymers Having Cross-linkable Soft Hydrophobic Blocks

1. Synthesis of hydrophilic structural modules

Branched hydrophilic block, PEG550$_3$-N$_3$ was synthesized by following the previously reported procedure (Scheme S3-1). PEG550$_3$-(*3,5*)-N$_3$ was synthesized by coupling the corresponding benzyl alcohol and methyl 3,5-bis(azidomethyl)benzoic acid.

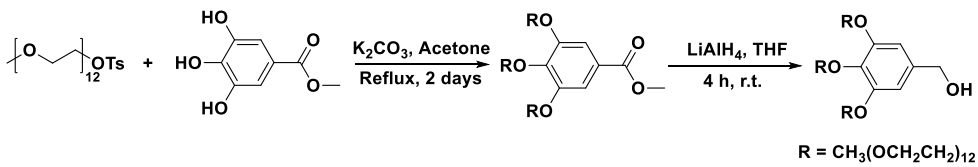

Scheme S4. Synthesis of PEG550$_3$-OH.

PEG550$_3$-OH. It is synthesized in multi-gram quantity by following the literature methods.

^{1}H NMR (400 MHz, $CDCl_3$) 6.64(s, 2H), 4.58(d, *J*=5.6 Hz, 2H), 4.18(t, *J*=5.2 Hz, 4H), 4.14(t, *J*=5.2 Hz, 2H), 3.93-3.45 (m, -CH_2CH_2O-), 3.39(s, 9H), 2.52(t, *J*=5.6 Hz, 1H) ppm; **^{13}C NMR** (400 MHz, $CDCl_3$) 152.60, 137.49,137.22, 106.50, 72.29, 71.95, 70.77-70.57, 69.83, 68.79, 64.86, 59.07 ppm; **GPC** M_n = 2590 g mol^{-1}, $Đ$ = 1.03.

Methyl 3,5-dimethylbenzoate. A few drops of H_2SO_4 (95%) were added into methyl 3,5-dimethylbenzoic acid (10 g, 66 mmol) in methanol (100 mL). The solution was refluxed at 70 °C for 10 h. The

reaction mixture was quenched with ice and extracted with ether. The organic layer was washed with Na_2CO_3 saturated solution, dried over $MgSO_4$, and removed under reduced pressure. The crude product was purified by column chromatography using *n*-hexane as an eluent. The compound was obtained as colourless oil. Yield 9.8 g (89.63%) ^{1}H NMR (400 MHz, $CDCl_3$) 7.66 (s, 2H), 7.19 (s, 1H), 3.90 (s, 3H), 2.36 (s, 6H).

Methyl 3,5-bis(bromomethyl)benzoate. Methyl 3,5-dimethylbenzoate (5.8 g, 35.3 mmol) and N-bromosuccinimide (13.83 g, 77.70 mmol) were added into benzene (250 mL). The solution was degassed by bubbling N_2 for 15 min. Azobisisobutyronitrile (0.58 g, 3.53 mmol) was added into the solution and stirred at 95 °C for 12 h. The precipitate was filtered off and washed with hot benzene. The combined filtrate was washed with a saturated $NaHCO_3$ solution and brine. The organic layer was dried with $MgSO_4$ and removed under reduced pressure. The crude product was purified by column chromatography using hexane as an eluent. Yield 3.33 g (30.61%) ^{1}H NMR (400 MHz, $CDCl_3$) 8.00 (s, 2H), 7.62 (s, 1H), 4.50 (s, 4H), 3.93 (s, 3H).

Methyl 3,5-bis(azidomethyl)benzoate. Methyl 3,5-bis(bromomethyl)benzoate (3.33 g, 10.34 mmol) and NaN_3 (2.68 g, 41.37 mmol) were added into DMF (50 mL). The solution was stirred at 65 °C for 3 h. It was diluted with water and then extracted with ethyl acetate (EA). The organic layer was dried with $MgSO_4$. The solvents were removed under reduced pressure. The crude product was purified by column chromatography using hexane as an eluent. Recrystallization

in hexane gave a white crystalline solid. Yield 2.23g (87.57%) ^{1}H NMR (400 MHz, $CDCl_3$) 7.97 (s, 2H), 7.49 (s, 1H), 4.49 (s, 4H), 3.95 (s, 3H).

Methyl 3,5-bis(azidomethyl)benzoic acid. A solution of 2M LiOH (10ml) was added into methyl 3,5-bis(azidomethyl)benzoate (1g, 4.06 mmol) in methanol (70 mL). The reaction was stirred at room temperature for 12 h. The solvents were removed under reduced pressure and monitored by thin layer chromatography (TLC). Then, 2M HCl solution was added into the mixture until pH was dropped to pH 5~6. Mixture was extracted with ethyl acetate and brine, and then dried with $MgSO_4$. The solvents were removed under reduced pressure. A white solid was collected. Yield 0.91 g (71.95%) ^{1}H NMR (400 MHz, $CDCl_3$) 8.04 (s, 2H), 7.56 (s, 1H), 4.49 (s, 4H).

PEG550$_3$-(3,5)-N$_3$ (3). Methyl 3,5-bis(azidomethyl)benzoic acid (0.475 g, 1.54 mmol), *N*,*N*′-dicyclohexylcarbodiimide (0.367 g, 1.78 mmol), and 4-dimethylaminopyridine (0.007 g, 0.059 mmol) were dissolved in dry CH_2Cl_2 (50 mL) at 0 °C. The mixture was slowly added to the CH_2Cl_2 solution (50 mL) of PEG550$_3$-OH (0.7 g, 0.297 mmol) at 0 °C. The resulting mixture was gradually warmed to room temperature. After 24 h, the crude mixture was cooled, and urea was removed by repeated filtration with cold EA. Then mixture was purified by flash column chromatography using silica gel (CH_2Cl_2:MeOH = 95:5 v/v). ^{1}H NMR (400 MHz, $CDCl_3$) 8.00 (s, 2H), 7.50 (s, 1H), 6.68 (s, 2H), 5.25 (s, 2H), 4.45 (s, 4H), 3.93–3.45 (m, -CH_2CH_2O-), 3.38 (s, 9H). GPC M_n = 3060 g mol^{-1}, $Đ$ = 1.04.

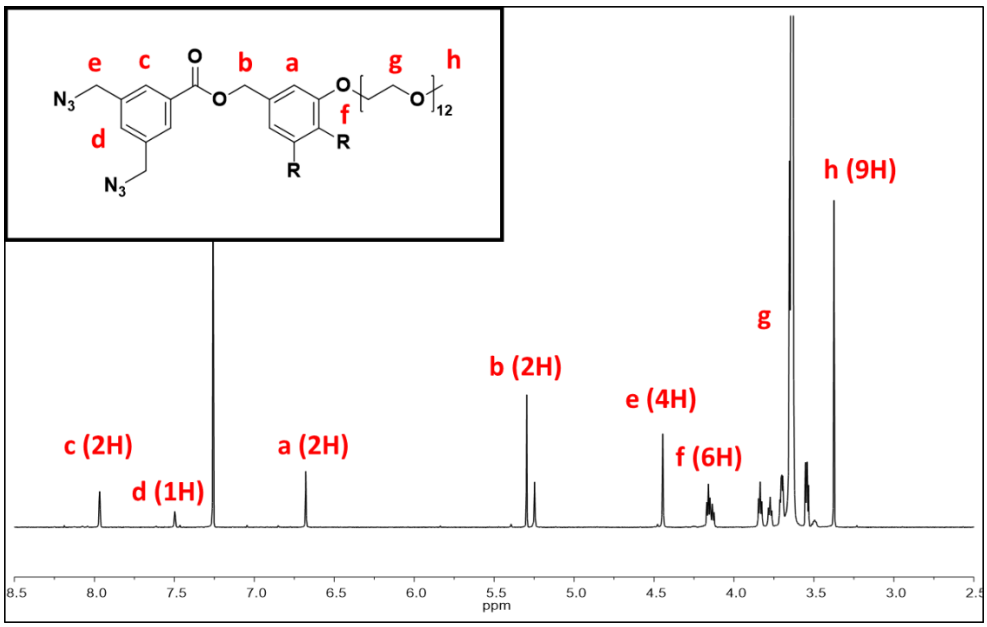

Figure S5. ^{1}H NMR (500 MHz, $CDCl_3$) spectrum of branched hydrophilic block.

2. Synthesis of hydrophobic structural modules

5-triethylsilyl-4-pentynyllithium (TESP-Li). A 10-fold excess of lithium (0.8 g, 0.11 mol) over the (5-chloro-1-pentynyl)triethylsilane (TESP-Cl) (2.5g, 0.011mol) was used. Dry cyclohexane (50 mL) was added to the lithium placed in a 100 mL two neck flask with a reflux condenser under an argon atmosphere. The reaction mixture was vigorously stirred for 30 min at 50 ℃. Then, TESP-Cl was added dropwise to this solution, and the solution was stirred for 4h at 50 ℃ and overnight at room temperature. The reaction mixture was then filtered through a fritted Schlenk filter to afford a clear red-orange solution. ^{1}H NMR (400 MHz, $CDCl_3$) 2.15 (t, 2H), 1.45(m, 2H), 0.97–0.82 (m, 12H), 0.49 (m, 6H).

Polymerization of α-acetylene-functionalized polyisoprene. All polymerization was performed in a dry condition under inert

atmosphere in Glove box. Isoprene was pre-dried over CaH_2 for 24 h, which was distilled prior to use. A desired amount of isoprene was dissolved in dry cyclohexane and THF in a vial. The prepared TESP-Li was introduced to the solution at once. The polymerization was monitored by GPC at 30 min intervals. After 2h, the reaction was quenched by injecting degassed methanol. The solution was evaporated under reduced pressure and precipitated into methanol for 3 times. Colourless viscous product was obtained after drying. Then, the product and tetrabutylammonium fluoride trihydrate (TBAF) (5 eq. to polyisoprene) were dissolved in THF and stirred at room temperature for 4 h. Then, the solution was precipitated in methanol and dried. Colourless viscous product was obtained. In case of 1,2-addition, polymerization was going under –78 °C. ^{1}H NMR (400 MHz, $CDCl_3$) 6.1–5.5 (1,2, -CH-), 5.10 (1,4, -CH-), 4.8–1.6 (1,2, -CH_2), 4.75 (3,4, -CH_2), 2.03 (1,4, -CH_2-), 2.0 (3,4, -CH-), 2.0–1.8 (1,4, -CH_2-), 1.8–1.2 (1,2, -CH_2), 1.65 (1,4, -CH_3), 1.64 (3,4, -CH_3), 1.36 (3,4, -CH_2-), 1.15-1.0 (1,2, -CH_3).[3]

3. Synthesis of block copolymers by click chemistry

CuBr(I) (40 mg) was dried in vacuum for 15 min. *N*,*N*,*N'*,*N''*,*N''*-pentamethyldiethylenetriamine (PMDETA) (80 mg) mixed with THF (1.5 mL) was added and the mixture was stirred in N_2 for 15 min. To this solution, a solution of the hydrophilic PEG block and deprotected polyisoprene (4 eq. to the hydrophilic module) in THF (5 mL) was added. The mixture was degassed by bubbling N_2 for 15 min. After degassing, the click reaction was proceeded at 40 °C until completion. The extent of the reaction was monitored by GPC. The reaction was quenched by exposing the solution to air, followed by dilution with chloroform. The cooled solution was filtered through aluminum oxide

(basic) with $CHCl_3$ to remove the Cu catalyst. The filtered solution was concentrated on a rotary evaporator, and then crude products were filtered through a pack of silica with CH_2Cl_2 to remove the excess homo PI. To collect the click product, a mixed eluent (dichloromethane:methanol = 90:10 v/v) was used. The filtered solution was concentrated on a rotary evaporator to afford a pure block copolymer as a pale yellow gummy product. If necessary, the resulting block copolymer was purified by preparatory size exclusion chromatography.

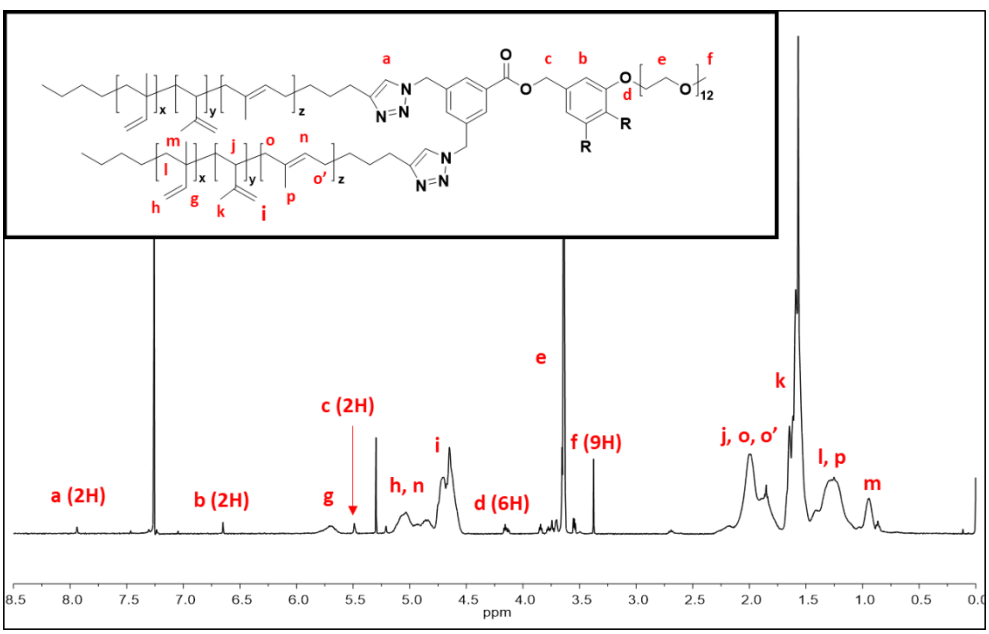

Figure S6. ^{1}H NMR (500 MHz, $CDCl_3$) spectrum of PEG550$_3$-*b*-PI$_2$.

4. Solution self-assembly and cross-linking of block copolymers

Typically, BCPs (10 mg) was dissolved in 1,4-dioxane (1 ml) in a 20 mL capped vial with a magnetic stirrer. The solution was stirred for two hours at room temperature (800 revolutions per minute). To this solution, 1 mL of water was slowly added at a rate of 2 mL h^{-1} by using a syringe pump. To the solution (dioxane:water = 1:1 for volume ratio), 5 mg of 2-Hydroxy-4'-(2-

hydroxyethoxy)-2-methylprophenone (Igarcure 2959) was added for cross-linking. The suspension was stirred for 30 min and exposed to UV light (λ = 365 nm, 15 W) for 5 h with mild stirring, followed by dialysis against water. All BCPs were self-assembled and cross-linked under identical conditions for comparison. The cross-linking of PI chains was confirmed by changing the suspension medium from water to THF.

Cross-linking experiment. The cross-linking of vinyl group in PI chain was confirmed with polymersomes of PEG550$_3$-PI(33K) which is the simplest self-assembled structures in this study. In the presence of photoradical generator, the formation of covalent bonds between PI blocks could maintain the structures upon exchanging the solvent from water to THF, of which the average diameter was increased from 455.2 nm in water to 610.1 nm in THF. Cross-linked polymersomes could also be observed with conventional TEM due to their enhanced physical stability. It indicates that the membrane of the polymersomes showing swelling behaviour was covalently stabilized by cross-liking of polyisoprene domains in the bilayer membrane.

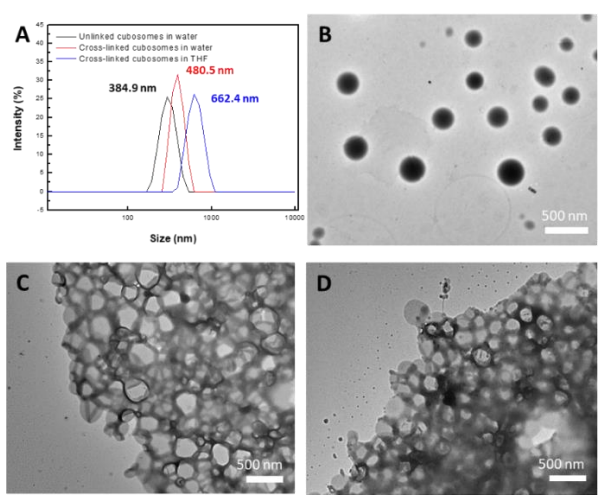

Figure S7. (A) Dynamic light scattering (DLS) size plots of the uncross-linked (black) and cross-linked (red) polymersomes in aqueous and THF (blue). TEM images of (B) uncross-linked vesicles in water, and cross-linked vesicles (C) in water and (D) in THF.

Chapter 4. Block Copolymers Composed of Main-Chain Cyclic Polymers: Morphology Transition and Covalent Stabilization of Self-Assembled Nanostructures via Intra- and Inter-chain Cyclization of Styrene-*co*-Isoprene Blocks

1. Synthesis of hydrophilic structural modules

Branched hydrophilic block, $PEG750_3$-N_3 was synthesized by following the previously reported procedure.

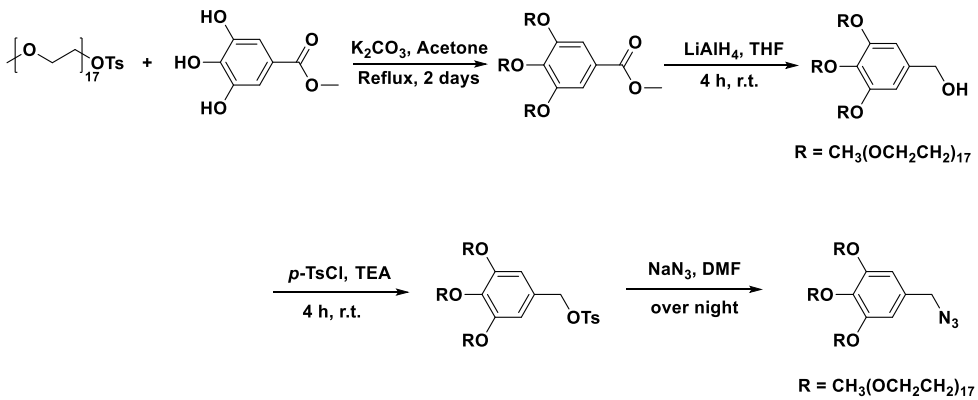

Scheme S5. Synthesis of $PEG750_3$-N_3

$PEG750_3$-N_3. It is synthesized in multi-gram quantity by following the literature methods.

^{1}H NMR (400 MHz, $CDCl_3$) 6.64(s, 2H), 4.58(d, *J*=5.6 Hz, 2H), 4.18(t, *J*=5.2 Hz, 4H), 4.14(t, *J*=5.2 Hz, 2H), 3.93-3.45 (m, -CH_2CH_2O-), 3.39(s, 9H), 2.52(t, *J*=5.6 Hz, 1H) ppm; ^{13}C NMR (400 MHz, $CDCl_3$) 152.60, 137.49,137.22, 106.50, 72.29, 71.95, 70.77-70.57, 69.83, 68.79, 64.86, 59.07 ppm; **GPC** M_n = 2590 g mol^{-1}, $Đ$ = 1.03.

2. Synthesis of random copolymers of p(St-*co*-Ip)

Polymerization of acetylene-functionalized poly(styrene-*co*-isoprene). The random copolymers were prepared by following polymerization procedure found by Kamigaito and co-workers. Styrene and isoprene were pre-dried over CaH_2 for 2 h, which was distilled prior to use. The copolymerization was initiated by adding premixed St/Ip mixture (1 to 1 ratio) by a syringe pump into the solution containing cyclohexane, THF, and *n*-butyl lithium. After 1 h, the reaction was quenched with 1-Chloro-5-triethylsilyl-4-pentyne. The solution was evaporated under reduced pressure and precipitated into methanol. Colorless viscous product was obtained after drying. Tetrabutylammonium fluoride trihydrate (TBAF) was added into the silane-protected product in THF. The mixture was stirred at room temperature for 2 h. The solution was precipitated in methanol and dried again to afford a colorless viscous acetylene-functionalized product. ^{1}H NMR (500 MHz, $CDCl_3$) 7.4–6.7 (styrene, -CH), 5.10-4.3 (1,4, -CH- and 3,4, -CH_2), 2.5-1.3 (styrene, -CH_2- and -CH-) 2.3-2.0 (1,4, -CH_2-), 2.0 (3,4, -CH-), 2.0–1.8 (1,4, -CH_2-), 1.65 (1,4, -CH_3), 1.64 (3,4, -CH_3), 1.36 (3,4, -CH_2-).

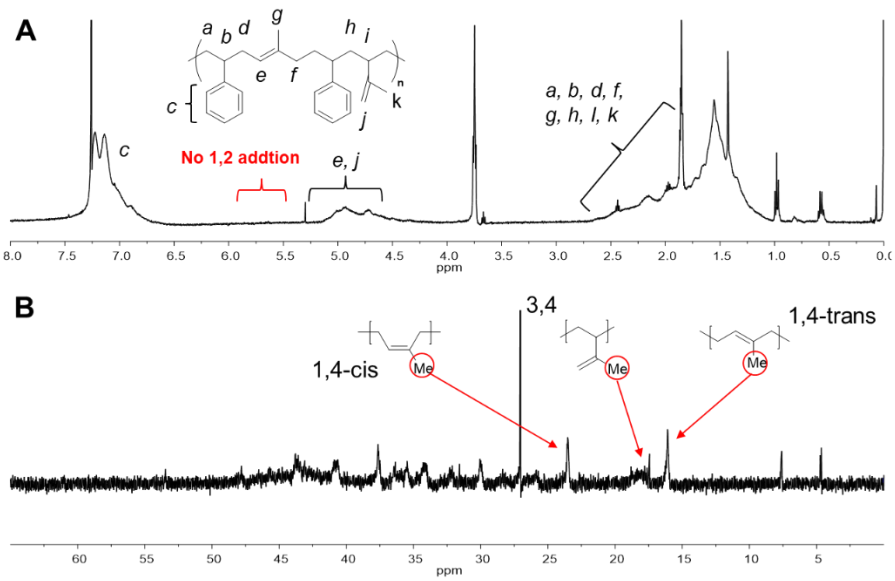

Figure S8. (A) ^{1}H NMR and (B) ^{13}C NMR spectra of random copolymer, p(St-*co*-Ip)(1,4). The regiospecificities of the isoprene units showed predominantly 1,4-rich repeating unit (1,4-: 1,2-: 3,4- = 70-73: 0: 27-30) along the copolymer chain.

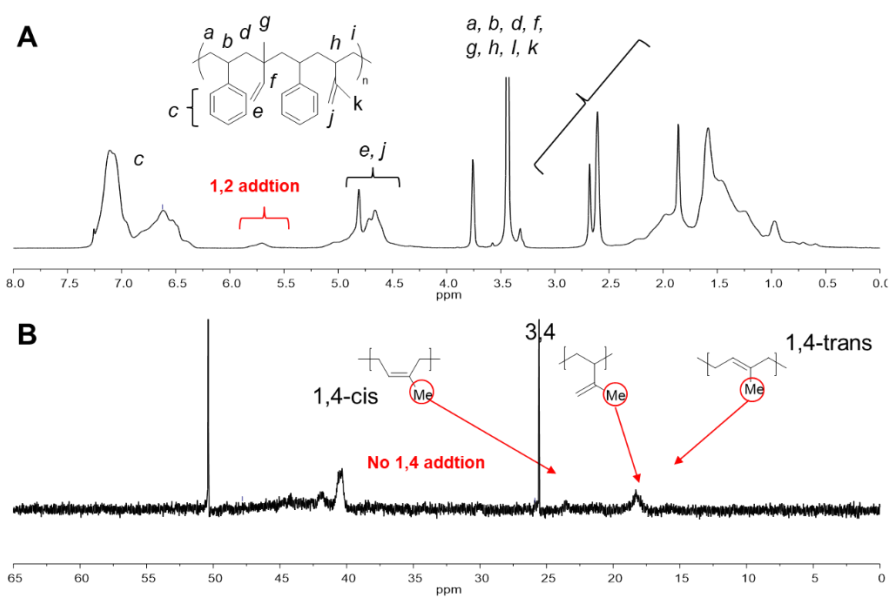

Figure S9. (A) ^{1}H NMR and (B) ^{13}C NMR spectra of random copolymer, p(St-*co*-Ip)(3,4). The regiospecificities of the isoprene units showed predominantly 3,4-rich repeating unit (1,4-: 1,2-: 3,4- = 0: 25-29: 71-75) along the copolymer chain.

3. Intramolecular Friedel-Crafts cyclization of poly(styrene-*co*-isoprene)

The cyclization was initiated by adding CF_3SO_3H into the random copolymer in cyclohexane at room temperature. After 2 h, the cyclization was terminated with 1 % aqueous solution of Na_2CO_3. The quenched solution was extracted with CH_2Cl_2 and washed with water three times to remove salt residues. It was precipitated into methanol, filtered, and vacuum-dried to give the product as a powdery product. The cyclization of poly(St-*co*-Ip) was confirmed by consumption of peaks for double bonds (4.5-5.2 ppm) in NMR analysis.

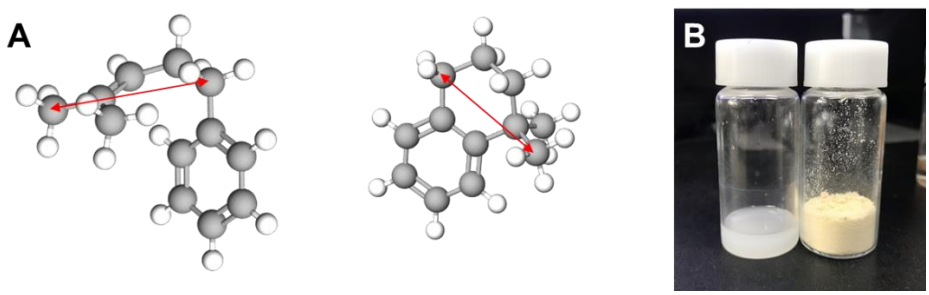

Figure S10. 3-D images of (A) 1,4- units and bicyclic structure generated by the intramolecular Friedel-Craft cyclization of between isoprene units and the benzene ring of the adjacent styrene unit. (B) The reaction leads to a high T_g and robust mechanical properties to the random copolymer. The gummy product was converted to the powdery compound.

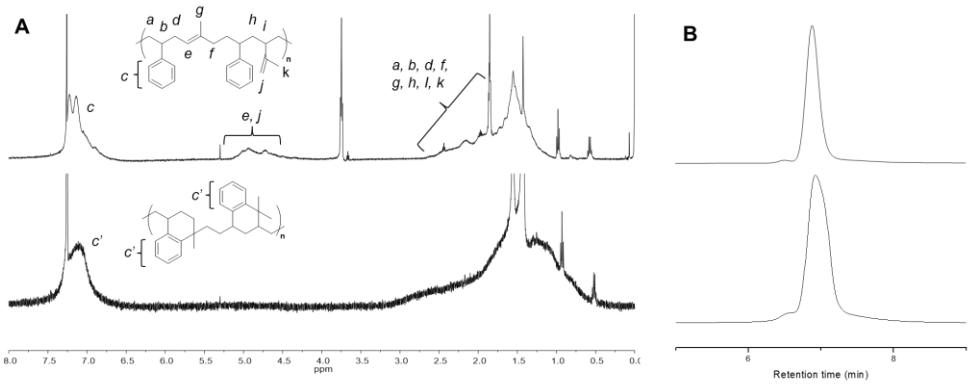

Figure S11. (A) ^{1}H NMR and (B) gel-permeation chromatography spectra of random copolymers, p(St-*co*-Ip)(1,4) and its cyclized product. Cationic cyclization of the obtained polymer was examined using CF_3SO_3H in cyclohexane. $[CF_3SO_3H]_0$ = 5 wt%.

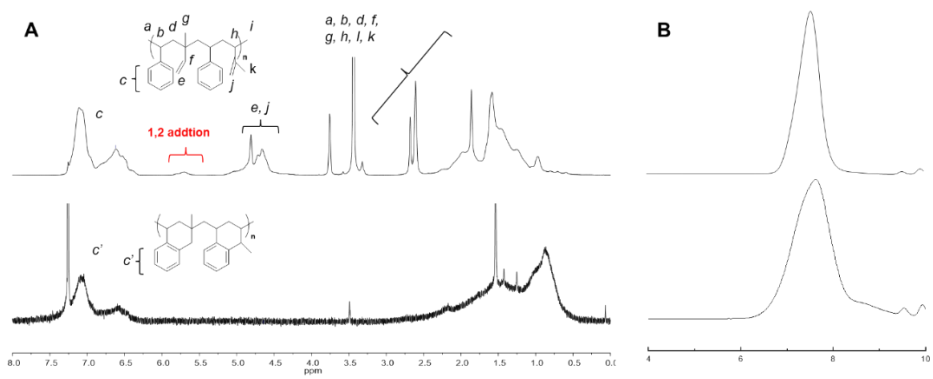

Figure S12. (A) ^{1}H NMR and (B) gel-permeation chromatography spectra of random copolymers, p(St-*co*-Ip)(3,4) and its cyclized product. Cationic cyclization of the obtained polymer was examined using CF_3SO_3H in cyclohexane. $[CF_3SO_3H]_0$ = 5 wt%.

4. Preparing random copolymers of amphiphilic block copolymers

Synthesis of poly(styrene-*co*-isoprene)-*b*-poly(ethylene glycol) by click chemistry. CuBr (30 mg) was dried in vacuum for 15 min. *N*,*N*,*N'*,*N''*,*N''*-pentamethyldiethylenetriamine (PMDETA) (0.060 mL) and THF were added into the flask. The resulting mixture was stirred in

N_2 for 15 min. To this mixture, a solution of the hydrophilic PEG block (M_n = 2450 g mol^{-1}, 127 mg) and deprotected poly(styrene-*co*-isoprene) (M_n = 14500 g mol^{-1}, 1.07 g) in THF was added. The mixture was degassed by bubbling N_2 for 15 min. After degassing, the click reaction was proceeded at 40 °C until completion. The extent of the reaction was monitored by GPC. The reaction was quenched by exposing the solution to air, followed by dilution with chloroform. The cooled solution was filtered through aluminum oxide (basic) with $CHCl_3$ to remove the Cu catalyst. The filtered solution was concentrated on a rotary evaporator, and then crude products were filtered through a pack of silica with CH_2Cl_2 to remove the excess unreacted hydrophobic block. To collect the product, a mixed eluent (dichloromethane:methanol = 90:10 v/v) was used. The filtered solution was concentrated on a rotary evaporator to afford a pure block copolymer as a pale yellow gummy product (M_n = 15300 g mol^{-1}, 0.350 g (% yield = 39.97%)). If necessary, the resulting block copolymer was purified by preparatory size exclusion chromatography.

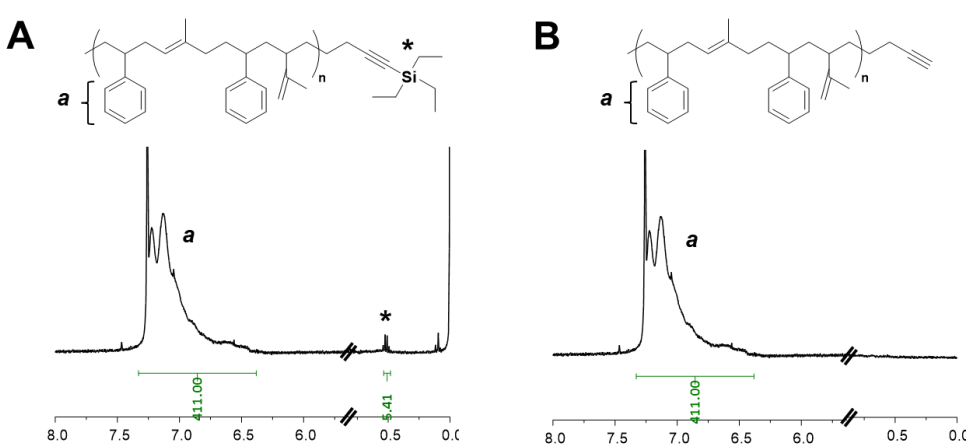

Figure S13. ^{1}H NMR spectra of random copolymer, p(St-*co*-Ip)(1,4) (M_n = 14.5k) showing the disappearance of Si-CH_2 protons upon deprotection.

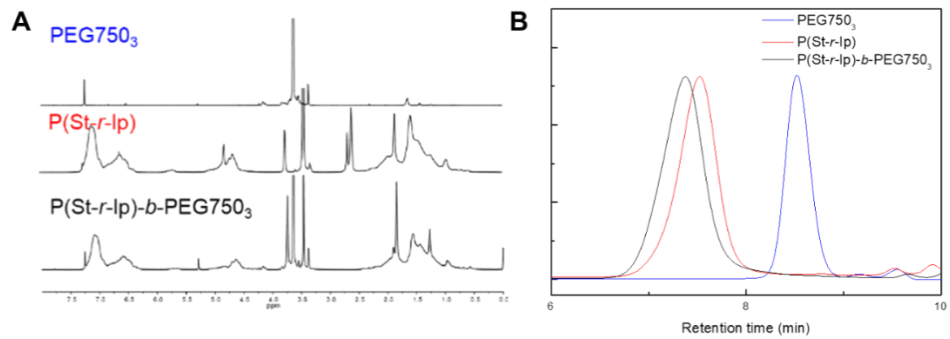

Figure S14. (A) ^{1}H NMR spectra and (B) GPC spectra of synthesis of p(St-*co*-Ip)(3,4)-*b*-PEG750$_3$ block copolymers by click chemistry: PEG (blue), p(St-*co*-Ip) (red) structural module, and p(St-*co*-Ip)-*b*-PEG (black).

5. Intramolecular Friedel-Crafts cyclization of poly(styrene-*co*-isoprene)-*b*-PEG BCPs

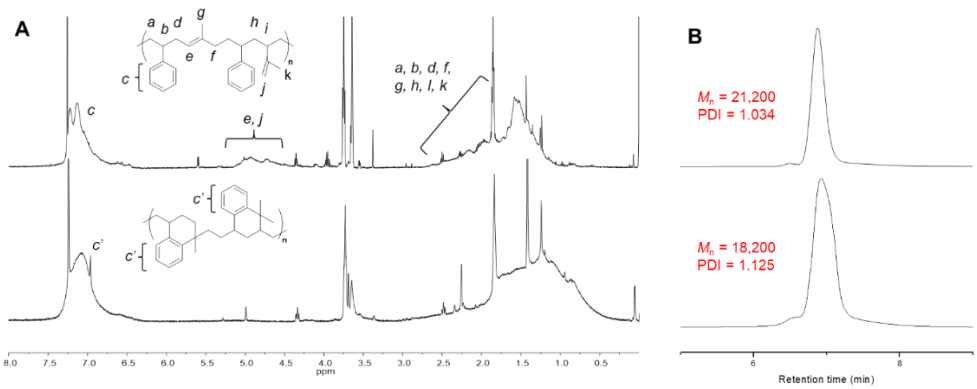

Figure S15. (A) ^{1}H NMR and (B) Gel-permeation chromatography spectra of random copolymers containing dominantly 1,4-microstructures and its cyclized product. Cationic cyclization of the obtained polymer was examined using CF_3SO_3H in cyclohexane. $[CF_3SO_3H]_0$ =5 wt%.

6. Observation of self-assembled structures of BCPs by cryo-TEM

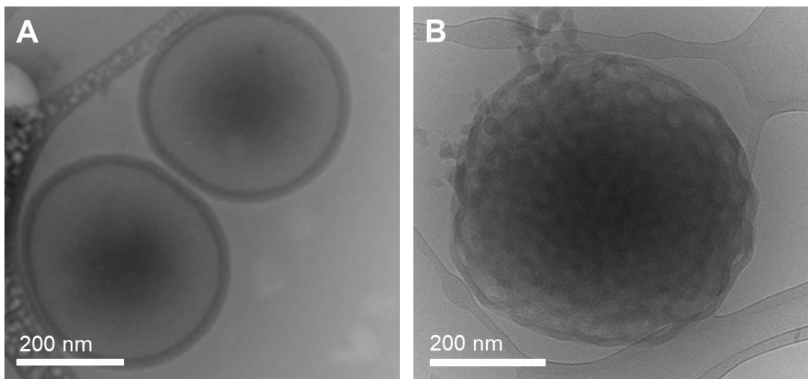

Figure S16. Cryo-TEM images of self-assembled structures of (A) p(St-*co*-Ip)(1,4)-*b*-PEG750$_3$ (21.2k) and (B) p(St-*co*-Ip)(1,4)-*b*-PEG750$_3$ (25.0k).

7. Comparison of the thickness of the bilayer membrane consisting of the self-assembled structures

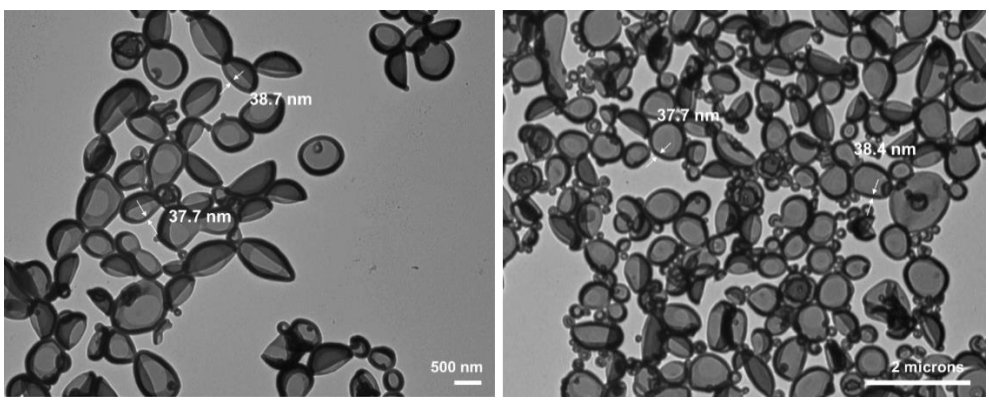

Figure S17. TEM images of self-assembled structures showing the thickness of the bilayer membrane: (A) polymer vesicles of p(St-*co*-Ip)(3,4)-*b*-PEG750$_3$ (M_n = 19.2K) and (B) polymer vesicles of its cyclized BCPs.

8. Cross-linking of self-assembled structure of p(St-*co*-Ip)-*b*-PEG750$_3$ via intermolecular cyclization

10 mg of BCPs was dissolved in 1,4-dioxane (2 mL) in a 20 mL capped vial with magnetic stirrer. To this solution, 2 mL of water was slowly added at a rate of 2 mL h^{-1} by using a syringe pump. It was followed by dialysis against

water. The solvent medium should be exchanged from water to acetonitrile via dialysis for 24 h. To provide acidic condition in the acetonitrile medium, 100 wt% of CF_3SO_3H was added. After 3 h stirring, it was followed by dialysis against water. All BCPs were self-assembled and cyclized under identical conditions for comparison.

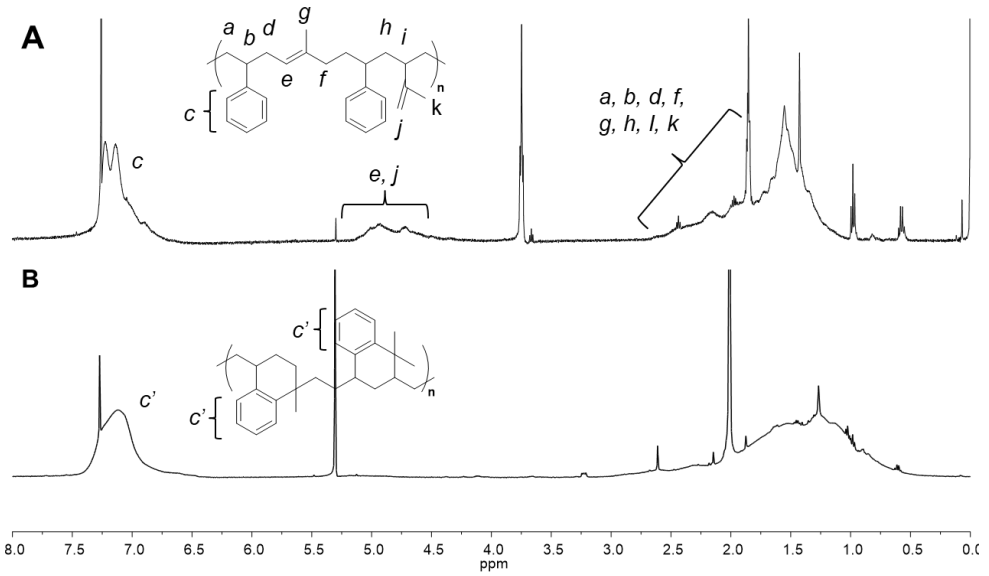

Figure S18. ^{1}H NMR of (A) random copolymers, p(St-*co*-Ip)(1,4) and (B) its cyclized product. Cationic cyclization of the obtained polymer was examined using CF_3SO_3H in acetonitrile. $[CF_3SO_3H]_0$ = 5 wt%.

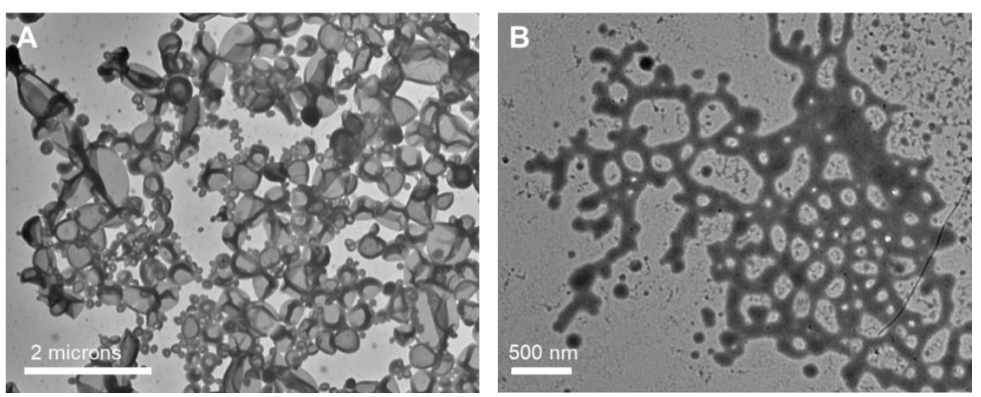

Figure S19. TEM images of (A) polymer vesicles of the cyclized p(St-*co*-Ip)(1,4)-*b*-PEG750$_3$ (M_n = 13.8K) in acetonitrile and (B) the uncross-linked polymer vesicles in THF.

Chapter 5. Shape Transformation of Nanoparticles Driven by Light-Induced Conformational Change of Hydrazone-Based Photoswitches

1. Preparation of hydrazone-based photo-switches

Hydrazone-based photo-switches (THP-H1-COOH) was synthesized by following the previously reported procedure.

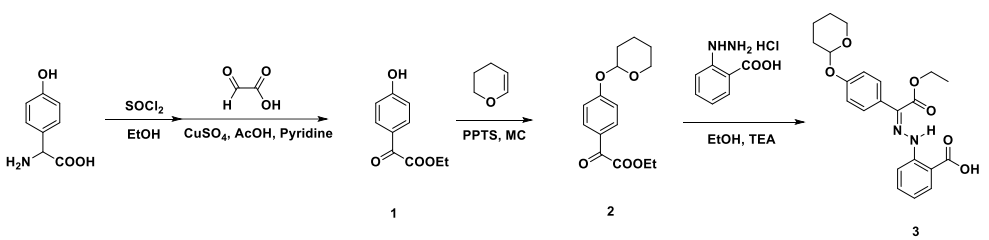

Scheme S6. Synthesis of hydrazone-based photo-switches.

THP-H1-COOH (3). It is synthesized in multi-gram quantity by following the literature methods.

^{1}H NMR (500 MHz, $CDCl_3$) δ 13.67 (s, 1H), 8.02 (dd, J=8.0, 1.5 Hz, 1H), 7.94 (d, J=8.0 Hz, 1H), 7.64 (d, J=9.0 Hz, 2H), 7.54 (t, J=8.5 Hz, 1H), 7.07 (d, J=9.0 Hz, 2H), 6.95 (t, J=8.0 Hz, 1H), 5.48-5.47 (m, 1H), 4.45 (q, J=7.0 Hz, 2H), 3.95-3.90 (m, 1H), 3.64-3.61 (m, 1H), 2.05-2.00 (m, 1H), 1.90-1.87 (m, 2H), 1.70-1.55 (m, 3H), 1.39 (t, J=7.0 Hz, 3H) ppm; ^{13}C NMR (125 MHz, CD2Cl2) δ 169.42, 162.97, 157.66, 147.26, 135.57, 132.74, 132.03, 130.08, 130.04(2C), 120.45, 117.49, 116.31(2C), 114.86, 96.84, 62.51, 61.92, 30.73, 25.64, 19.25, 14.41 ppm.

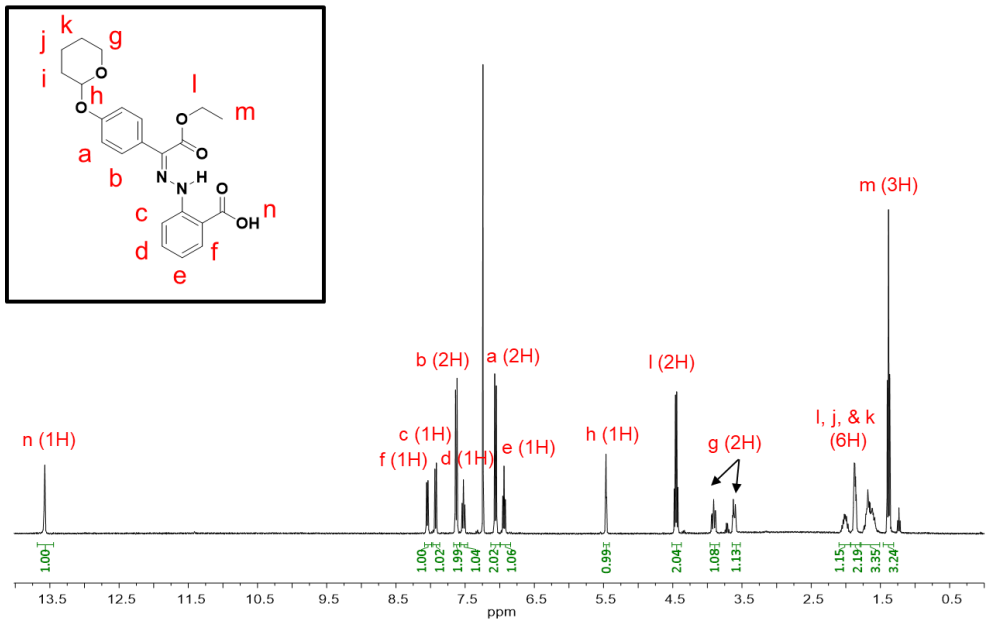

Figure S30. [1]H NMR spectra of hydrazone-based photo-switches (THP-H1-COOH).

2. Procedure for the convergent growth of poly(phenyl lactic acid)s

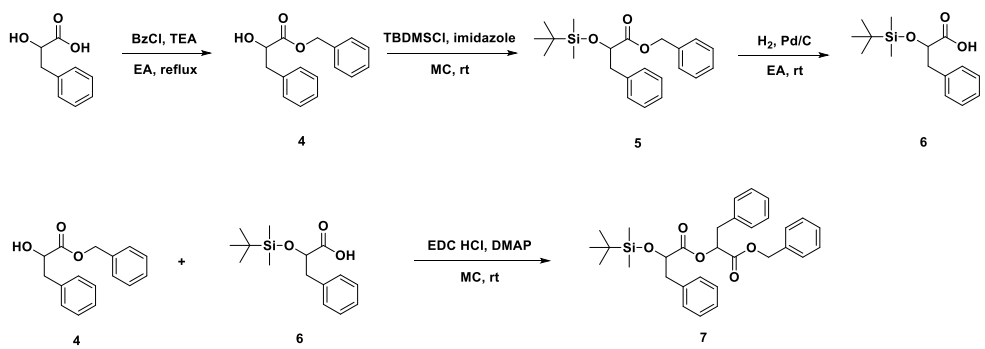

Scheme S7. Synthesis of pheynyl lactic acid dimer (**PLA_2**).

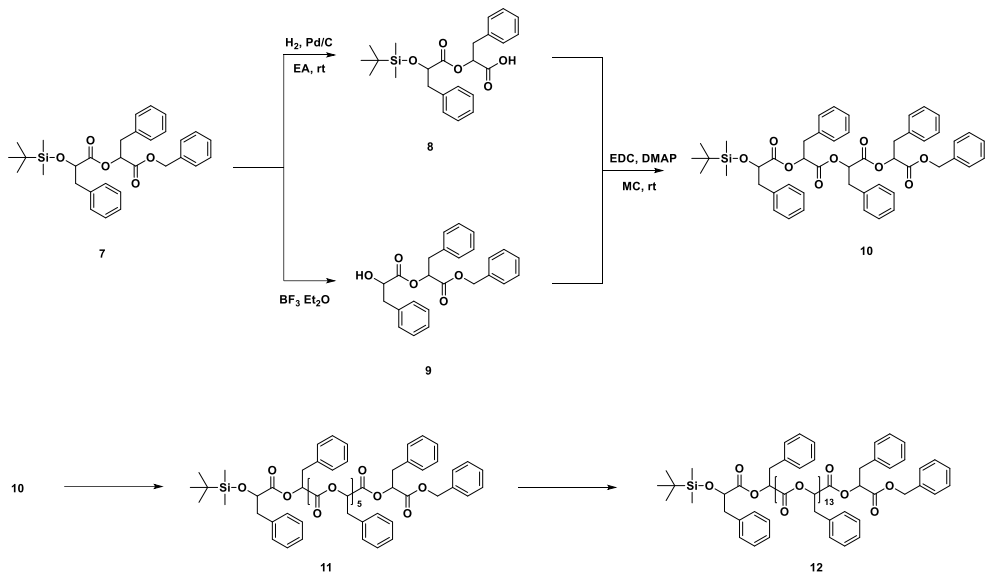

Scheme S8. Synthesis of discrete poly(pheynyl lactic acid)s (d**PPLAs**).

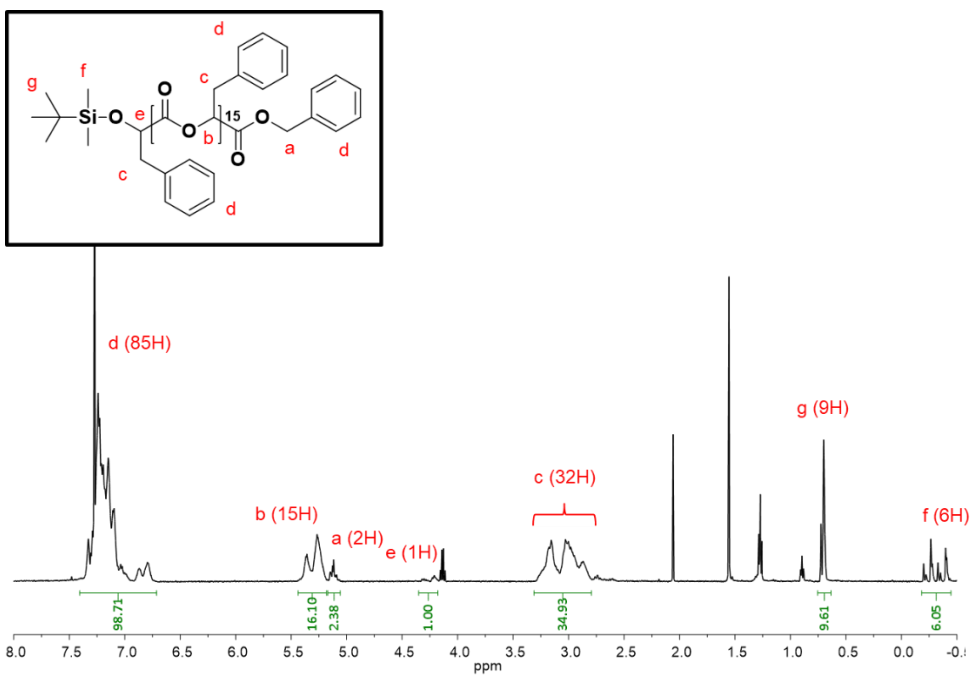

Figure S21. ^{1}H NMR spectra of poly(phenyl lactic acid) 16-mer ($PPLA_{16}$).

$PPLA_{16}$ (12). It is synthesized in multi-gram quantity by following the literature methods.[2]

^{1}H NMR (500MHz, $CDCl_3$): 7.37-7.01 (m, 85H, Ph-H), 5.32 (m, 15H, COO-CH(CH_3)C=O), 5.14 (m, 2H, Ph-CH_2-O), 4.30 (ddd, J = 29.2, 9.2, 3.4 Hz, 1H, SiO-CH(CH_2Ph)C=O), 2.90 (m, 32H, Ph-CH_2-CH), 0.71 (d, J = 91. Hz, 9H, $(CH_3)_3$C-Si), - 0.29 (dd, J = 51.5, 23.9 Hz, 6H, $(CH_3)_3$C-Si(CH3)2-O) ppm.

3. Synthesis of block copolymers having hydrazone-based photo-switches

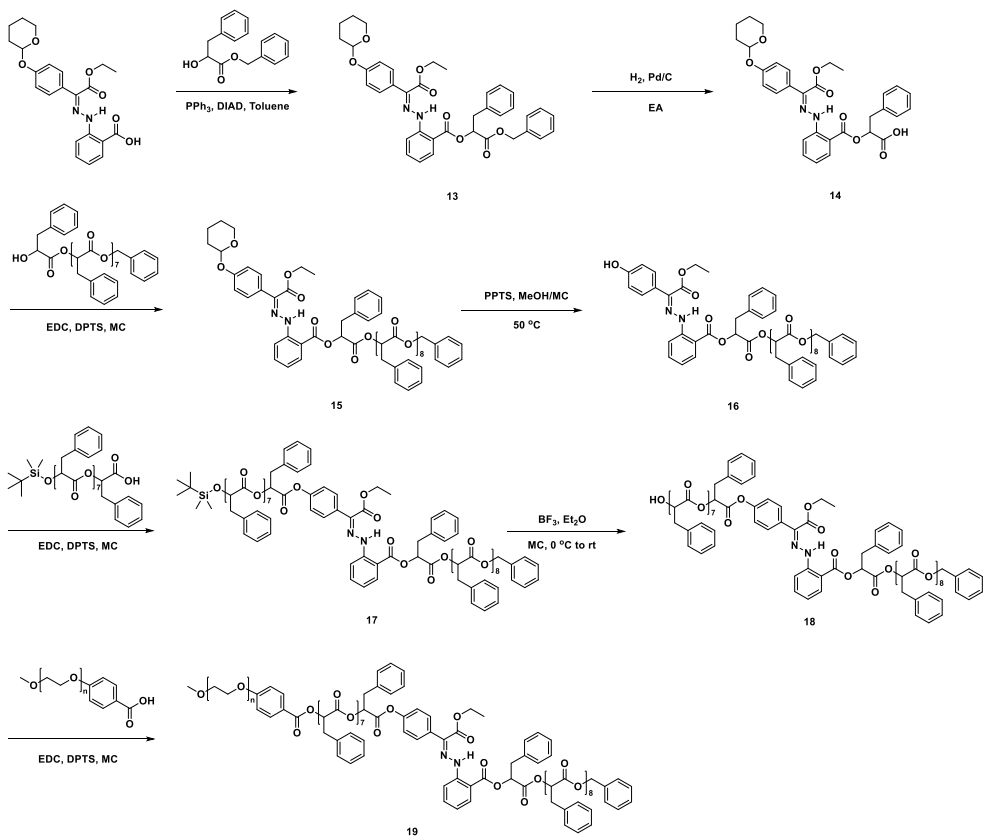

Scheme S9. Synthesis of block copolymer having hydrazone-based photo-switches (PEG-$PPLA_8$-H1-$PPLA_9$).

13: DIAD was added to a solution of hydrazone **3**, HO-PLA-Bn, and PPh_3 in toluene at 0 °C. The reaction was stirred at room temperature overnight. After removal of the solvent under vacuum, the product was purified by flash column chromatography affording a yellow oil.

14: Palladium on activated charcoal (10% Pd/C) was added to the solution of THP-H1-$PPLA_9$-Bn in EA. The suspension was purged with nitrogen for 15 min. The nitrogen atmosphere was then replaced with hydrogen atmosphere, and the reaction mixture was stirred at room temperature. Upon completion of the reaction, the suspension was filtered through a Celite cake to remove Pd/C. The product was obtained by removing the solvent from the filtrates under reduced pressure.

15: EDC was added to a solution of THP-H1-PLA-COOH (14), HO-$PPLA_8$-Bn, and DPTS in MC at 0 °C. The mixture was stirred at room temperature overnight. After removal of the solvent under vacuum, the product was purified by flash column chromatography affording a yellow oil.

16: A mixture of THP-H1-$PPLA_9$-Bn (15) and PPTS in MC/MeOH was heated to 50 °C and then stirred for 4 h. After removal of the solvent under vacuum, the product was purified by flash column chromatography to afford the *Z*-isomer product.

17: EDC was added to a solution of TBS-$PPLA_8$-COOH, HO-H1-$PPLA_9$-Bn, and DPTS in MC at 0 °C. The mixture was stirred at room temperature overnight. After removal of the solvent under vacuum, the product was purified by flash column chromatography affording a yellow oil.

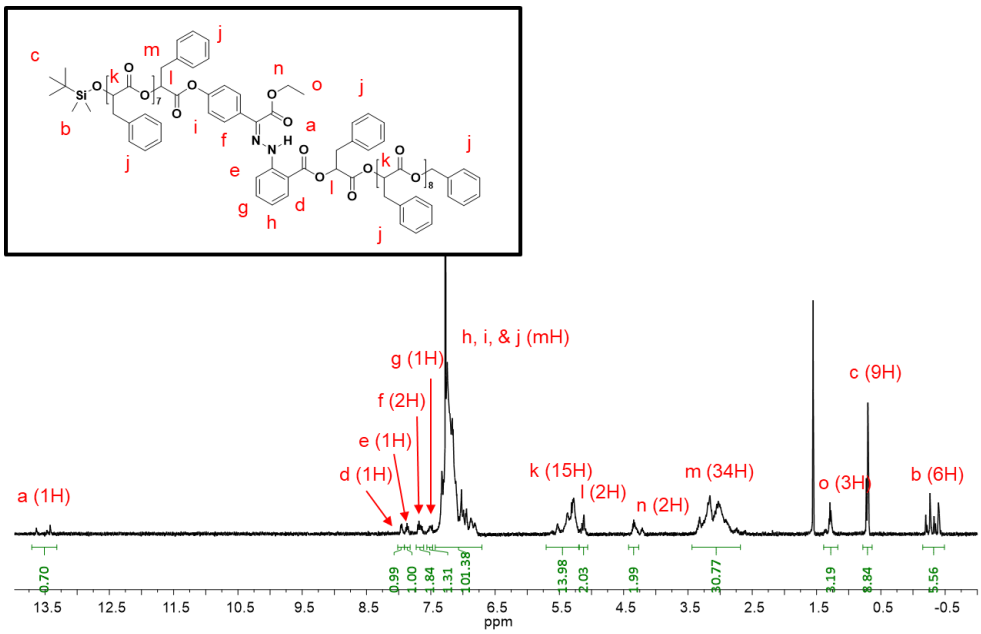

Figure S22. ^{1}H NMR spectra of hydrophobic block (TBS-PPLA$_8$-H1-PPLA$_9$-Bn).

18: The hydrophobic chain, TBS-PPLA$_8$-H1-PPLA$_9$-Bn (17), was dissolved in dry MC. The solution was cooled to 0 ºC on an ice bath, and boron trifluoride diethyl etherate (BF_3 Et_2O) was added dropwise. The reaction mixture stirred at room temperature for 4 h. Upon completion of the reaction, the reaction was quenched with saturated $NaHCO_3$ followed by dilution with water. The organic layer was separated and washed with brine. The combined organic layer was dried over $MgSO_4$, and the solvent was removed under reduced pressure. The crude product was purified by column chromatography affording a yellow viscous oil.

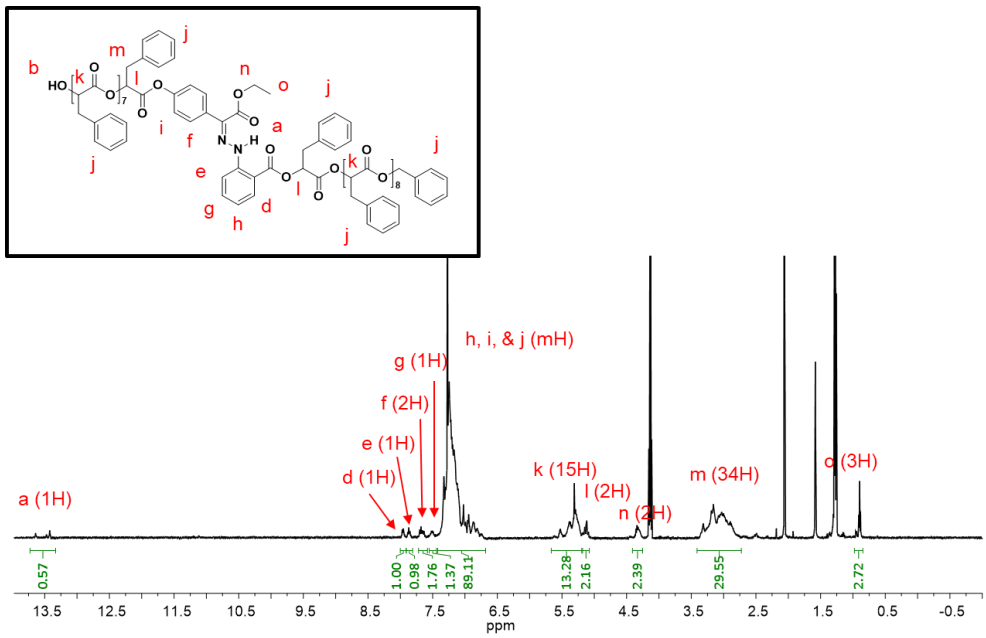

Figure S23. ^{1}H NMR spectra of hydrophobic block (HO-PPLA$_8$-H1-PPLA$_9$-Bn).

19: The deprotected hydrophobic block, HO-PPLA$_8$-H1-PPLA$_9$-Bn (18), and the hydrophilic block, PEG$_{550}$-COOH, were dissolved in dry MC. The mixture was cooled to 0 °C on an ice bath. To the mixture, 1-(3-dimethylaminopropyl)-3-ethylcarbodiimide hydrochloride (EDC HCl) and DPTS were added. The reaction mixture was stirred overnight at room temperature. Upon completion of the reaction, the reaction mixture was washed with water and brine. The combined organic layer was dried over $MgSO_4$, and the solvent was removed under reduced pressure. The crude product was purified by column chromatography affording a yellow viscous oil.

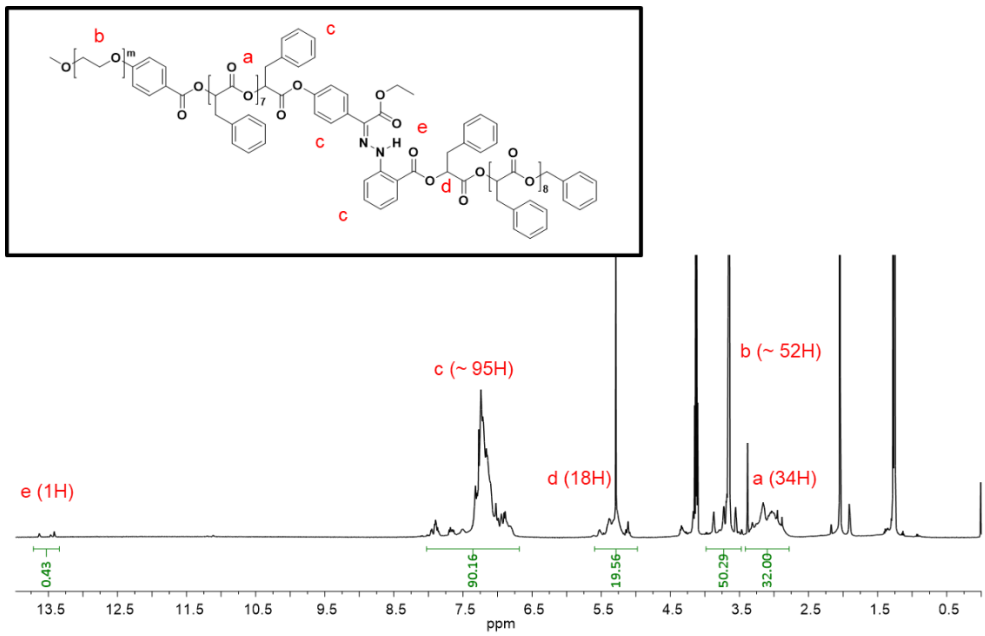

Figure S24. ^{1}H NMR spectra of amphiphilic block copolymer (PEG-PPLA$_{8}$-H1-PPLA$_{9}$).

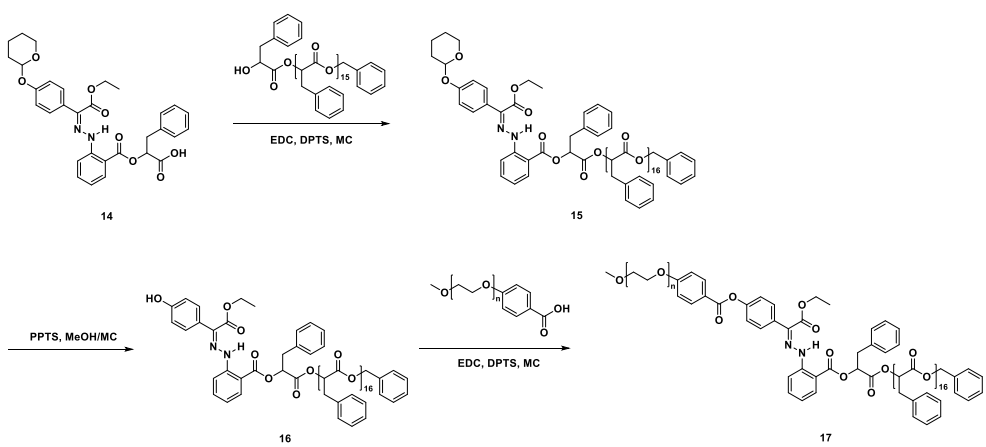

Scheme S10. Synthesis of block copolymer having hydrazone-based photo-switches (PEG-H1-PPLA$_{17}$).

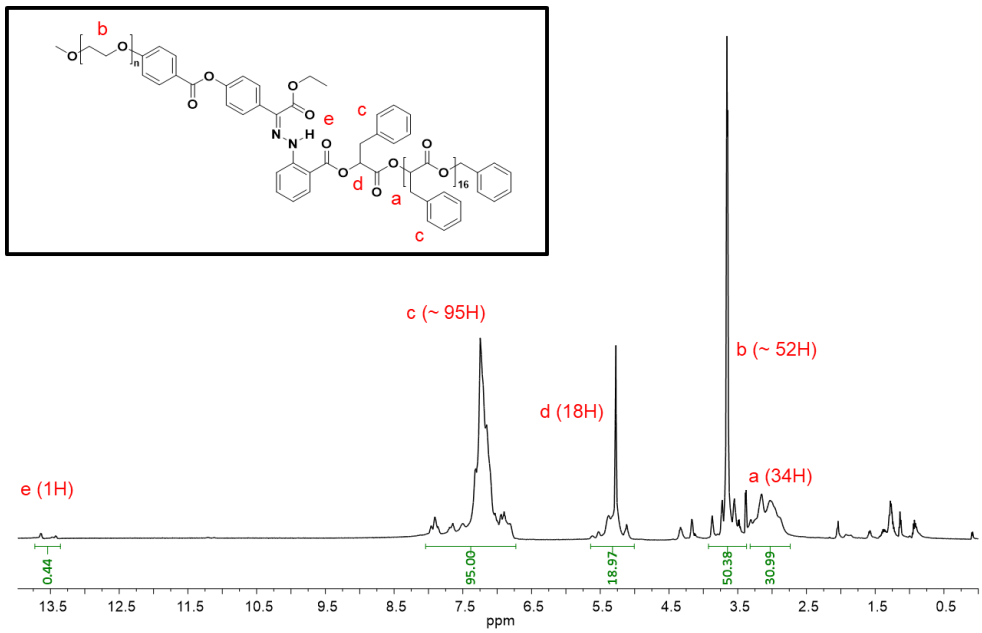

Figure S25. ^{1}H NMR spectra of amphiphilic block copolymer (PEG-H1-PPLA$_{17}$).

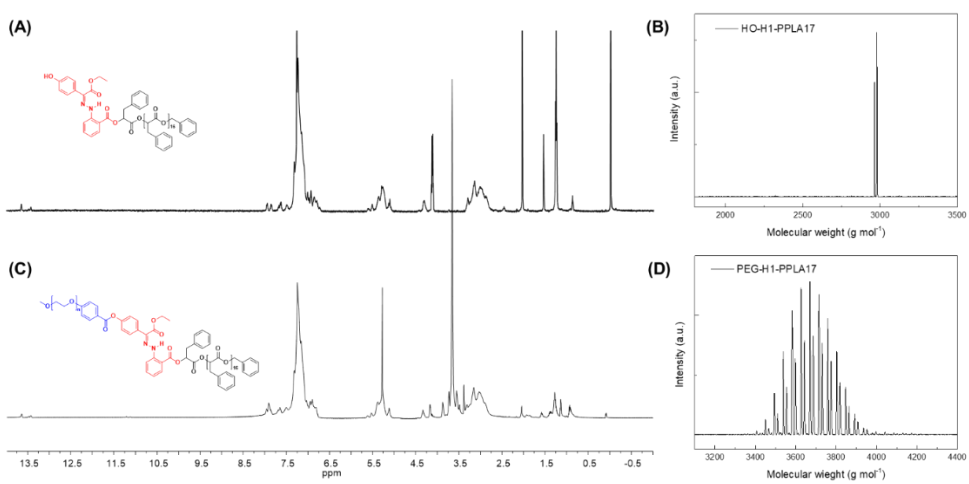

Figure S26. (A and C) ^{1}H NMR spectra in $CDCl_3$ and (B and D) MALDI-TOF spectra of monodisperse hydrophobic block (HO-H1-PPLA$_{17}$) and amphiphilic block copolymer (PEG-H1-PPLA$_{17}$) respectively.

4. Solution self-assemblies of BCPs via co-solvent method

5 mg of BCPs was dissolved in dioxane (1 mL) in a 20 mL capped vial with magnetic stirrer. The solution was stirred for 1 h at room temperature (860 rpm). A syringe pump was calibrated to inject water at a speed of 0.5 mL/h. The vial cap was replaced with a rubber septum, and water was added to the polymer solution over 2 h using a syringe pump with a 6-mL syringe equipped with a steel needle. The resulting suspension was subjected to dialysis (molecular weight cutoff 12-14 kDa (SpectraPor, Rancho Dominguez, CA)) against water for 24 h.